WATER AND MACROMOLECULAR TRANSPORT INTO THE WALLS OF VESSELS WITH DIFFERING ATHEROGENIC SUSCEPTIBILITIES

by

Yixin Shou

A dissertation submitted to the Graduate Faculty in Engineering in partial fulfillment of the requirements for the degree of Doctor of Philosophy, *The City University of New York*

2005

UMI Number: 3187390

UMI Microform 3187390

Copyright 2005 by ProQuest Information and Learning Company.
All rights reserved. This microform edition is protected against unauthorized copying under Title 17, United States Code.

ProQuest Information and Learning Company
300 North Zeeb Road
P.O. Box 1346
Ann Arbor, MI 48106-1346

This manuscript has been read and accepted by the Graduate Faculty in Engineering in satisfaction of the dissertation requirement for the degree of Doctor of Philosophy.

August 1st, 2005
Date

Professor David S. Rumschitzki
Chair of Examining Committee

August 1st, 2005
Date

Professor Mumtaz K. Kassir
Executive Officer

Professor Bing-Mei Fu

Professor Kung-ming Jan
College of Physicians and
Surgeons, Columbia University

Professor Charles Maldarelli

Professor David Rumschitzki

Professor John Tarbell

Professor Sheldon Weinbaum

Supervisory Committee

The City University of New York

Abstract

Water and Macromolecular Transport into the Walls of Vessels with Differing Atherogenic Susceptibilities

by
Yixin Shou

mentor: David Rumschitzki
co-mentor: Kung-ming Jan

Large arteries such as the aorta and the coronary arteries are atherogenic. Transendothelial transport of lipid into and its spread in the subendothelial intima of large arteries, together with its subsequent accumulation therein are believed to be the earliest steps leading to plaque formation. The pulmonary artery can develop the disease when it is under prolonged pulmonary hypertension. Veins are only disease-prone after grafting a vein as an arterial bypass. This thesis focuses on experimental studies on the water filtration, tracer transport and ultrastructures of the rat aorta, pulmonary artery and the inferior vena cava, as representatives of the three classes of large vessels, in order to understand their very different atherogenicity. In addition, we investigate the contribution of the trans-membrane water channel Aquaporin to the aortic hydraulic conductivity and propose a preliminary model for understanding the water filtration processes through the walls of the three vessels.

This thesis begins by studying the ultrastructures of the pulmonary artery (PA) and the inferior vena cava (IVC) and comparing them with that of the aorta. Using the elastin-specific stain orcein, we find that the PA has continuous endothelium and complete internal elastic lamina (IEL). Its structure is similar to that of the aorta, but has a thinner wall and fewer and thinner elastin sheets. The vein has a very different structure; it has a continuous endothelium, a very incomplete IEL, only sparse bits of elastin and considerably more collagen than the arteries.

Both the PA and IVC show ruthenium red stains at the luminal and abluminal sides of the endothelium, indicating the existence of a subendothelial intima in these vessels, albeit the IVC does not have a complete IEL to outline an intima

We measure the hydraulic conductivity Lp for each vessel as a function of transmural pressure ΔP, both with intact and denuded endothelium on the same vessel. Aortic Lp is high at 60 mmHg, drops by ~40% at 100 mmHg and is pressure-insensitive beyond. The trends are similar in the PA and IVC, dropping 42% from 10-40 mmHg and flat to 100 mmHg for the PA and dropping 33% from 10-20 mmHg and essentially flat to 60 mmHg. Endothelial removal renders Lp(ΔP) flat; it increases the aortic Lp by ~75%, doubles Lp of the PA and quadruples Lp of the IVC. The specific resistance (1/Lp) of the aortic endothelium is ~47% of the total resistance. The PA value is 55% above 40 mmHg and the IVC value is 23% at 10 mmHg. The Lp's of the intact aorta, PA and IVC have magnitudes of 10^{-8}, 10^{-7} and $5x10^{-7}$ cm/(s mmHg) and wall thicknesses 145.8±9.3, 78.9±3.3 and 66.1±4.1 (mean ± SD) μm. These data are consistent with the differing wall structures of the three vessels. The rat aortic Lp data suggest that intimal compression under pressure loading may also play a role in Lp(ΔP) in these other vessels. Despite different ΔP's in these vessels, their nominal transmural water fluxes are surprisingly similar, and therefore cannot alone account for their different disease susceptibilities.

We also experimentally examine the transport of the macromolecular tracer horseradish peroxidase (HRP) across the endothelium of the vessels. In all the vessels, HRP traverses the endothelium in focal spots for short times. The PA's spots have a radius of 53.2±10.4 μm (mean ± SD) at 30s which is comparable to the aorta (54.6±8.75 μm) at 30s. The spots grow quickly from 30s to 1 min (40%, $P<0.05$) and more slowly afterwards ($P>0.05$). The trend is also similar to the aorta, which suggests that the PA has a similarly sparse intima. With HRP introduced

through a femoral vein (FV) cannulation, the IVC spot was very large (192.56±62.8 μm) even at 30 s. The tracer spot grew little with longer circulation time ($P>0.05$). With carotid artery (CA) cannulation, the tracer takes longer to reach the IVC and the tracer is more diluted in the blood, and thus the 30 s tracer spot in the IVC is a bit smaller (132.86±37.32 μm) than the analogous FV-cannulation, but still much larger than that of the PA. The spot grew only 28% ($P<0.05$) from 30 s to 60 s and, with either cannulation, was much flatter than the artery curves. Transverse EM sections of these vessels after circa 10 min. HRP circulation times showed thin, intense staining immediately beneath the vessels' endothelia. This indicates the existence of a sparse, sub-endothelial intima in these vessels, even in the absence of an IEL, as in the IVC.

To gain more insight about the nature of Lp, we further study how ubiquitous water channel protein aquaporin (AQP) plays a role in transendothelial water transport. We use the aquaporin blocker mercuric chloride ($HgCl_2$) to assess the fraction of the endothelial and of the overall vessel wall Lp attributable to AQP-1. The Lp's of excised rat aorta were measured as a function of ΔP, first in the absence and then in the presence of $HgCl_2$ on the same vessel. Without $HgCl_2$ Lp has a high value at 60 mmHg, drops about 27% at 100 mmHg ($P<0.05$) and remains flat to 140 mmHg. Introduction of 10 μM $HgCl_2$ depresses Lp over the entire range 60-140 mmHg, but most (27.5%) at 60 mmHg, equivalent to a 41% drop with the pooled data. Higher $HgCl_2$ concentrations led to Lp artifacts at higher pressures that exceeded the control values, and probably indicated $HgCl_2$ being forced into and interfering with the normal junctions.

Finally, we propose a set of theoretical models for the filtration water flow through the PA and IVC walls, and contrast them with the established model for the filtration problem in the aorta. We present these solutions and briefly discuss the parameters needed thereof. We leave a detailed numerical study of these equations to future work.

To my family

Acknowledgements

I would like to express my deepest gratitude and appreciation to my mentor Professor David Rumschitzki and co-mentor Dr. Kung-Ming Jan. I have gained so much inspiration from their physical insights and suggestions throughout this research work.

I also would like to thank my mom for her undying support and love. I especially thank my husband, Hsien-Hung Wei, who is also my best colleague, for always being concerned about me and for listening to me without complaints.

I am very grateful to Dr. Christ Chan, Dr. John J. Lee and Dr. Daniel Lemons of Biology Department to let me use their facilities enable to complete this research. Also a special thank to Dr. Jorge Morales of Biology Department for constant help with the electron microscopy.

This work is supported by NSF Grant CTS-0077520 and NIH Grant 5-R01-ML 067383.

List of Content

List of Figures

Chapter 1

Chapter 2

Chapter 5

Chapter 6

Chapter 1

Introduction

Atherosclerosis is a disease mainly of large arteries. It appears to begin with the delivery of cholesterol from the blood into the vessel wall, where it accumulates (Vander 2001). Blood-borne monocytes enter the arterial intima in regions with high sub-endothelial lipid concentration, becoming macrophages that, along with media-derived smooth muscle cells (SMC), attempt to scavenge the extracellular cholesterol. When overwhelmed, they progress to form foam cells, and this accumulation of lipid and necrotic cells appears to comprise the earliest lesions. Eventually, such lesions can lead to stenoses that can burst, sending debris into the blood stream and can compromise the cross section for blood flow rendering it susceptible to clogging by a clot, causing the heart to be overworked and possibly leading to heart attack.

It is well known that there is more than one type of lipoprotein cholesterol, and they are usually grouped by their corresponding fraction upon centrifugation. Low Density Lipoprotein (LDL) is termed the "bad" cholesterol because of its high concentration in atherosclerotic lesions. One LDL "molecule", about 22 nm in diameter, is comprised of about 2000 cholesterol and cholesterol ester molecules, all surrounded by a phospholipid coat to make it water/blood soluble, and an apoprotein B molecule that allows cell surface receptors to specifically recognize and bind it (Figure 1). Cholesterol in moderate concentrations is needed by cells to produce membranes. Nature has evolved two delivery methods to supply it to all cells: the exogenous and endogenous pathways. In the former, cholesterol and other lipids absorbed from the intestines enter the blood stream and make their way to the adipose tissue and muscles for storing energy in liver. In the latter, the liver packages cholesterol and other lipids into lipoprotein packets that transport the cholesterol through the bloodstream to the body's cells for use in cell membranes

and in hormone production (Brown 1984). An overabundance of cholesterol due to a high blood LDL concentration can lead to plaque formation and atherosclerosis.

Atherosclerosis normally occurs in the large arteries and/or in the aortic valve but not in the pulmonary artery (PA) or in veins. In humans, the pulmonary artery is vulnerable only in the presence of pulmonary hypertension (Duff 1951). (Curiously, some data suggest that rabbit pulmonary artery appears to be similar to rabbit aorta in its proclivity toward developing atherosclerosis (Schwenke 1997) and a comparison of the PA of the rabbit with that of an animal without this unusual susceptibility is worthy of study.) Veins normally do not develop atherosclerosis. However, when veins, such as the saphenous vein, which is frequently used in coronary bypass procedures, are placed in arterial conditions, i.e., high pressure, atherosclerosis often develops (Lever 1996) along with vessel remodeling. After 6 to 12 years, 71% of such vein grafts develop atherosclerosis and their structures resemble arterial fatty streaks (Berceli 1991). If the triggering events for the disease are lipid transport across the vessel endothelium and its sub-endothelial accumulation, it is natural to wonder if these processes are radically different in disease-resistant and disease-prone vessels. One of the first questions that one needs to ask in order to develop an understanding of the mass transport in these vessels is whether such transport is diffusion-driven, convection-driven or a combination of the two.

Before considering what might distinguish resistant vessels from susceptible ones, let us briefly review what is known about the earliest atherogenic events in susceptible vessels, such as the aorta. The aorta is lined with a monolayer of cells called the endothelium. Endothelial cells (EC) have junctions that are tight enough (~7 nm) ((Bell 1974), (Bell 1974), (Majno 1961), (Packham 1967), (Sprague 1980)) to severely restrict the trans-endothelial migration of molecules with sizes as small as that of albumin (~7 nm diameter) (Levick 1994). This raises the

question: how can a 22 nm LDL particle penetrate the endothelium's tight junction? Many groups tried to explain the LDL's penetration of the endothelium. With the use of electron microscopy and electron-dense cytochemistry, early investigators believed that plasmalamellal vesicles transported macromolecules across the endothelium (Simionescu 1978). These investigators proposed that the free vesicles in the cytoplasm of the endothelium represented the shuttling vesicles transporting macromolecules between the lumen and the tissue fronts of endothelium. Frokjaer-Jensen (Frokjaer-Jensen 1980) used the technique of ultra-thin serial sections and electron microscopy to study macromolecular transport across the endothelium and reported that the vesicles that, in isolated sections appeared to be free, were in fact bound to one or the other surface of the endothelium in another plane. Chien and Weinbaum (Chien 1981) purposed a theoretical model to estimate the percentage of LDL transport by vesicles. This percentage turned out to be very small compared to observed LDL accumulation.

Our collaborators and others then proposed (Weinbaum 1988b), (Wen 1988), (Stemerman 1986), (Yuan 1991) and Lin *et al*., ((Lin 1988), (Lin 1989)) and substantiated the hypothesis that an important pathway for large molecule to cross the aortic endothelium (in the rat) was via the junctions that surround rare, isolated cells, many of which are dying or dividing, whose junctions are not tight and therefore leak transiently. Experiments showed that 99% of the cells in mitotic (M) phase were associated with Evans blue albumin conjugate (EBA) leakage and that 80% of cells in M phase were to LY-LDL (Lucifer yellow-LDL). Figure 2 shows a dual-staining experiment exhibiting the coincidence of tracer leakage and (via hematoxylin staining) a cell in M phase of mitosis. The bright area indicates the tracer's presence under the endothelium. However, dying cell and cell mitosis do not appear to be the only causes of macromolecular

leaks. Truskey, *et al*., (Truskey 1992) used autoradiography to determine that mitotic or dying cells accounted for only about 25% of the total leaks found.

Chuang *et al*. (Chuang 1990) injected rats through the femoral vein with horseradish peroxidase (HRP) as a tracer and let it circulate for various amounts of time before animal sacrifice. These experiments showed the growth of the tracer spot in the aorta's subendothelial space as a function of tracer circulation time. Surprisingly the HRP tracer spots in the rat's aorta grew extremely fast, reaching 200 μm in diameter in only 2 min. These results were consistent with earlier similar experiments by Stemerman *et al*. (Stemerman 1986). This rapid growth of the large spots at early times represented a challenge to the theorists.

Initially theorists assumed the tracer growth was either a one-dimension diffusion process ((Truskey 1981), (Fry 1985), (Fry, 1987)), which was incapable of addressing the issue of isolated tracer spots, or a two-dimension diffusion process (Weinbaum 1985), (Weinbaum 1988b), (Wen 1988). Later work recognized that Chuang's observed spot growth was too fast to be accounted for by a purely diffusive process with any reasonable diffusivity, and thus included convection ((Yuan 1991), (Huang 1994)) and some ultrastructural detail, including the vessel intima and internal elastic lamina (IEL) as a transport barrier (Yuan 1991), but were still unable to account for the rapid spot growth. Huang *et al.* (Huang 1994) recognized that Frank & Fogelman's (Frank 1989) ultra-rapid freezing/rotary shadow-etching experiments revealed the detailed structure of the thin extracellular matrix in the sub-endothelial intima that separated the endothelium and IEL, which is above the tunica media that comprises ~99% of the healthy vessel wall. The intima's matrix consists of two major components, collage and proteoglycans. The etchings showed that this thin matrix turned out to be far more porous (0.84~0.88 for albumin) than the media (0.08 for albumin) (Tedgui 1987). Lark *et al*., (Lark 1988) immunolocalization

studies with monoclonal antibodies revealed that one reason for this was that the intima has different proteoglycan than the media. Huang *et al*'s (Huang 1994) *ab intio* theory for the intima's transport parameters showed that it offered far less resistance to a filtration flow than the media and, as such, encouraged an intimal flow that was largely parallel to the endothelium. The matrix of the IEL fenestrae was a continuation of the intima instead of the media. Combination of the resulting intima parameters with a two-dimensional convection-diffusion model similar to Yuan *et al*'s was able to explain Chuang *et al*'s data quite satisfactorily and, in the process, provided new insights into the transport processes in the artery wall.

Again, if lipid transport and accumulation are indeed the keys to triggering early atherolsclerosis in large, susceptible, high-pressure arteries, a detailed understanding of the relevant transport process in each vessel type might be able to explain the large differences in vessel susceptibilities. This thesis focuses mainly on experimental approaches to this problem, with some codifying theory at the end. It asks, just how similar are the water filtration and macromolecular transport processes in the aorta to those in the PA and the inferior vena cava (IVC)? Our working hypothesis is that they are different and correlate with the differences in vessel susceptibilities. Specifically, we ask: 1. How do the wall structures that strongly influence these transport processes differ among these vessels? This includes questions about the thickness and structure of the vessel walls that present flow resistance. Do the vessels all have thin, sparse intima adjacent to thick, dense media? What is the elastin content of the vessel walls? 2. How do the resistances of the different layers of the vessels' walls to transmural water flow differ from those of the corresponding layers of the other vessels? How similar are they for the same vessel, but in different species? 3. What are the basic facts about macromolecular entry into these vessels' walls? Is such transport focal or uniform? Is it convection-driven, diffusion-driven, or

some combination of the two? 4. What is the nature of transmural water flow? Is it purely junctional, or does it involve parallel pathways, including, e.g., the ubiquitous aquaporin membrane water channel pathway? 5. Can we codify the insight and measurements mentioned above into precise mathematical models whose solution might both explain experimental results and shed some light both on the nature of the differences in transport between these vessels and, in the longer term, on the differences in their atherosclerotic susceptibilities? These questions form the motivation for this thesis and the outline below will reflect our investigations towards answering them. Each of the succeeding 5 chapters is intended to be self-contained. It contains its own abstract, introduction, literature review, methods, results and discussion sections. As such, at the cost of some repetition, one can read Chapters 2-6 in any order.

First this thesis begins with a little background on the other vessels. We focus on the rat model. Note that although rats do not naturally become atherosclerotic due to low blood cholesterol, rats can develop atherosclerosis when fed an atherogenic diet (Vlad 1995). The PA is normally exposed to a low transmural pressure (16 mmHg) and has lower blood oxygen (Po_2=40 mmHg) than the aorta (Po_2=100 mmHg). The normal PA has a thinner wall (78.9±3.3μm in rat; see Chapter 2) than the aorta (145±9.7 μm in rat; see Chapter 2). The basic structure of the PA is similar to the aorta, containing a monolayer of endothelial cells with an associated intima and tunica of media, which has a repeated structure of elastin and smooth muscle cells (SMC). These two layers are separated by an internal elastic lamina (IEL) with numerous fenestrae (see Chapter 2). The IVC experiences an even lower transmural pressure (5 mmHg) than the PA, and its blood has the same oxygen tension as the PA. Since the vein is exposed to very low pressures, it has a thinner wall than the arteries (Lever 1990) - about 66.1±4.1 μm for rat vena cava (see Chapter 2). Its wall structure is different from that of the arteries. It has a larger lumen, less SMCs, a lower

elastin content, and a much higher distensibility, thereby providing a much lower hydraulic resistance than arterial walls (Mountcastle 1968). Chapter 2 will delve further into the structural differences between these vessels at different magnification. With the help of orcein, a specific stain for elastin, and the electron-dense ruthenium red general stain for proteoglycans ((Luft 1971), (Gerrity 1977)), one of the major constituents of the aortic intima (Frank 1989), we will be able to identify the proteoglycan in the extracellular matrix above and below the endothelium. In this chapter, we will compare the ultrastructures of the pulmonary artery, the inferior vena cava and the aorta and identify the matrix layers in the three vessels.

An important transport feature determined by details of the vessel's structure is the resistance (or its inverse, the hydraulic conductivity Lp) that it presents to transmural water flow. This bears directly on whether convection plays as strong a role in the mass transport in these lower-pressure vessels as it does in the large arteries. After reviewing the methods that have been used previously for measuring Lp, Chapter 3 adapts the *ex vivo* approach pioneered by Tedgui and Lever (Tedgui 1984) and later used by Baldwin and Wilson ((Baldwin 1992), (Baldwin 1993)) on the rabbit model to the much smaller rat model. This technique allows us to measure Lp of each of these three vessels in male, Sprague-Dawley rats, both with intact and denuded endothelium on the same vessel and to calculate the Lp of the endothelium from these measurements. We analyze the trends evident in these measurements and their implications. In particular, in rabbit, Lp of the intact vessel decreased with increasing pressure and then leveled off above 100 mmHg ((Tedgui 1984), (Baldwin 1992), (Baldwin 1993)). A theory by Hunag *et al* (Huang 1997) proposed and the same authors experimentally confirmed (Huang 1998), that the aortic intima compressed under pressure, causing the endothelium to block IEL fenestrae. The associated change in intimal flow accounted for the decrease in Lp with pressure, which,

consistent with this concept, disappeared with denudation. We shall examine the likelihood that similar phenomena occur in these other vessels. Finally, it is the *combination* of the measured Lp and the transmural pressure – *not* Lp alone - for different vessels and conditions that determine the overall transmural flows of the vessel and whether convection is likely substantial in transendothelial transport. Chapter 3 will assess this for the PA and IVC.

Chapter 4 turns to macromolecular transport in these vessel walls. In particular, we circulate horseradish peroxide for up to 5 minutes in rat, sacrifice the rat and investigate whether HRP penetrates the endothelia of these vessels focally rather than uniformly. After establishing that it crosses focally, we adapt the procedure of Chuang *et al*.'s (Chuang, 1990) HRP tracer spot size experiments to study HRP tracer spot growth in the PA and IVC and compare the results to those in the aorta. In the aorta, the HRP tracer spot growth demonstrates that this transport is a convection-dominated process driven by a large driving force– the high lumen pressure of 100 mmHg. Since the PA and the IVC are under lower pressures, 16 mmHg and 5 mmHg, respectively, it will be interesting to see if this is still the case? We use the Lp measurements of the vessels and of their endothelia from Chapter 3 to explain the results. We proposed a crude simple model to interpret the tracer spot size growth in the three vessels.

Chapter 5 addresses the issue of the pathways for water transport through the endothelium. Recent well-publicized work has shown that there is a family of transmembrane proteins – the aquaporins (AQP) - that transport only water molecules and reject everything else ((Murata 2000), (Sui 2001)). AQP exist in plants (Johanson 2001), red blood cells (Cho 1999), epithelium and endothelium (Nielsen 1993), and many other cell types. In Chapter 5, we modify the design of the Lp measurement from Chapter 3 and introduce mercuric chloride ($HgCl_2$) a well-established water channel inhibitor. We measure the Lp of the aorta as a function of

transmural pressure, first without, then with, this known aquaporin blocker on the same vessel. By comparing endothelial Lp values before and after the inhibitor, we estimate the contribution of AQP to the known endothelial resistance.

Finally, Chapter 6 considers how these accumulated results impact the formulation of a model for the filtration flow in each of these vessel walls and how these should compare with the model by Huang *et al*., (Huang 1994) discussed above. The solutions to these models should settle the question of whether intimal convection parallel to the endothelium is significant in these vessels. If so, and thus if transmural macromolecular transport indeed turns out to be convection-dominated, one would expect the filtration front in the intima to at least roughly explain the HRP spot size growth observed in Chapter 3. This chapter provides the governing equations, boundary conditions and solutions for the filtration models for the PA and IVC. It briefly discusses the model parameters and their relation to the experiments of the previous chapters, but leaves detailed numerical solutions for future work.

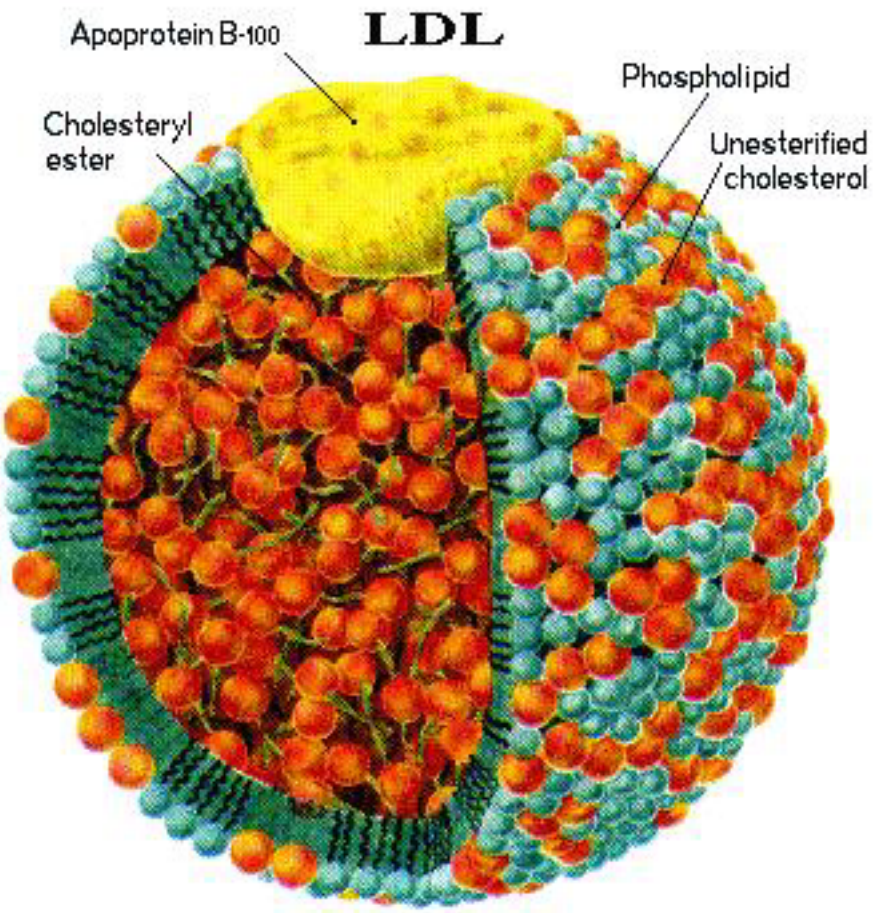

Figure 1. LDL molecule consist ~2000 undesterifed cholesterol and cholesteryl ester. The Apoprotein B receptor was recognized by most of surface cell receptors. The LDL has the diameter of ~22 nm.

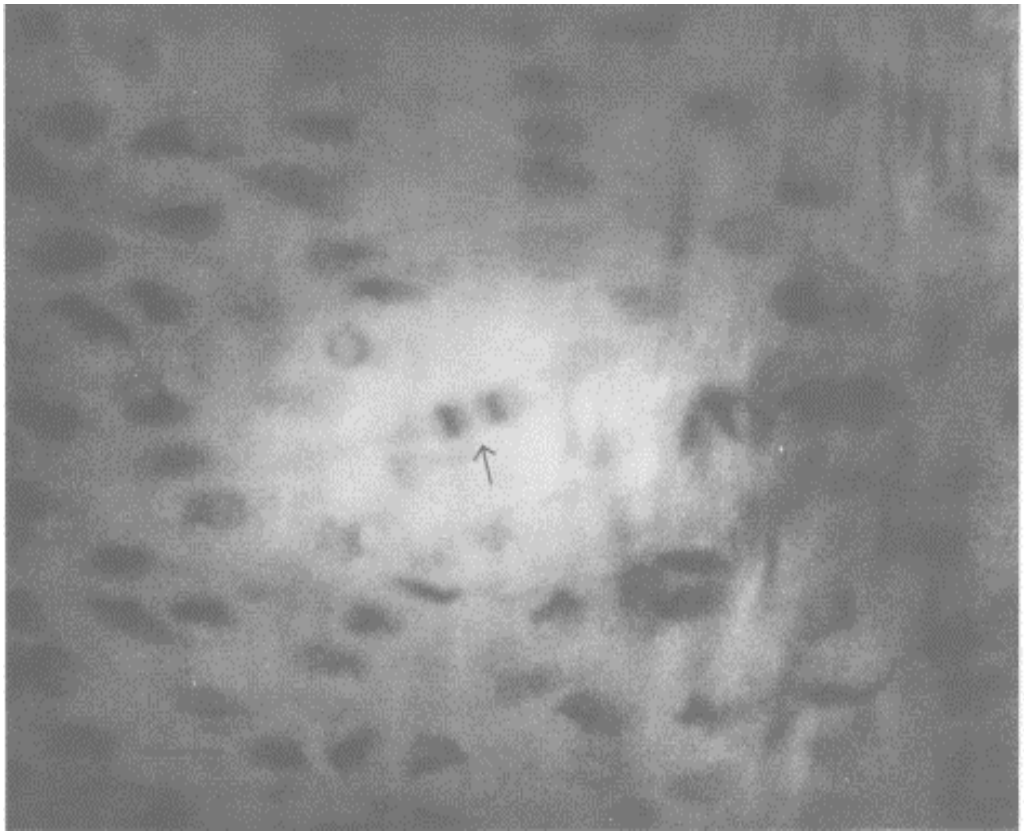

Figure 2. An Evans blue albumin leaky spot with a dividing endothelial cell (arrow) comparing with normal endothelial cells (dark area). ({Lin, 1988 #10})

Chapter 2

Ultrastructural studies of the rat aorta, pulmonary artery and inferior vena cava with orcein and ruthenium red

1. Introduction

Atherosclerosis is the leading cause of death in the Western countries. Atherosclerosis appears to begin with the accumulation of extracellular lipoproteins in the artery wall and develops into lesions (Vander 2001). This accumulation, associated with high plasma low-density lipoprotein (LDL) concentrations, reduces the cross section of blood flow and can lead to deadly consequence. It is thus critical to understand early lesion formation ((Ross 1986), (Steinberg 1983)).

In humans, large, high-pressure, thick-walled arteries such as the aorta are the primary target of disease, unlike the lower-pressure pulmonary artery (PA) and the even lower-pressure veins. However, the PA can also develop atherosclerosis under pulmonary hypertension (Duff 1951). Schwenke has reported that normal rabbit PA develops atherosclerosis as avidly as the rabbit aorta (Schwenke 1997). When veins are placed in arterial condition, i.e., high transmural pressures, as in coronary bypass procedures, atherosclerosis often develops rapidly even as the vessel remodels (Lever 1996). The saphenous vein is often used in the bypass surgery. After 6 to 12 years, 71% of the vein grafts develop atherosclerosis whose structures resemble the arterial fatty streaks (Berceli 1991).

Much is known about the structure and transport properties of the aorta. It consists of a monolayer of endothelial cells, a subendothelial intima comprised mainly of extracellular matrix (proteoglycans and collagen fibers), an internal elastic laminar (IEL) with fenestrae ~2.0 μm apart (Huang 1998) and a tunica of media. The media, a repeated structure mainly of elastin, smooth muscle cells (SMC) and extracellular matrix, comprises ~99% of the total healthy wall thickness.

Large tracers such as LDL (~22nm) or even, in short circulation times (<~5 min), horseradish peroxidase (HRP, ~5 nm, (Chen 1995)), cross the endothelium focally and not uniformly (Stemerman 1986). The subsequent growth of a leakage spot with tracer circulation time is initially very rapid, quickly reaching a large size and seeming to level off in on the order of 4 min (Chuang 1990). Electron micrographs of transverse sections of the aorta after 5 min HRP circulation show that the HRP reaction product localizes overwhelmingly in the region between the endothelium and the IEL ((Huang 1992), (Chen 1995)) These experiments suggested there was a very thin intima space between the endothelium and IEL comprised of extracellular matrix, with a thickness of 100-500nm (Huang 1998), consisting less than 1% of the total aortic wall. However, one cannot neglect this thin layer. Huang *et al*.'s (Huang 1994) two-dimensional convection/diffusion tracer transport model demonstrated that including this layer and its transport properties in detail was necessary to explain the very rapid spot growth. The structure of the intimal matrix, as determined from Frank and Fogelman's (Frank 1989) ultra rapid freezing, rotary shadow freeze-etchings, turned out to be significantly sparser than the media. It thus offered much less resistance to a spreading flow in the intima near an endothelial leak, thereby accounting for the large spots.

This sparse matrix also is susceptible to compression under pressure loading, which can explain the pressure-dependence of the hydraulic conductivity Lp ((Baldwin 1993), (Huang 1997)). The total Lp of the aorta has a high value at low transmural pressure. Upon increasing the pressure, the Lp drops quickly and then remains flat. Endothelial denudation yields a higher, value of Lp that is independent of the transmural pressure. Huang *et al*, (Huang 1997) proposed a theoretical model to explain these results based on the idea that this porous intima was easily compressed under pressure loading. At low pressure, the intima is uncompressed and its Lp is large. Upon increasing the pressure, the intima, unlike the dense media, compresses, increasing the intima matrix density, and more importantly, causing the endothelium to block some IEL fenestrae, thereby lowering Lp. The stiff collagen in the intima prevents it from further compression and the resistance becomes pressure independent. Deendothelialization destroys the intima and Lp is larger, but independent of the pressure (Huang 1997).

The intima consists mainly of three elements, proteoglycan, collage and elastin (Frank 1989) and proteoglycan staining is used to identify the intima. Ruthenium red (RR) is a common dye used to identify the proteoglycan in the blood vessel. It reacts with glycosaminoglycans and produces electron-dense precipitates (Luft 1971a). Gerrity *et al*. (Gerrity 1977) used RR staining with transmission electron microscopy to identify the region of the proteoglycan staining in the pig aorta. Wight & Ross (Wight 1975) carried out light and electron microscopic studies on the pigtail monkey aorta. The RR granules were found within the basement membrane beneath the endothelium and surrounded the SMCs. Lark *et al*.'s (Lark 1988) immunolocalization study with monoclonal antibodies revealed that the intima had a vastly different proteoglycan structure than the media of the bovine aorta.

Clearly the aorta's structure and, in particular, its intima, play an important role in macromolecule transport and accumulation that precede atherosclerosis. Here we focus our attention on the atherosclerosis-resistant PA and the disease-immune inferior vena cava (IVC) that are normally exposed to lower transmural pressures, 16 and 5 mmHg, respectively. The IVC has a thinner wall, a larger lumen, less SMCs, and elastin content, much higher indistensibility and much lower in resistance than the arteries (Mountcastle 1968). The vein does not have a complete IEL, and it is tempting to assume it therefore has no subendothelial intima. Below we focus on the wall structures of the PA and the IVC and consider whether their wall structures are consistent with and can explain their different transport properties, which may underlie their different atherosclerotic susceptibilities. We shall, in particular, quantify the elastin content and IEL integrity of each vessel, see whether each has a sub-endothelial intima and investigate and measure its endothelial surface glycocalyx layer.

2. Methods

We examine vessel ultrastructures by sectioning and staining for light microscopy and transmission electron microscopy. All protocols below were IACUC-approved.

2.1. Light and Electron Microscopy

The structural studies of the aorta, PA and IVC using light and electron microscopy each used three male Sprague-Dawley (SD) rats weighing 250-350 g were used to study An overdose of 1% (w/v) pentobarbital sodium (Sigma, MO) (30 mg/kg body weight) sacrificed the rats. The vessels of interest were excised and fixed in 1% then 2% (v/v) glutaraldehyde (Sigma, MO) for 1

hour each. The specimens were post-fixed with 2% (v/v) osmium tetroxide (Ted Pella, CA) for 90 minutes at room temperature.

2.1.1. Light microscopy: The specimens were washed with distilled water and dehydrated by a series of ethanol and propylene oxide. All tissues were embedded with Epon 12 (Ted Pella, CA). Sections with thickness of 100 nm were cut with a glass knife on the MT-1 ultramicrotome ((Huang 1998), (Bozzola 1992)). The sections were adhered to a glass slide with 2% gelatin (Ted Pella, CA), stained with orcein (0.4% (w/v) for the arteries and 1% (w/v) for the vein) (for details see Chapter 3) and examined under the light microscope (Olympus BX51, Japan).

2.1.2. Electron Microscopy: The specimens were enblock stained with 2% (w/v) uranyl acetate (EMS, PA) at 60^{o}C overnight, washed with distilled water and dehydrated by a series of ethanol and propylene oxide. All tissues were embedded with Epon 12 (Ted Pella, CA). We cut pale gold to silver sections (60-70 nm thickness) (Bozzola 1992) with a diamond knife on the LKB III ultramicrotome and stained them with lead citrate for examination under the transmission electron microscope (Zeiss 902, German).

2.2. Ruthenium Red (RR) Staining

The RR staining study used two male SD rats weighing 250 to 350 g. After anesthetizing the rats with 1% pentobarbital sodium, we injected them with 0.5 ml heparin intravenously to prevent blood clotting 30 sec. prior to sacrifice. The rats were sacrificed with 2 ml of 1% glutaraldehyde in 0.1 M sodium cacodylate buffer (pH 7.0, EMS, PA) (Luft 1971a) containing 0.2% (w/v) RR (Sigma, MO) intravenously. We excised the vessels of interest, i.e., the aorta, PA and IVC, fixed them in the same fixative for one hour, and then for another hour in a 2%

glutaraldehyde solution with the same concentration of the RR. We post fixed the specimens with 2% osmium tetroxide in a 0.1 M sodium cacodylate buffer (pH 7.0) with 0.2% RR and used Uranyl acetate (2%) at 60^{o}C overnight to enblock stain. After rinsing the excess staining, we dehydrated the specimens with a series of ethanol and propylene oxide. After infiltration, all tissues were embedded in Epon 12 (Ted Pella, CA). Pale gold and silver sections were cut with a diamond knife on the LKB III ultramicrotome and examined under the transmission electron microscopy (Zeiss 902) without lead citrate staining.

3. Results

3.1. Light Microscopy study

As noted, the rat aorta has an endothelial monolayer, a continuous IEL, and a media. The orcein stain clearly shows the media's IEL and its parallel sheets of elastins (Figure 1a). The spacing of the aorta's elastins is about 11.4±2.7 μm (Chapter 3), comparable to the diameter of the smooth muscle cells (SMC) that, along with collagen fibers and proteoglycans, are between the elastins. The vessel is 145±9.3 μm thick (Chapter 3).

The thick section, low magnification Figure 1b gives an overview of the PA's media. With orcein staining, we can see the continuous IEL and elastin sheets. The elastins appear wavy because the vessel is under zero pressure in the figure. The maximum space between two adjacent elastins is about 14.9±2.9 μm (Chapter 3), as in the aorta, which is about the diameter of a SMC. The PA has a thinner (78.9±3.3 μm, Chapter 3) wall than the aorta. The orcein stain of thick sections of the IVC media reveals that the IVC has a very incomplete IEL and only discreet, barely visible bits of elastin (Figure 1c). The wall is 66.1±4.1 μm (Chapter3).

3.2. RR-free ultrastructure of blood vessels

Figure 2 shows a more detailed and highly magnified electron micrograph of the aortic structure. Its IEL is 4.5±1.6 μm thick and displays SMCs just below it. Notice that the space between the two adjacent elastin of Figure 2 is again the diameter of the SMC. The electron micrograph shows collagen fibers in the subendothelial region.

Figure 3a is an electron micrograph of the PA that exhibits its endothelium, its intima that contains collagen fibers, IEL, and its media that contains repeat structure of elastin and SMCs. The PA and the aorta clearly have similar structures, but the PA appears to have thinner elastins (3.2±0.7 μm) than the aorta. The PA's SMCs again have a rough diameter of 10 μm that is consistent with the light micrograph. Figure 3b shows the normal endothelial cell junction. The arrow points to the inter-endothelial cell tight junction.

The micrograph in Figure 4 reveals that the IVC has an endothelial monolayer, an abundance of collage fibers and far fewer SMCs than the arteries. There is a thin layer of extracellular matrix that contains collage fibers between the endothelium and start of the SMCs. Since the IVC has a very incomplete IEL, the boundary of the intima is not well defined as in the arteries.

3.3. RR-stain of the proteoglycan

With the RR staining, the aortic endothelium shows a rough coating of the glycocalyx at both its abluminal and luminal sides (Figure 5a), the former being its intima (~200 nm). The

fenestra of the IEL shown contains collagen fibers and granules of the RR staining similar to the intima, indicating that the fenestra also contains proteoglycans (Figure 5b).

Figures 6 shows intense RR stain of the PA. RR stain again appears on both luminal and abluminal side of the EC (Figure 6a). This corresponds to a rough coating of glycocalyx (383±181 nm thick) at the luminal side and to the intimal proteoglycans (~200nm) on the abluminal side. The fenestrae of the IEL also show ruthenium red staining, again resembling that in the intima (Figure 7b). The collagen fiber appears as a negative staining ((Luft 1971b)) and the space between the fibers shows staining. The endothelial cell junction also shows the rough ruthenium red coating (Figure 7c).

Figure 7 shows the RR stained region between the endothelial cell and a piece of the discontinuous IEL of the IVC, which shows collagen fibers and proteoglycans. The boundary of intima is not nearly as clear as in the aorta or the PA where it is separated from the media by the thick, complete IEL. There is a rough coating of EC at the lumen side. The glycocalyx layer has a thickness of (121±22 nm).

4. Discussion

As the introduction has explained, the loose structure of the subendothelial intima matrix relative to the dense structure of the media, and the existence of a barrier IEL play a major role in dictating the overall transmural convective flow and associated macromolecular transport in the large arteries. In particular, it caused water to sweep tracer that crossed the endothelium focally in a direction parallel, rather than normal, to the endothelium in the intima, thereby generating rapid tracer spot growth, before seeping into the denser media. The two-dimension

convection/diffusion model (Huang 1994) could account for this growth only by including this density/porosity mismatch. We shall now see which structural features carry over to the PA and IVC and what this may mean for macromolecular transport into their walls.

4.1. The ultrastructures of the blood vessels and their effects on transmural transport processes

4.1.1. PA: The PA has a physiological pressure of 16 mmHg. Our light microscopy studies show a continuous IEL and parallel subsequent elastin layers in both the aorta and the PA (Figures 1). The PA has a thinner wall (78.9±3.3 μm) than the aorta (145±9.3 μm, Chapter 3). The IEL of the PA (3.2±0.7 μm) is thinner than the aorta (4.5±1.6 μm). The electron micrographs show that both vessels have continuous endothelium and IEL (Figures 2 & 3a). Each vessel has a thin, proteoglycan-filled space between its endothelium and IEL. The media of the two vessels has a repeat structure of elastin sheets and SMCs.

Proteoglycans and collagen are the two main constituents of the aorta's subendothelial intima, and the IEL (elastin) denotes its lower boundary (Frank 1989). Intimal collagen is visible without RR staining in both arteries' intimas, Figure 5a's RR stain shows the proteoglycan content of the aortic subendothelial intima and is consistent with Wight and Ross (Wight 1975). The same stain appears in the same subendothelial space of the PA (Figure 6a), consistent with the existence of a similar subendothelial intima in the PA. Recall the porosity mismatch of the aortic intima and media causes the large and fast growth of the tracer spot sizes ((Chuang 1990), (Huang 1994)). This similarity suggests it may be reasonable to assume that this thin intima matrix of the PA also has a loose structure. Moreover, Figures 5b & 6b show very similar structures for the IEL fenestra in the aorta and the PA. Since the matrix of the IEL fenestra of the

aorta is similar to its intima matrix (Lark 1988), it is reasonable to assume that the fenestral pore of the PA also has a similar matrix to its intima. We therefore argue that the structure of the PA is sufficiently similar to that of the aorta to warrant postulating a transport model for this tissue that is similar to that of the aorta, albeit with different parameters. (For example, the hydraulic conductivity in the PA ($2.0\pm0.23\text{x}10^{-7}$ cm/s/mmHg) is larger than that of the aorta ($2.79\pm0.72\text{x}10^{-8}$ cm/s/mmHg). As such, one would expect a qualitatively, although not necessarily quantitatively, similar transport picture, with convective tracer spreading parallel to the endothelium in the PA's intima.

To be specific, recall that the intima/media density/porosity mismatch, leading to a large mismatch in flow resistances, was crucial in explaining the rapid growth of localized tracer spots ((Chuang 1990), (Huang 1994)). Moreover, the sparseness of the aortic intima matrix led to a theory based on the hypothesis, later confirmed in experiment ((Huang 1998)) that the intima compresses under pressure loading that accounts for the observed variation in Lp with transmural pressure and with endothelial denudation. The structural similarities of the two arteries may suggest that these aspects carry over to the PA.

First, we have studied the growth of HRP spots in the PA as a function of circulation time (Chapter 4). We found that, despite the much lower transmural pressure across the PA's wall, the spot sizes as a function of HRP circulation time in the PA were quite similar to those in the aorta. This supports the idea that the PA also has a large density/porosity mismatch, leading to a flow resistance mismatch, between the intima and the media. Second, our Lp measurements of the intact PA wall (Chapter 3) show it to be 5 times larger than that of the aorta. This is consistent with its thinner elastin and thinner overall wall that has fewer layers providing less flow

resistance. Third, interestingly, even though aorta's and the PA's Lp's have different magnitudes, the trends for Lp as a function of transmural pressure and of endothelial denudation are qualitatively (not quantitatively similar) (Chapter 3). This supports the notion that the PA's intima may also be compressible under transmural pressure load. Thus, positing a transport theory with at thin, porous, compressible intima for the PA that is similar to the existing theory for the aorta seems very reasonable. Naturally, only a comparison of the quantitative results of such a theory with experiments can be definitive, and this is beyond the scope of this paper.

RR is intensely reactive with certain lipids particularly the acidic phospholipids (Luft 1971a). The PA's normal inter-endothelial cell junctions appear clearly outlined without RR stain in the EM (Figure 3b). Nevertheless, Figure 6c shows it to be mostly filled with the electron dense RR product stain. Judging from the nuclei, these two adjacent cells appear to be normal endothelial cells. This indicates that this cellular junction is likely loaded with proteoglycan matrix that can increase the water flow resistance through the junction. These proteoglycans may also serve as a sieve for macromolecules trying to pass through the cellular junction.

4.1.2. IVC: The physiological pressure of the IVC is much lower (5 mmHg) than either the PA or the aortic pressure (100 mmHg) and, as such, it is no surprise that the IVC's wall has a very different structure than the arteries. The light micrograph (Figure 1c) shows that the IVC has an incomplete IEL and only sparse, discontinuous elastins, rather than continuous sheets. The spacing between two adjacent elastin bits is much larger than that in the aorta. The higher magnification electron micrograph shows the IVC structure in more detailed (Figure 9). It has a monolayer of the endothelium, scattered SMCs and a much larger amount of collagen fibers in the venous media than the in the tunica media of the aorta and the PA (Figures 2 & 3a). The flow

resistance across the vein's wall has proven to be far less than across the aorta's (Chapter 3), and these figures allow us to infer that its thin vessel wall and near absence of media elastin layers, in addition to its higher porosity (Lever 1990) are the reason.

One might suspect that the IVC has no intima because of its lack of a complete IEL to separate it from the media. However, the RR stain shows the accumulation of RR reaction product granules that indicate a high concentration of proteoglycans beneath the basal membrane of the IVC endothelial cells (Figure 7). Since this RR staining resembles the staining of the aorta and PA intimas, one may reason that the IVC has an intima matrix adjacent to its endothelium similar to the aorta, even though its boundary is not as nearly clearly due to the absence of a complete IEL. This similarity to the aorta and PA leads one to also suspect a mismatch in IVC intima/media porosity. The IVC's very different wall structure from that of the arteries and its absence of an IEL suggests that its transmural water and macromolecular transport may be quite different from the analogous processes in the arteries.

The indications here of a thin, porous IVC intima suggest that there could be significant tracer spread in the subendothelial IVC intima. On the other hand, the small pressure drop supplies little driving force for such a flow. Moreover, since it is the mismatch in the intima/media porosities and not the absolute intima porosity that results in the rapid intimal spread of tracer in the model of the aorta's transport, a more porous media would lower this mismatch and decrease spot growth. We have measured the growth of HRP tracer spots in the IVC as a function of circulation time (Chapter 4) and found spots that are initially much larger (see Chapter 4 for explanation), but that grow much more slowly than those in the arteries. This is consistent with the IVC wall transport being qualitatively different from that in the arteries.

Since the IVC has only a very sparse and discontinuous IEL, it cannot constitute a significant water barrier. This and its much thinner wall and apparently much less dense media should contribute to a much lower hydraulic resistance. Indeed, our measurements of Lp experiment, the vein has by far the largest Lp of these three vessels (Chapter 3), both with ($6.01\pm1.50\times10^{-7}$ cm/s/mmHg, mean±SD) and without ($25.44\pm4.90\times10^{-7}$ cm/s/mmHg) intact endothelium (values at 10 mmHg). Compare these with the pulmonary artery Lp ($2.34\pm0.27\times10^{-7}$ cm/s/mmHg with endothelium, and $2.73\pm0.57\times10^{-7}$ cm/s/mmHg without endothelium, at 10 mmHg) and the aorta Lp ($2.79\pm0.72\times10^{-8}$ cm/s/mmHg with endothelium, $4.89\pm1.01\times10^{-8}$ cm/s/mmHg without endothelium, at 100 mmHg). Finally, Lp of the IVC as a function of transmural pressure and of endothelial denudation seems to follow similar qualitative, although very different quantitative, trends to the arteries. The initial drop in Lp with increasing transmural pressure appears to be present in the IVC as well, being although of slightly lower magnitude (24% IVC, 42% PA and 40% aorta) and statistical significance. This may be consistent with the IVC's intima still being compressible under transmural pressure loading, but since the vein has only a sparse IEL, IEL fenestra blocking cannot be a significant factor. In addition, if the vein's media is indeed much less dense than the arteries' media, then it may also exhibit some compressibility which may also contribute to this initial drop in Lp with pressure.

Figures 5, 6, and 7 show the RR coating of endothelium's luminal side, meaning it has a glycocalyx layer, of thickness 121±22 nm. The glycocalyx serve as a macromolecular sieve (Hu 2000). Unfortunately, the thickness of endothelial glycocalyx layers in general is still in dispute. The rabbit carotid artery endothelium has a glycocalyx thickness of 81±2 nm (Haldenby 1994). In the hamster cremaster muscle capillary, the glycocalyx is about 400 to 500 nm thick (Vink

1996). Other evidence suggests the glycocalyx might be collapsed by the dehydration step of the electron microscopic preparation (Silberberg 1990), and therefore EM measurements of its thickness may not represent its true *in vivo* extent and density.

5. Summary

The goal of this paper has been to study and compare the wall structure of three vessels representing atherosclerosis-prone (aorta), usually resistant (pulmonary artery) and immune (inferior vena cava) vessels. We have used light microscopy with elastin-specific orcein stain and TEM both with and without the proteoglycan-marking dye Ruthenium Red. The results show that the aorta and the PA have similar structures of endothelial monolayers, thin, proteoglcan and collagen filled (and likely very porous and therefore compressible) subendothelial intimas, continuous IELs and thick, dense media comprised of repeated, continuous sheets of elastin separated by SMCs and proteoglycans. The intima is the LDL accumulation site of the aorta (Frank 1989). The proteoglycan has been implicated in early LDL accumulation in the artery wall and in subsequent calcification (Wight 1987). These results are consistent with measurements reported elsewhere of similar tracer spot growth with tracer circulation time and of similar trends in Lp as a function of transmural pressure and of endothelial denudation in these two vessels. In contrast, the IVC has a very incomplete IEL and only sparse bits, rather than continuous sheets, of elastin in its media. Yet it appears to still have an intima that is similar to the arteries, despite a lack of an IEL Its media also appears to be significantly less dense than the arteries' media. This consistent with the much slower HRP spot growth and much larger Lp of the IVC, and suggests a different transport picture in the vein from that in the arteries.

Ruthenium Red is a general dye for proteoglycans, but it is unable to distinguish the detailed compositions of proteoglycans e.g., hyaluronic acid, keratan sulfate, heparin and heparan sulfate, dermatan sulfate or chondroitin sulfate. The detailed composition, accessible using monoclonal antibodies (Lark 1988), can provide information relevant for investigating the binding mechanism of LDL. For example, Iverius has demonstrated that dermatan sulfate was the greatest binding affinity of all the proteoglycan tested for LDL (Iverius 1972). For definitive studies of intimal porosity, ultra-rapid freezing/rotary shadow etching (Frank 1989) has proven to be an invaluable tool.

This results above constitute the first step in constructing models for transport in these vessel walls and, potentially, to understanding the basis for their very different susceptibilities to atherosclerosis.

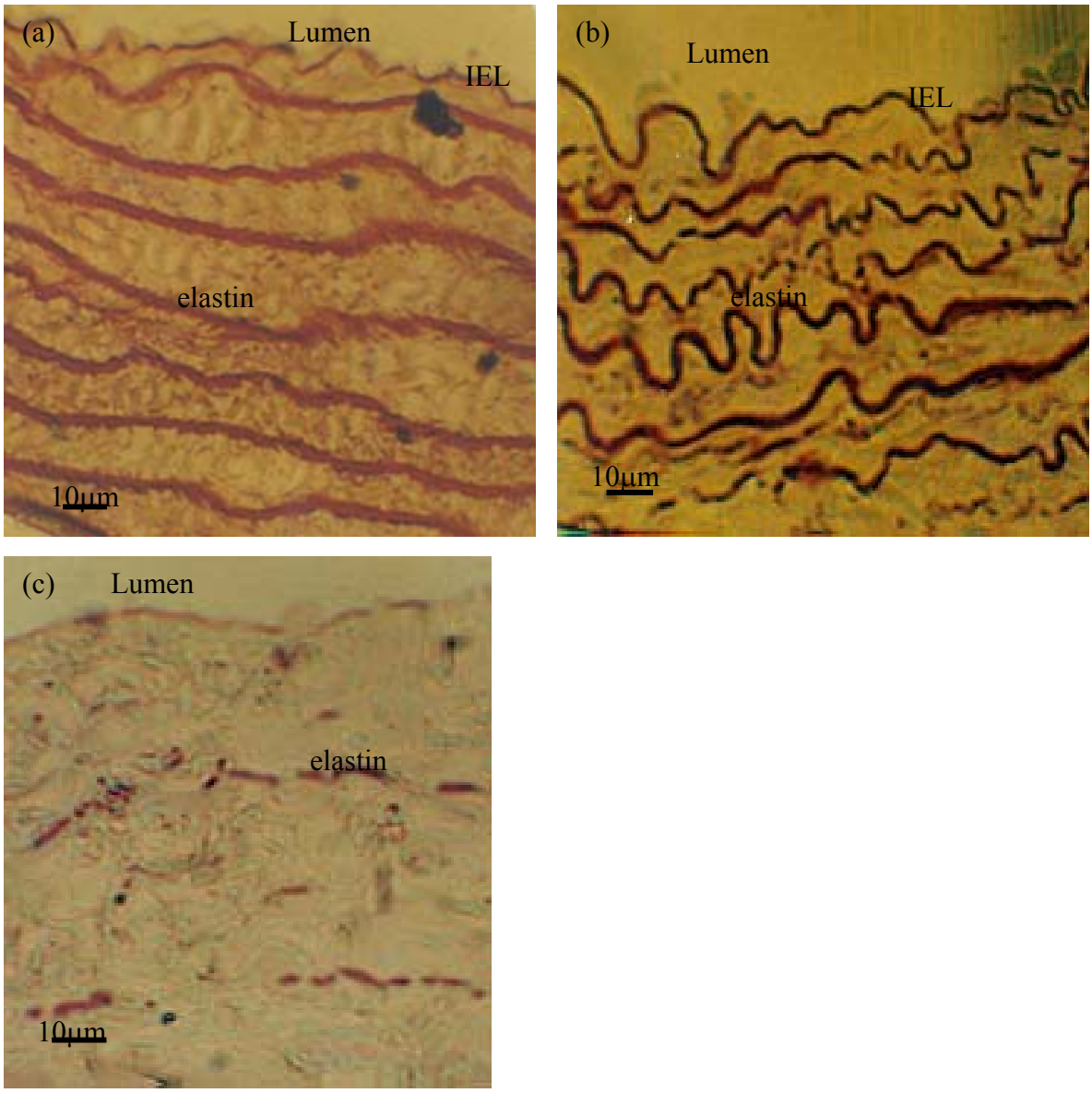

Figure 1. Orcein stain of thick section (100 nm) viewed by light microscopy. (a) The aortic media stain with 0.4% orcein with a wall thickness of 145±9.7μm at zero pressure (Lp paper). It has a complete IEL (4.6±1.6 μm) and continuous layers of elastin (red lines) (b) The PA media stained with 0.4% orcein has a wall thickness of 78.9±3.3 μm (mean± SD) at zero pressure. It has a complete internal elastic lamina (IEL) (3.2±0.7 μm thick) and continuous wavy layers of elastin (dark red lines). (c) The inferior vena cava has a wall thickness of 66.1±4.1 μm at zero pressure. It has an incomplete IEL (the broken red line just below the lumen) and only sparse bits of elastin throughout (1.0% orcein stain). . Bar represents 10 μm.

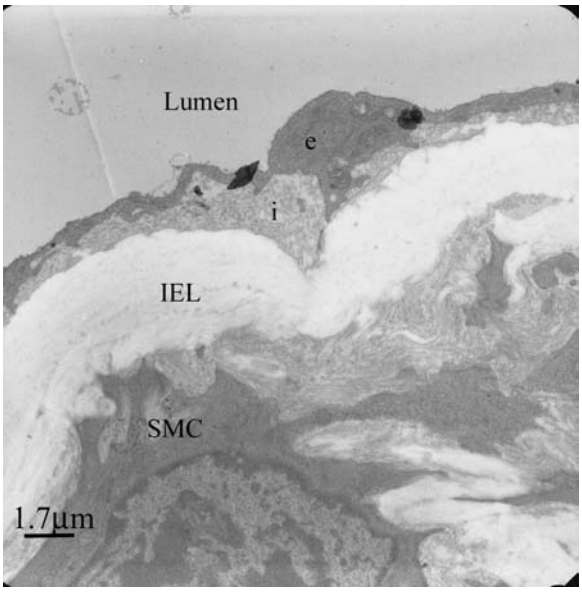

Figure 2. Electron microscopy of the rat aortic wall. The lumen side is lined with monolayer of endothelium; intima separates the endothelium and IEL; beneath is SMC of the media (e: endothelium; IEL: internal elastic lamina, SMC: smooth muscle cell).

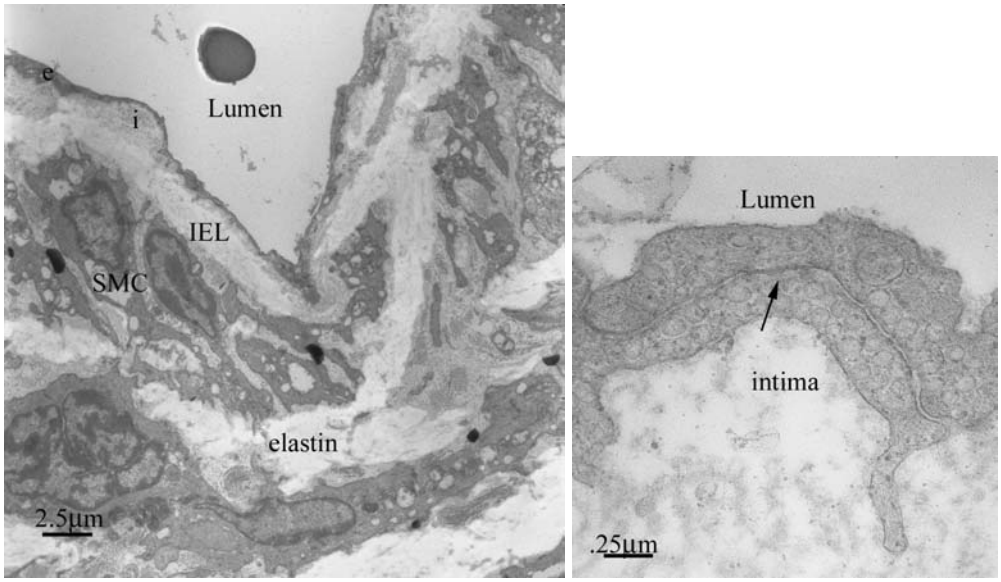

Figure 3. Electron microscopy of rat PA wall (e: endothelium; IEL: internal elastic lamina, SMC: smooth muscle cell). (a) lumenal side is lined with a monolayer of endothelium; intima separates the endothelium and IEL; beneath is the tunica media with SMC and elastin. (e: endothelial cell; IEL: internal elastic lamina; SMC: smooth muscle cell) (b) Normal endothelial cell junction (arrow pointing the tight junction)

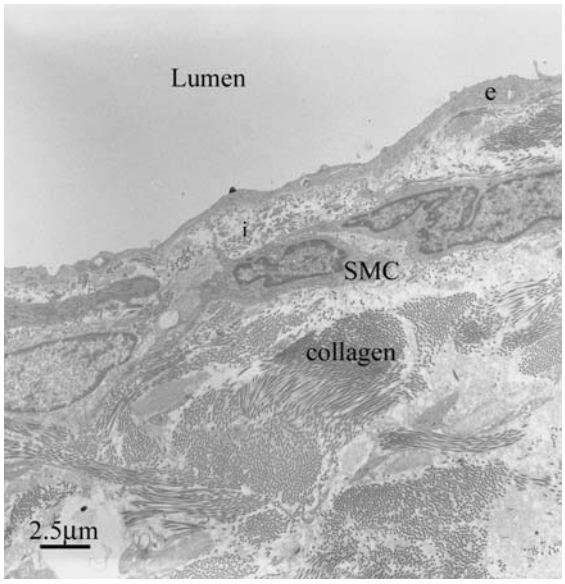

Figure 4. Electron microscopy of the IVC (e: endothelium; IEL: internal elastic lamina, SMC: smooth muscle cell). The luminal side is covered with a monolayer of endothelia. The media contains SMC and collagen fibers (cross-section) with few elastic fibers.

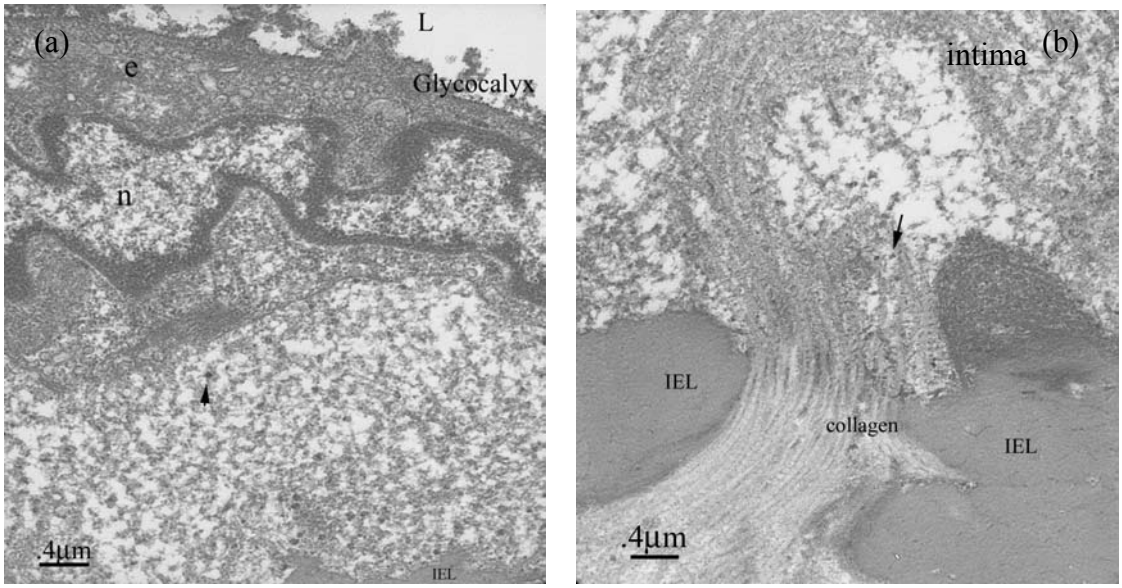

Figure 5a, b. Electron microscopy of rat aorta with Ruthenium Red stain. (a)The granule of the proteoglycan appears in the intimal region (arrow). (b) The granule appears in the fenastra (arrow). (L: Lumen; e: endothelial cell; n: nuclear; IEL: internal elastic laminae)

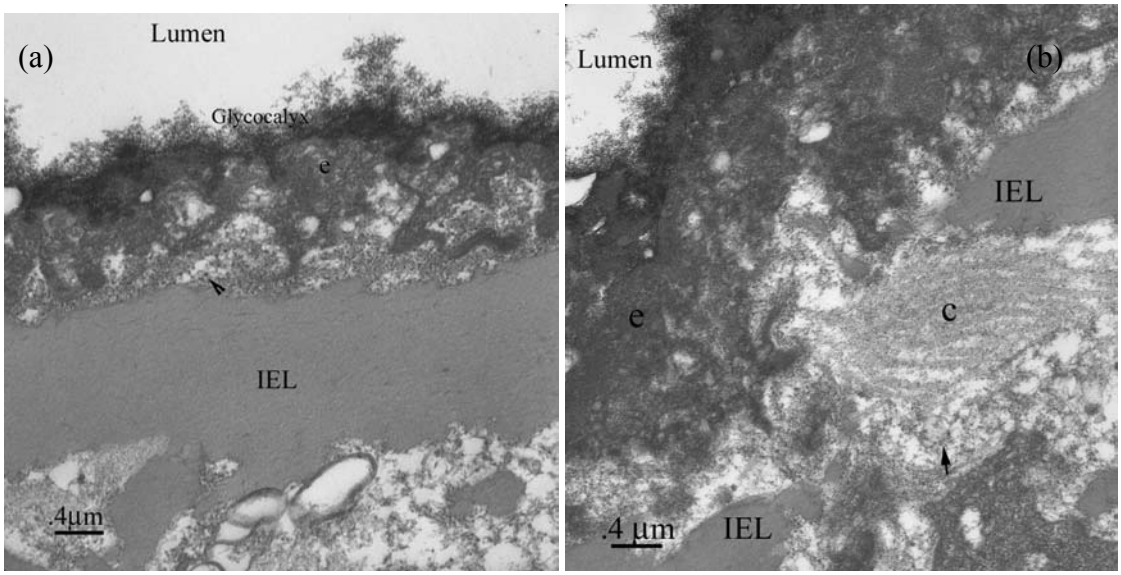

Figure 6. Electron microscopy of rat pulmonary artery with Ruthenium Red stain. (a) The granule of the stain shows in the intima region (arrow). (b) the stain also shows in the fenestra (arrow) (e: endothelial cell; IEL: internal elastic laminae; c: collagen)

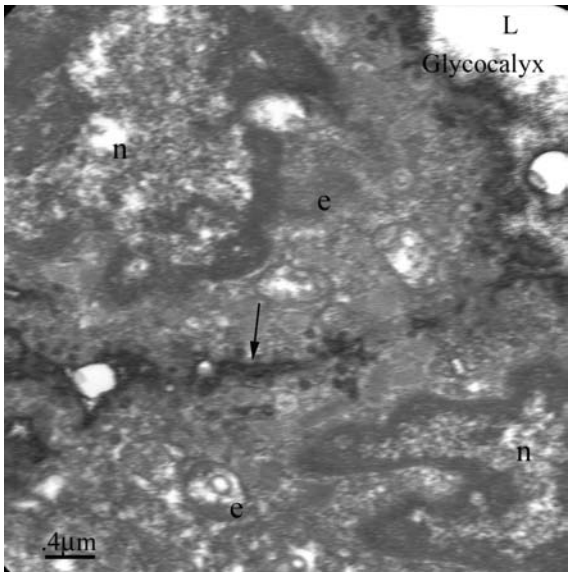

Figure 6c. Electron microscopy of rat pulmonary artery with Ruthenium Red staining. The rough coating of the stain shows in cell junction of two endothelial cells (arrow). The two nuclei suggest the two normal cells (e: endothelial cell; n: nuclear; L: lumen).

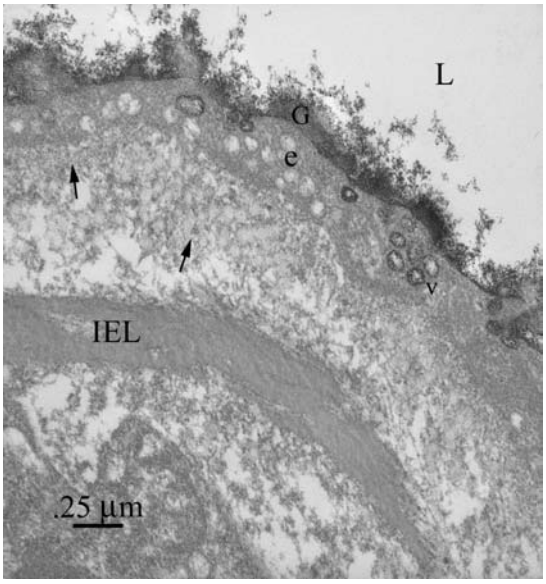

Figure 7. Electron microscopy of rat inferior vena cava with ruthenium red stain. The RR granule of the proteoglycan appears in the intimal region (arrows). (L: lumen; e: endothelial cell; IEL: internal elastic lamina; v: vesicle; G: glycocalyx).

Chapter 3

The hydraulic conductivities of the aorta, pulmonary artery and inferior vena cava with intact and denuded endothelia

1. Introduction

Atherosclerosis is a disease that develops in large arteries and valves ((Wilson 1991), (Ross 1986)). It begins with low-density lipoprotein (LDL) cholesterol delivery into the vessel wall and its accumulation there. Blood-borne monocytes enter the arterial intima in regions with high sub-endothelial lipid concentration, becoming macrophages that attempt to scavenge the extracellular cholesterol (Vander 2001). When overwhelmed, they form the foam cells. Lipid and necrotic cells accumulate to comprise the earliest lesions ((Steinberg 1983), (Simionescu 1986)). Such lesions mature and thicken the arterial wall, which, eventually can compromise the cross section for blood flow and increase the potential of a blockage (Vander 2001), rupture or clot formation.

Atherosclerosis normally occurs in the large arteries and/or in the aortic valve but not in the pulmonary artery (PA) or in veins. In humans, the pulmonary artery is vulnerable only in the presence of pulmonary hypertension (Duff 1951). (Curiously, some data suggest that rabbit pulmonary artery appears to be similar to rabbit aorta in its proclivity toward developing atherosclerosis (Schwenke 1997) and a comparison of the PA of the rabbit with that of an animal without this unusual susceptibility is worthy of study.) Veins normally do not develop atherosclerosis. However, when veins, such as the saphenous vein, which is frequently used in coronary bypass procedures, are placed in arterial conditions, i.e., high pressure, atherosclerosis often develops (Lever 1996) along with vessel remodeling. After 6 to 12 years, 71% of such vein

grafts develop atherosclerosis and their structures resemble arterial fatty streaks ((Berceli 1991)). If the triggering events for the disease are lipid transport across the vessel endothelium and its sub-endothelial accumulation, it is natural to wonder if these processes are radically different in resistant and disease-prone vessels. One of the first questions that one needs to ask in order to develop an understanding of the mass transport in these vessels is whether such transport is diffusion-driven, convection-driven or a combination of the two. In previous mass transport studies of the aorta, rats were injected with a macromolecular tracer, such as horseradish peroxidase (HRP), of relatively large molecular size, and were sacrificed after different circulation times ((Stemerman 1986), (Chuang 1990)). By examining the animals' aortas *en face*, the HRP was found to traverse the endothelium in rare localized spots, rather than uniformly. Measuring the sizes of the HRP spots as a function of tracer circulation time, these investigators found tracer spot growth that was sufficiently fast as to be consistent only with a convection – dominated transport mechanism; for any reasonable value of the diffusivity, these data were not consistent with a diffusion-dominated process. The same was true of Tompkins *et al*'s (Tompkins 1989b) ^{125}I-LDL tracer spots, localized just below the endothelium, in squirrel monkey. Huang *et al*. (Huang 1994) and Yuan *et al*. (Yuan 1991) mathematically modeled how macromolecules such as HRP, albumin and LDL leak through the rare, widened inter-endothelial junctions, whereas water passes through all junctions. Huang *et al*. (Huang 1994) developed a new convection-diffusion transport model that divided the subendothelial space into the subendothelial intima and media and, with strong ultrastructural evidence, postulated that the intima was the much more porous; it thus offered a much smaller hydrodynamic resistance, than the media. The resulting convection-dominated transport theory predicted the observed growth rate of HRP tracer spots. Thus an understanding of water flow in the artery wall is central.

Again, if lipid transport and accumulation is indeed the key to triggering early atherosclerosis, a detailed understanding of the relevant transport process in each vessel might be able to explain the differences in vessel susceptibilities. This paper asks, just how similar are the water filtration processes that drive convective lipid transport in the aorta to those in the PA and the inferior vena cava (IVC)? Our initial hypothesis is that they are different and correlate with the differences in vessel susceptibilities. The PA is normally exposed to a low transmural pressure (16 mmHg) and has lower blood oxygen (Po_2=40 mmHg) than the aorta (Po_2=100 mmHg). The normal PA has a thinner wall (78.9±3.3μm in rat; see Results) than the aorta (146 μm in rat; see Results). The basic structure of the PA is similar to the aorta, containing a monolayer of endothelial cells with an associated intima and tunica of media, which has a repeated structure of elastin and smooth muscle cells (SMC). These two layers are separated by an internal elastic lamina (IEL) with numerous fenestrae. The IVC experiences an even lower transmural pressure (5 mmHg) than the PA, and its blood has the same oxygen tension as the PA. Since the vein is exposed to very low pressures, it has a thinner wall than the arteries (Lever 1990) - about 66.1±4.1 μm for rat vena cava (see Results). Its wall structure is different from that of the arteries. It has a larger lumen, less SMCs, a lower elastin content, and a much higher distensibility, thereby providing a much lower hydraulic resistance than arterial walls (Mountcastle 1968).

Given these differences among vessels, it is important to assess whether convection plays as strong a role in the mass transport in these lower-pressure vessels as in the large arteries. Transmural pressure differences are the driving force for convection, and the hydraulic conductivity (Lp) is the critical transport parameter that provides a relationship between the water flux and the pressure driving force. If the *combination* of the measured Lp and the

transmural pressure – *not* Lp alone - for different vessels and conditions leads to transmural flows whose magnitudes correlate with vessel susceptibility to atherosclerosis, this would lend support to the proposition that convective lipid transport is a leading determining factor in the prelesion triggering events. We have already noted the lower driving pressures in the PA and the IVC and now need to measure their Lps to assess the roles of convection in these vessels. In particular, if the relation between the very low driving force and the associated specific flow resistance (the inverse of Lp used in Tedgui and Lever ((Tedgui 1984), (Vargas 1986)) or the vessel flow resistance (1/(LpAS), where AS is the vessel's outer surface area) in the vein leads to negligible transmural water flow, diffusion likely dominates macromolecule mass transport over convection and convection may not be important in these vessels.

Yamartino *et al*. (Yamartino 1974) used a slab of rabbit aorta stuck to a rigid porous background, and found a low value of Lp. Vargas *et al*. (Vargas 1979) maintained the rabbit aorta's cylindrical shape, and used a weighing method to measure the transmural flow rate. Tedgui and Lever (Tedgui 1984) calculated the transmural flow at 70 mmHg and 180 mmHg on the same vessel by measuring the velocity of an air bubble in a horizontal catheter connecting the pressurized water source with the rabbit's isolated vessel's lumen. Baldwin and Wilson (Baldwin 1993) extended the pressure range of this experiment on rabbit aorta from 50 mmHg to 150 mmHg at 25 mmHg increments. To date, no one appears to have applied this technique to vessels other than the aorta. Both groups found a high value of Lp at low pressure (Baldwin and Wilson's lowest pressure measurement had a uniquely large error bar), which dropped sharply by 44% by 75 mmHg and then remained pressure-independent. This low-pressure high Lp value disappeared upon nitric oxide inhibition (Baldwin 1993). Mechanical endothelial denudation increased Lp significantly and appeared to make it pressure-insensitive. Dhar *et al*. (Dhar 1996),

on the other hand, found that Lp of chemically denuded rabbit aorta decreased with increasing transmural pressure, although they subjected each vessel to only a single pressure. Finally, Tedgui and Lever (Tedgui 1984) used their measurements to infer the Lp of the aortic endothelium and to calculate the percentage of the wall's total resistance to flow due to the endothelium. Tarbell *et al*. (Tarbell 1999), working in cultured bovine aortic endothelial cells, addressed Lp of the endothelium directly. They found Lp underwent a transient increase with sudden pressure change that relaxed in ~1 hr to background.

McCandless *et al*. (McCandless 1991) found a very high value for Lp ($20.1\pm5.2 \times 10^{-5}$ cm/s/mmHg) for cultured sheep pulmonary artery endothelial cells. Their method may have suffered from large leaks of water around the chamber's edges, and this may explain their reported high value. Moreover, measurement on a cultured monolayer only accesses Lp of the endothelium and not of the other components of the wall. Vargas *et al*. (Vargas 1986), using dog vena cava, measured Lp by the volume clamp method. The vessel was hung from a force transducer that was calibrated to measure weight. The volume change of the vessel was constantly monitored. The weight loss was transmitted to a polygraph and a controller; the feedback loop then injected fluid into the vessel lumen to maintain the lumen at constant volume. By the conservation of mass, the rate of the fluid injected into the vessel equaled the rate of fluid loss through the vessel wall.

To explain the behavior of rabbit aortic Lp with transmural pressure and with endothelial denudation, Kim and Tarbell (Kim & Tarbell 1994) developed a theory based on whole wall compaction, while Huang *et al*. (Huang 1997) proposed a new mathematical model that invoked the ultra-high intimal porosity to restrict pressure-compaction to the intima. They predicted that rising pressure compressed the intima, thereby decreasing its void space and increasing its

resistance, and the compressed endothelium could block IEL fenestrae, altering the water flow. At larger transmural pressures the intima is supported by the stiffer collagen and does not compress further, and so Lp becomes insensitive to pressure. Huang *et al*. (Huang 1998) experimentally confirmed this predicted intimal compaction behavior with increasing transmural pressure on the rat. This mechanism is also consistent with the disappearance of the high Lp value at 50 mmHg (and no change at other pressures) upon nitric oxide inhibition. With NO, the wall is relaxed, and a low transmural pressure pushes the endothelium against a media that has some give, and thus does not completely compress the intima; removal of NO stiffens the wall and fosters complete compression at the lower transmural pressure of 50 mmHg. Vessel-vessel variation in medial give might then account for the large error bars for the intact vessel at this apparent borderline pressure.

In this study, we examine rat aorta, PA and IVC. We measure Lp as a function of transmural pressure for the same vessel, both with and without an intact endothelium, to investigate the extent of similarities or differences among the vessels. Of primary importance is whether transmural convection has the potential to transport similar amounts of macromolecules into the walls of the PA and the IVC as it does into the aorta. The detailed measurements of Lp for the aorta will also both complete a consistent set of data, all taken on the rat, for Huang *et al*'s model and demonstrate whether the observed behavior of Lp with pressure and endothelial denudation observed in rabbit aorta, and attributed to intimal compression, also occurs in rat aorta. Note that although rats do not naturally become atherosclerotic due to low blood cholesterol, rats can develop atherosclerosis when fed an atherogenic diet (Vlad 1995).

2. Methods

2.1 Experimental Setup and Measurement Technique

A mercury sphygmomanometer controls the pressure of a large volume air reservoir that is connected to a solution reservoir. A three-way connector connects this solution reservoir, a 1-ml syringe and a horizontal, 120 mm Tygon catheter of inner diameter 0.5 mm mounted on a finely graduated ruler. The catheter is inserted into the isolated aorta that is closed off and immersed in a bathing solution (See Figure 1a). The syringe injects an air bubble into the catheter and, once its velocity reaches steady state (~30 min), its position is recorded 5-6 times at 5 min intervals. Solution incompressibility implies that the volume (bubble velocity times catheter cross section) that it traces out per unit time equals the flow rate through the vessel wall. All chemicals are obtained from Sigma (St. Louis, MO) unless otherwise stated. The solution entering the vessel contains 4% (w/v) bovine serum albumin (BSA, fraction V, Fisher Scientific) in phosphate buffered saline (PBS) solution, 10^{-3}M of sodium nitrate ($NaNO_3$) to reduce smooth muscle cell contraction ((Baldwin 1983), (Baldwin 1993)) and 0.03% (w/v) trypan blue, which serves two purposes: Blue dye appearing in the adventitia means the vessel has a leak (the dye's intensity relative to the clear bathing solution made even minute leaks easily visible), which we try to secure with string. If this is not successful, we discard vessel. Also trypan blue is a vital stain that penetrates the membrane of non-viable cells (Tedgui 1984), (Baldwin 1993). The bathing solution is identical, except for the absence of trypan blue, so as to keep the osmotic pressures on both sides of the wall the same. From its molecular size (Inglesby 2002), we estimate Trypan Blue's hydrodynamic radius to be ~1 nm and thus its reflection coefficient as ~0.0.64 (Levick 1994), as opposed to albumin's value of 0.8-1.0 ((Karmakar 1994), (Knox 1988)). Thus the dye's contribution to the osmotic pressure is negligible.

As in all previous similar studies ((Tedgui 1984), (Baldwin 1993)), we used mechanical calipers (accurate to ±0.1 mm) to measure diameters and lengths from tie to tie of pressurized, excised vessels. This method has the advantage that it does not destroy the vessel, and thus allows multiple measurements *on the same vessel* at a series of pressures and both with and without endothelium. To assess the accuracy and reliability of this method, we used it to measure the diameters at three different points along the length of two vessels (one aorta at 100 mmHg and one IVC at 60 mmHg), each three times. We then fixed the vessels under pressure, sliced each open along its axis, flattened it on a glass slide, viewed them and took images under the microscope, and measured the distance from edge to edge along its outer surface at thirty points along its length.

All protocols below were IACUC-approved.

2.2 Ttransmural flow rate and vessel dimensions

2.2.1 Aorta: Six healthy male Sprague-Dawley (SD) rats that weigh between 250 and 350 g on a normal diet were used. After anesthesia with 1% pentobarbital sodium (15 mg/500 g rat, i.p.), we injected ~0.5 ml of heparin (1,000 units) intravenously to prevent blood coagulation. A rodent respirator kept the rat ventilated. After opening the chest and carefully dissecting the fat, we exposed the aorta from the rest of the fat and connective tissue and ligated the first three pairs of intercostal arteries. The aorta was cannulated from the distal end and the lumen side was rinsed with the PBS solution described above, pressurized at 100 mmHg, the normal aortic pressure, to prevent vessel collapse. The aorta was ligated at the proximal end and excised. The segment of the aorta was immersed in a solution bath a described above at 37^{o}C. The solution bath was changed every 20 min and air was continuously bubbled through it to keep the vessel oxygenated. We were able to successfully transfer 6 of 8 rat aortas as reported below.

To begin the measurement, an air bubble was introduced into the horizontal catheter at low pressure, and then the pressure was increased to the desired value. The experimental pressures ranged from 60 - 140 mmHg with 20 mmHg increments. At each pressure, we determined the flow rate through the vessel wall by monitoring the movement of the bubble's front meniscus after it became steady, as described. The outer dimensions (length and diameter) of the vessel were measured. The same vessel was deendothelialized by inserting a glass rod with an Epon polymer tip of diameter 2.5 mm and working it back and forth. We recannulated, flushed and tested the vessel for leaks before restarting the measurements at the same pressures done with the endothelium intact. At this point, the excised vessel was outside the rat body for ~10 hours. After finishing the flow rate measurements, the vessel was fixed with 2% glutaraldehyde under pressure, stained with Harris' hematoxylin and examined under the light microscope to ensure that the endothelium had been totally removed. One Lp experiment was performed without $NaNO_3$, both with and without endothelium. The results were within the error band of those with this muscle relaxant.

2.2.2 Pulmonary Artery (PA): We used twelve healthy male Sprague-Dawley (SD) rats weighing 250 to 350 g on a normal diet for this protocol, six for the pressure range 20-100 mmHg and six for the range 10-40 mmHg. We begin with the former. The procedure is similar to that for the aorta. After anesthesia with 1% (w/v) pentobarbital sodium (15 mg/500g rat, i.p.), the femoral vein was cannulated with Tygon tubing and injected with ~0.5 ml of heparin (1,000 units) to prevent blood coagulation. A rodent respirator ventilated the rat during the operation. After opening the chest, we carefully dissected out the fat, exposed the PA from the remaining fat and connective tissue and ligated the left pulmonary branch near the pulmonary bifurcation. We cannulated the main pulmonary trunk through the right ventricle with a Tygon catheter and

washed the lumenal side of the vessel with the reservoir solution containing trypan blue that was pressurized at 20 mmHg to prevent vessel collapse that could damage its endothelium. The animal was sacrificed with an overdose of pentobarbital and the right pulmonary artery was tied near the lung. After the vessel was removed, at which point 1-1.5 hr had elapsed, the balance of the procedure, except the pressure range, was identical to the aorta.

A second set of six rats was used to measure Lp over the pressure range 10 to 40 mmHg. The procedure was identical to that above, except that both, rather than just one, PA branches were taken at the root of the lung.

2.2.3 Inferior Vena Cava (IVC): The procedure for the IVC was also similar to those described above. In brief, ten healthy male Sprague-Dawley (SD) rats, weighing 250 to 350 g, were used. After anesthesia, heparin was introduced intravenously and a rodent respirator attached to ventilate the rat. After opening the chest, we cannulated the vein through the right atrium with a catheter and pressurized the lumen of the vessel using the upstream manometer with the same solution described above at 20 mmHg to prevent vessel collapse. Although 20 mmHg is higher than the vena cava's normal pressure, the vessel's dimensions hardly changed (see Results) from their values at 10 mmHg. The animal was sacrificed and the vessel was tied at the diaphragm, removed and submerged in PBS solution as above. The rest of the procedure was identical to those above, except that the pressure range examined was 10-60 mmHg for the vena cava. Because a number of vessels sprang leaks at 50 –60 mmHg, we succeeded both with and without endothelium in four animals for 10-60 mmHg and two for 10-40 mmHg, and in two with and two without endothelium from 10-40 mmHg. The pressure setup was not stable at lower pressures such as 5 mmHg.

2.3 Structural Study

An overdose of 1% pentobarbital sodium was injected to sacrifice the rat. The blood vessels of interest, i.e., the PA, the IVC and the aorta, were removed and fixed with 1% then 2% (v/v) gluteraldehyde solution for 1 hr each, followed by PBS solution to wash out the fixative. The tissue was post-fixed with 2% (v/v) osmium tetroxide (Ted Pella, CA) for 90 min. After fixation, the tissue was rinsed with distilled water 3 times (about 1 min. each), dehydrated with ethanol in the series 30%, 50%, 75%, 80%, 90%, and 100%, (v/v) and propylene oxide (Ted Pella, CA) and finally, after infiltration, embedded in Epon 12 (Ted Pella, CA).

We sectioned the Epon blocks to a thickness of around 100-500nm (purple reflection ((Bozzola 1992), (Huang 1998)) using a glass knife with an MT-1 ultramicrotome (Dupont) and adhered the sections to a glass slide with 2% (w/v) gelatin (Ted Pella, CA). We then applied orcein stain to specifically highlight the elastic fibers in the vessel walls ((Huang 1998)). The slides were dried and observed under light microscopy. The vessel wall thicknesses were measured by using NIH ImageJ. For the aorta and the PA, which contain large amounts of elastin, we used a 0.4% (w/v) orcein solution (0.4 g, of orcein, dissolved in 100 ml 70% ethanol, with 0.6 ml of concentrated HCl then added), whereas for the IVC, which contains much less elastin, we used a 1% orcein solution.

2.4 Calculations

For the aorta, IVC and the first population of PAs, we assume the vessel is cylindrical, and thus its the outer surface area $AS=\pi(OD)L$, where OD and L are the vessel outer diameter and length, respectively. The second set of extracted PAs included both pulmonary branches, forming a Y-shape with the pulmonary trunk as the base. We calculated the vessel's surface area by breaking it up into four parts. First we calculated the area of each branch, as if the two

branches had met in a V-shape. Each of these areas is the product of the branch cross section's perimeter $\pi(OD)_i$, i=1,2, and the average of the smaller and larger lengths $(l_i+(l_i+\Delta l_i))/2$, i=1,2, from where the two branches would meet in a V to the vessel's far end. To this we add the surface area $\pi(OD)_T l_T$ of the trunk, from its far end to the point where it joins the branches. Finally, since the two branches meet the trunk before actually completing the V-shape, we subtract the area near the tip of the V. We approximate this tip area as that of a cone of base diameter OD equal to that of the trunk (OD_T) and of cone angle □, where □is the half angle of the branch bifurcation. Thus, $AS=\pi(OD)_1(l_1+(l_1+\Delta l_1))/2 +\pi(OD)_2(l_2+(l_2+\Delta l_2))/2 + \pi(OD)_T l_T - \pi(OD_T)^2/(4\sin$□. See Figure 1b for this construction.

The bubble velocity V was determined as V=□/t, where □ is the distance the bubble travels in a time t. Let ID be the inner diameter of the catheter. Since the solution is incompressible, the flow rate Q at steady-state through the vessel wall equals that traced out by the bubble in the tube, i.e., $Q=\pi(ID)^2V/4$. Q=Lp x AS x ΔP, where ΔP is the transmural pressure, allowed us to determine the hydraulic conductivity Lp as function of ΔP. For the intact vessel, it represents $Lp_{overall}$; for the deendothelialized vessels, it represents $Lp_{media+IEL}$. If, as is standard in the field ((Tedgui 1984), (Vargas 1986)), one assumes that Lp adds like linear capacitances in series, one calculates $Lp_{endothelium+intima}$ from $1/Lp_{overall}=1/ Lp_{media+IEL}+1/Lp_{endothelium+intima}$. To calculate the percentage resistance of the endothelium+intima, we take the average intact-vessel hydraulic conductivity for a particular rat at a particular pressure and call it $Lp_{overall}$, do the same for $Lp_{media+IEL}$ and then use this formula to calculate $Lp_{endothelium+intima}$ for that rat at that pressure. The fractional resistance of the endothelium is $(1/<Lp_{endothelium+intima}>) /(1/<Lp_{overall}>)$, where 1/Lp is a resistance and <•>signifies an average over all of the subject rats. As such, the average Lps do not satisfy the defining relation for $Lp_{endothelium+intima}$.

2.5 Statistics

Paired Student's t tests are used to compare Lp with and without endothelium. The same method is used to compare the values at different transmural pressures of each of the Lp, outer diameter and surface area of the vessels, both with and without endothelium. $P<0.05$ was chosen as the criterion for statistical significance. All data are presented as mean±SD.

3. Results

3.1 Accuracy of caliper measurements

The *enface* measurements of the sliced-open aorta (2.61±0.01mm) and IVC (2.88±0.03 mm) were in excellent agreement with the caliper measurements, 2.56±0.02 and 2.87±0.04 mm.

3.2 Structure

The structure of the vessel's wall plays an important role in determining its Lp. Figure 2a shows a cross-section of the aorta stained by orcein, a specific stain that highlights/colors the elastin sheets in the aortic media red. We find the gaps between elastin sheets that contain smooth muscle cells (SMCs) and proteoglycans are ~11.4±2.7 μm apart, roughly the diameter of the SMCs. The aorta has a complete IEL of thickness 4.5±1.6 μm and continuous elastin layers of thickness 5.71± 2.14 μm. Total wall thickness was 145.8±9.3 μm.

Transverse sections of the pulmonary artery (PA) show a large amount of the orcein (Figure 2b). The elastins in the pulmonary arterial media, which have thicknesses of 3.4±1.9 μm, account for a majority of (or for much of) the elasticity of the artery. The largest space between two adjacent elastin layers is 14.9±2.9 μm, which is again roughly the diameter of the SMCs. The elastin and SMCs are the two major components of the media, in addition to proteoglycans and collagen. The wall thickness is about 78.9±3.3 μm at 0 mmHg. The IEL is 3.2±0.7 μm thick.

The inferior vena cava (IVC) is normally under the low physiological pressure of circa 5 mmHg. The structure of the veins (Figure 2c) is quite different from those of the PA and the aorta. The vein has a thinner wall (66.1±4.1 μm at 0 mmHg), a discontinuous IEL, sparse elastin (note the very sparse orcein staining, despite the higher orcein concentration used) and fewer SMCs. Since the IVC wall is only 66.1±4.1 μm and because it contains far less elastin than the PA, we would expect it to present much less resistance to transmural water flow than even the PA.

3.3 Outer diameter and surface area

The aorta expands dynamically with increasing pressure. The outer surface area, normalized by its value at 60mmHg expands fairly linearly by ~42% from 60 to 140 mmHg transmural pressure ($P<0.05$) (Figure 3a). Since the outer diameter of the aorta only expands ~20% from 60 to 140 mmHg ($P<0.05$), the balance of the area expansion is due to the vessel's change in length. Removal of the aortic endothelium does not change these values significantly ($P>0.05$).

The outer diameter of the PA increases fairly linearly by 32.4% from 20 to 100 mmHg ($P<0.05$). (It is not plotted for the Y-shaped vessels.), although the outer diameter varies little between adjacent pressures, e.g., from 80 to 100 mmHg, $P>0.05$. Again, since the length of the vessel also varies with changing transmural pressure, Figure 3b plots both the vessel's absolute diameter and the ratio of its outer surface area AS as a function of transmural pressure compared with its value AS(20) at 20 mmHg. The outer surface area of the PA increases monotonically from 20 to a maximum at 100 mmHg of about 1.65 times AS(20). The surface area increases 71% from 10 to 40 mmHg ($P<0.05$). Both before and after deendothelialization, the outer diameter of the vessel displays a similar increasing trend, but the significance is lower ($P>0.05$)

with deendothelialization. The deendothelialized diameter increases about 26.7% from 20-100 mmHg ($P<0.05$). The difference between the outer surface areas of the vessel with and without its endothelium is within the curves' error bars ($P>0.05$) at each transmural pressure over the entire range 10-100 mmHg and the difference between the two groups of rats is statistically insignificant ($P>0.05$). Since the endothelium comprises a very small fraction of the vessel wall, it is no surprise that endothelial removal has no effect on AS, despite some wall hydration upon endothelial removal.

As noted, limitations in the accuracy of our pressure setup dictated a lowest transmural pressure of only 10 mmHg for the vena cava, rather than its physiological value (5) or less. Figure 3c, for the 4 rats measured over the entire pressure range both with and without endothelium, shows that the outer diameter of the vein monotonically increased 11.3% over its pressure range ($P<0.05$). The outer surface area, relative to its value at 10 mmHg, increased monotonically by only 25% over the pressure range of 10-60 mmHg, but this increase was not significant ($P>0.05$). Endothelial removal changed the measured outer diameters insignificantly ($P>0.05$), even though the curve appears much flatter, having increased only 2.1% over the pressure range ($P<0.05$). The vessel's normalized surface also increased similarly, albeit apparently more slowly, than that for the intact vessels (Figure 3c), falling within the error bars of the curve with endothelium ($P>0.05$). Again, the slower increases in OD than AS represents the vessels' lengthening with pressure.

3.4 Hydraulic conductivity Lp

The average value (n=6) of the hydraulic conductivity of the aorta at 100 mmHg (its time-average physiological pressure) with intact endothelium is $2.79\pm0.72 \times 10^{-8}$ cm/s/mmHg. The average Lp with intact endothelium at 60 mmHg has a higher value ($4.69\pm1.20 \times 10^{-8}$

cm/s/mmHg) than at the rest of the transmural pressures examined. The average Lp decreases with increasing pressure, dropping about 40% in the range from 60 mmHg to 100 mmHg (Figure 4a) ($P<0.05$), but remains flat thereafter ($P>0.05$). Deendothelialization increased Lp by roughly 3/4 ($P<0.05$). The average Lp without endothelium at 100 mmHg is $4.89\pm1.01 \times 10^{-8}$ cm/s/mmHg. In contrast to the intact vessel, the variation in Lp over the pressure range is insignificant (Figure 4a) ($P>0.05$).

Measurements of the aorta's Lp with and without endothelium allow a decomposition of the resistance roughly into an endothelial and a media component. $<Lp_{endothelium+intima}>$ at 100 mmHg is $5.9\pm3.5 \times 10^{-8}$ cm/s/mmHg, which translates to about 47% of the total wall resistance deriving from the endothelium at that pressure.

We measured the hydraulic conductivity Lp of the PA in six rats at five pressures from 20-100 mmHg with intact endothelium, denuded, and then repeated the measurements at the same five pressures. Unfortunately, the time required to extend these measurements to include 10 mmHg, including waiting for steady state at this low pressure, was long enough so that the vessel was no longer viable for both sets of measurements. Therefore we repeated the procedure on a second population of the same rats for 10, 20 and 40 mmHg. As Figs. 3b and 4b illustrate, the two populations agree very well (no significant difference, $P>0.05$) in the overlap region.

Lp with intact endothelium is $1.90\pm0.36 \times 10^{-7}$ cm/s/mmHg at 20 mmHg. It drops about 31% from 20 to 40 mmHg ($P<0.05$). Beyond 40 mmHg, Figure 4b shows that Lp varies little with pressure ($P>0.05$). Lp of the intact vessel is $2.34\pm0.27 \times 10^{-7}$ cm/s/mmHg at 10 mmHg and drops 42% from 10 to 40 mmHg ($P<0.05$).

The average magnitude of Lp for the deendothelialized PA over the entire pressure range is more than double its value with its wall intact ($P<0.05$). At 20 mmHg, the average Lp is

$2.99\pm0.49 \times 10^{-7}$ cm/s/mmHg, but it does not vary significantly with the increasing pressure ($P>0.05$) (Figure 4b). The same is true for the second group of rats; there was no significant difference ($P>0.05$) between the rats in the two pressure ranges. From Lp of the intact and deendothelialized walls one calculates the Lp of the endothelium $Lp_{endothelium+intima}=6.02\pm1.89 \times 10^{-7}$ cm/s/mmHg, or about 32% of the total wall specific resistanceat 20 mmHg, in contrast to its average value of 55% over the pressure range 40-100 mmHg.

The average Lp of the vein (six rats) with intact wall is $5.79\pm1.53 \times 10^{-7}$ (n=8) or $6.01\pm1.50 \times 10^{-7}$ (n=6) cm/s/mmHg at 10 mmHg, the former including two rats whose endothelia were not subsequently denuded. Figure 4c shows that the hydraulic conductivity drops 33.2% (n=8), 33.4% (n=6) at 20 mmHg ($P=0.012<0.05$ (n=8), $P=0.011<0.05$ (n=6)) and varies little with increasing transmural pressure ($P>0.05$) until 50mmHg, where n=4 and the error bars are larger; thus the (increasing) value is less meaningful. Considering this rise, it may be appropriate to consider the average curve flat. Since some of the vessels sprung leaks at 50-60 mmHg, only four vessels were available over the entire range. As Figure 5a illustrates, if the higher Lp at low pressure is real, the shape for the Lp vs. transmural pressure curve is similar in all vessels, at least for the lower four IVC pressures.

The Lp of deendothelialized IVCs at 10mmHg is $24.94\pm5.91 \times 10^{-7}$ (n=8), $25.44\pm4.90 \times 10^{-7}$ (n=6) cm/s/mmHg, roughly four times its intact value ($P<0.05$). The average Lp in the endothelium-free preparation is relatively flat ($P>0.05$) and insensitive to pressure change (Figure 4c), although the individual traces show some (inconsistent) variation. The calculated average Lp of the vena cava's endothelium is $Lp_{endothelium+intima}=7.80\pm2.53 \times 10^{-7}$ (n=8), $8.32\pm2.62 \times 10^{-7}$ (n=6) cm/s/mmHg, representing about 74% (n=8), 72% (n=6) of the total wall

resistance at 10 mmHg. The Lp vs. transmural pressure trends for all deendothelialized vessels are similar (Figure 5b).

4. Discussion

The Introduction noted that lipid transport from the lumen into the arterial wall and its binding to extracellular matrix therein are the likely earliest triggering events for atherogenesis. It is natural to suspect that the very disparate susceptibilities of different vessels to atherosclerosis derive from differences in these processes. Experimental and theoretical evidence implies that LDL transport in large, susceptible arteries is convection-dominated, with Lp the governing parameter for transmural water flow. The primary goals of this study are to measure and compare Lp for the aorta, PA and IVC in rat, and, with the known transmural pressures typically suffered by these vessels, estimate and compare transmural convection in these vessels. To address these questions we have measured the transmural water flow and the outer surface area of isolated rat aorta, PA and IVC as a function of pressure. We subjected each vessel to a full set of measurements at six different pressures, both with and without intact endothelium, and calculated Lp at each pressure for both vessel conditions. Figures 3 show the geometric variation.

4.1 Diameter and surface area.

The agreement of the two methods for measuring vessel geometry is excellent and so we employ the vessel-preserving caliper-based method. The vessel diameter adjusts to a change in transmural pressure and this enters into the definition/calculation of Lp from the measured data of total flow vs. transmural pressure. The aorta's surface area increases about 42% ($P<0.05$) from 60 to 140 mmHg but the data suggest a leveling off at the higher pressure ($P>0.05$) beyond

120 mmHg. The outer diameter of the aorta changed about 20% from 60-140 mmHg, as in Figure 3a. Endothelial denudation did not change this behavior (P>0.05) (Tedgui 1984). The PA's outer diameter rises 32.4% from 20 to 100 mmHg, but rises insignificantly between 80 and 100 mmHg (P>0.05). Its surface area, with or without endothelium, increases 71% over the pressure range of 10 to 40 mmHg similar to the aorta (Figures 3). These expansions of the outer diameter and surface area are due to the elastic properties of the artery wall's complete and continuous elastin sheets. The stiffness of the collagen causes the high-pressure plateaus ((VanBavel 2003)), having been stretched to its maximum. The endothelium makes up less than 1% of the total wall thickness and takes up a negligible amount of the vessel's hoop stress; consequently, deendothelialization does not significantly change the pressure dependence of the outer diameter and surface area.

In contrast, the IVC's surface area increases only about 25% with pressure from 10-60 mmHg, and this increase is relatively linear (Figure 3c). This means that the vein expands uniformly with an increase in pressure, both with and without endothelium. This is consistent with the pressure-volume relationship developed by Brown and Heistad (Brown 1986), who found that the volume of the vena cava did not increase significantly with pressure beyond 5 mmHg. The vein's limited area increase may be due to its lack of continuous elastin that can account for vessel elasticity and to its abundance of collagen fibers that provide its stiffness, both unlike the arteries (VanBavel 2003).

4.2 Magnitude of $Lp_{overall}$ in intact vessels.

Recently, DeMaio *et al*. (DeMaio 2003) studied the sealing effect that transiently reduces the Lp of bovine aortic endothelial cells (BAEC) cultured at zero pressure after a sudden rise in its transmural pressure. In our study we measure Lp of the vessels accustomed to and extracted

under physiological pressure. Moreover, DeMaio *et al*'s transients returned to background in circa 60 minutes. We assess the flow rate for 30 minutes at a given pressure until steady state appears to have been reached and then subsequently measure the transmural flow 5-6 times, with 5 min intervals, to infer Lp. We observe transients in this first ~30 min period, but these appear negligible in the subsequent measurements.

Figures 5 show the results for Lp for all three types of vessels. The average values over all pressures measured of Lp for rat aorta is $3.16\pm0.87 \times 10^{-8}$ (n=6 rats used), for rat PA is $1.85\pm0.49 \times 10^{-7}$ (n=6) and $1.48\pm 0.13 \times 10^{-7}$ (n=6), averaging from 10- 40 and 40-100 mmHg respectively, and for rat IVC is $4.85\pm1.10 \times 10^{-7}$ cm/s/mmHg (n=8), $4.95\pm1.08 \times 10^{-7}$ cm/s/mmHg (n=6), averaging from 10-40 mmHg.

In order to explain the large increase in Lp from aorta to PA to IVC, we examine the wall structures of these vessels. The media of the PA appears to have a similar structure to the aorta, with parallel sheets of elastin. The PA's IEL (3.2±0.7 μm) and other elastins (3.4±1.9 μm) appear thinner than the aorta's (4.5±1.6 and 5.7±2.1 μm) (Figures 2a,b). Since the PA's wall (78.9±3.3 μm) is thinner than the aorta's (145.8±9.3 μm; at zero pressure, but the distance between adjacent sheets is similar (~10 μm, the diameter of the smooth muscle cells in the media) the PA has fewer elastin sheets than the aorta. The vein's structure is very different from those of the arteries (Figure 2c). The media of the vein contains no discernable IEL and only sparse bits of elastin, as well as collagen fibers and SMCs. It is not nearly as densely packed as in the aorta or the PA and the IVC has the thinnest wall (66.1±4.1 μm). These factors contribute to and are consistent with the relative magnitudes of Lp in the three vessels.

In an earlier paper we (Huang 1998) reported a zero-pressure thickness of the aortic wall of 107 μm, in contrast to the present value of 145.8±9.3 μm. The reason for the difference is that

in the earlier study, the vessel was perfusion fixed at near zero pressure while still in the rat so as to be comparable to aortas fixed in the animal under pressure. In contrast, the present values were determined from histology done by fixing the excised vessels. In the rat, the vessel is stretched and excising it releases this stretching, allowing it to retract in length and thus expand in thickness. Each set of measurements was reproducible.

4.3 Shape of Lp vs. ΔP curve:

a. Trends: We measure Lp on the same animal's aorta, both with and without endothelium, as a function of its transmural pressure. We find that the Lp of the intact rat aorta starts out high (4.69±1.20 x 10^{-8} cm/s/mmHg) at low pressure, drops circa 40% from 60 to 100 mmHg and then remains pressure-independent beyond. For the PA, we examine the pressure regimes 10 to 40 and 20-100 mmHg because the mean physiological pressure of the PA is 16 mmHg and can exceed 100 mmHg for pulmonary hypertension (Brossman 1992), when the PA becomes susceptible to atherosclerosis. In the PA, Lp=2.34±0.27x10^{-7} cm/s/mmHg at the low transmural pressure of 10 mmHg and quickly drops 42% by 40 mmHg ($P<0.05$). Further increasing the pressure doesn't affect the Lp significantly ($P>0.05$). In the IVC, the hydraulic conductivity is high (5.79±1.53 x 10^{-7} cm/s/mmHg (n=8), 6.01±1.50 x 10^{-7} cm/s/mmHg (n=6)) at low pressure (10 mmHg), drops ~33.2% (n=8), 33.4% (n=6) when the pressure increases (20 mmHg), and remains flat until rising at the large-error bar values of 50 and 60 mmHg, which may indicate that the curve should best be considered flat. Endothelial denudation sharply increases Lp by 3/4, more than double and more than quadruple, respectively, in the three vessels, and renders Lp pressure-independent (Figures 4), i.e., the transmural water flux becomes linear with transmural pressure. The trend is clearly very similar in the aorta and the PA, and somewhat similar in the IVC, despite the differences in vessel wall structure and in absolute

magnitude of Lp (Figures 5). The IVC's lack of a complete IEL (see below) argues against a drop in Lp from 10-20 mmHg which would suggest an even higher value of Lp at the vessel's normal physiological pressure of 5 mmHg.

b. Interpretation: Earlier investigators ((Tedgui 1984), (Baldwin 1993)) found similar trends for Lp(ΔP) for the rabbit aorta, and we have now confirmed that the rat aorta's Lp was both qualitatively and quantitatively similar to the rabbit's. In fact, the average values for both intact and denuded rat aorta are almost identical to Tedgui and Lever's rabbit data (Figure 6) used in Huang *et al* (Huang 1994) and thereby provide Huang *et al* with a complete set of rat-derived data. Baldwin's (Figure 6) high value at low-pressure had a uniquely large error bar, reflecting that the trend was not consistent in all individual traces. Their Lp values were roughly double Tedgui and Lever's (Tedgui 1984). A quantitative factor of two is also roughly the variation in magnitude that one can observe between the aortas of different animals of the same species, even when their trends with varying ΔP and with deendothelialization are qualitatively similar. Kim and Tarbell (Kim & Tarbell 1994) attempt to explain the trend with a wall compaction hypothesis that invoked a variation of void fraction with distance into the wall. Huang *et al*. (Huang 1997) constructed a theory based on a large observed disparity in matrix structure and void volume between the intima (~90% void for albumin) and media (a few per cent void for albumin) (Tedgui 1987). Their theory suggested that the intima easily compresses under pressure until its stiff collagen matrix carries the load and allows no further compression, but the dense media is incompressible. The compressed intima would make it denser and more resistant (a small effect) and the juxtaposition of the endothelium and the IEL would block the IEL's fenestrae and thereby severely curtail transmural flow. Clearly, endothelial removal eliminates this effect and makes Lp pressure-independent. This theory is also consistent with

both Baldwin's (Baldwin 1992) large error bar at 50 mmHg and Baldwin *et a*l'*s* (Baldwin 1993) use of a nitric oxide inhibitor that eliminated the high Lp value at 50 mmHg, but left Lp at other pressures unchanged, as explained in the introduction. Thus this theory successfully explained the rabbit aorta data, and the similarity in structure and Lp trends between rat and rabbit aortas suggests the theory is equally valid in rat aorta. Huang *et al*. (Huang 1998) confirmed intimal compaction under pressure load in rat experiments, finding that its intima indeed compresses 80-85% from zero pressure to 100 mmHg.

The similarity in the structures of the PA's and the aorta's walls, with both containing complete, fenestrated IELs and discernable intimas, suggests that a similar qualitative explanation likely explains the Lp(ΔP) curves for the PA. The IVC, in contrast, does not have a fenestrated IEL and, as such, fenestral blockage by an impinging endothelium is not a potential explanation for the insignificant drop in Lp with Δp. Intimal compaction could still decrease the intima's contribution to flow resistance, since there is evidence (Zeng 2005) from the valve leaflet that the absence of an IEL does not preclude the existence of a thin, sparse, subendothelial intima. Further support comes from Tompkins *et al* (Tompkins 1989a), who injected a radioactive ^{125}I-LDL tracer into squirrel monkey 30 min. before sacrifice and used quantitative autoradiography to measure the average LDL concentration vs distance from endothelium for different vessels, including the aorta, PA and IVC. Each of these profiles had a high immediately subendothelial (intimal) value; a sharp drop near the luminal side and then a flat, low value in the media. The aorta's profile differed only in magnitude from the PA's and IVC's, being lower in magnitude. This sharp concentration drop is consistent with a high-void subendothelial intima juxtaposed against the dense media in all three vessels. Tracer may also bind with the intimal

extracellular matrix ((Frank 1989), (Yin 1997)), thereby magnifying the difference between intimal and medial concentrations.

4.4 Dhar et al's observations

In contrast to the literature results on rabbit cited, Dhar *et al.* (Dhar 1996) observed that Lp of denuded rabbit aorta decreased with increasing transmural pressure. They attributed this drop in Lp to media compressibility, and constructed a corresponding theory. Unlike in our experiment, Dhar *et al*. (Dhar 1996) used solutions of different albumin and saline concentrations on opposite sides of the vessel wall. They then made a major assumption that the media of the aorta was very porous so that they could neglect the reflection coefficients, σ, and thus the osmotic pressure difference across the rabbit aortic wall. In fact the media is roughly 42% porous to sucrose but only a few percent porous to albumin (Tedgui 1987). This indicates that most of the albumin cannot traverse the aortic wall. Knox *et al* (Knox 1988) and Karmakar *et al* (Karmakar 1994) estimated σ for a 4% BSA solution in PBS as between 0.8-1.0, which directly contradicts Dhar *et al*'s assumption. Thus the albumin will result in an osmotic pressure drop across the aortic wall, which is consistent with Lever and Sharifi's (Lever 1987) finding of a lower aortic wall Lp with higher albumin gradient across the wall. At higher pressures the initial transmural flow would be higher and could thus lead to a larger steady unstirred layer than at lower pressures. Neglecting the resulting transmural osmotic pressure difference would lead to an underestimate of Lp, and the magnitude of this underestimate would increase with ΔP; this could account for their observed drop in Lp with ΔP. This interpretation is consistent with Baldwin *et al*.'s observation (Baldwin 1992) of an Lp decrease with time at fixed pressure due to differing BSA concentrations in the perfusate and surfusate that disappeared when the solutions had the same BSA concentration. Thus, at the very minimum, such differences are known to

cause Lp artifacts. Finally, the theoretical model that Dhar *et al.* adapted from Tarbell and coworkers (Klanchar 1987) used a material property *M* that had to be negative for Lp to decrease with increasing pressure. However, a more recent study by Johnson and Tarbell (Johnson 2001) corrected the sign of this coefficient, which could not be negative when the permeability decreased with compression.

During vessel expansion, the lumen expands with increasing transmural pressure and, even if the density of the wall remains unchanged, the aortic wall becomes thinner as it reconfigures around the larger lumen at constant media volume. The product h·AS estimates the media volume when h is much less than the lumen radius. Therefore a decrease in the thickness h with transmural pressure is not necessarily indicative of wall compression. Unfortunately, Dhar *et al* (Dhar 1996) do not report their surface area measurements, which would allow one to assess the contribution of reconfiguration. A back of the envelope calculation below using h data from Huang *et al* (Huang 1998) and our AS data, both taken in our lab, but on different sets of rats and by different investigators, suggests that AS grows at least as fast as h shrinks with pressure.

One can also examine media compressibility empirically in rat. Huang *et al*. (Huang 1998) measured the aortic wall thickness as a function of transmural pressure by fixing each vessel at a different pressure *in situ*, sectioning transversely and examining each section under light microscopy. They reported that the wall thicknesses are 107 μm, 88 μm, 85 μm, and 82 μm at 0, 50, 100, 150 mmHg, respectively. The wall thickness at 0 mmHg is about 10-15% of the aorta's inner radius (Huang 1998). One can fit these data to either an exponential or to a hyperbolic function to calculate that the wall thickness at 60 and 100 mmHg should be 87 and 85 μm, respectively. As such, the fractional change in wall thickness from 60 to 100 mmHg is

roughly 2-3%, much less than the change of 40% in Lp for the same pressure range (see Figures 4). The small percentage drop in wall hat high Δp indicates that the media is not as compressible as one might suspect.

4.5. Lp of the endothelium

Removal of the endothelial cells removes one layer of flow resistance. In terms of Huang *et al* (Huang 1998), it also removes the possibility of fenestral blockage at high transmural pressures. As a result of these two effects, mainly the latter, the hydraulic conductivity without endothelium exceeds that with endothelium. Our calculation of Lp for the rat aorta shows that ~43% of the resistance comes from the endothelium plus intima at 100 mmHg; the rabbit has about the same percentage endothelial resistance (Baldwin 1993). Lp of the endothelium may be pressure dependent.

4.6 $Lp_{media+IEL}$ and $Lp_{endothelium+intima}$.

As noted above, the $Lp_{overall}$'s of the PA and IVC are, on average, 4.7 (40-100 mmHg) and 15.4 (n=8), 15.7 (n=6) times $Lp_{overall}$ of the aorta. We examine how much of this difference derives from the different media structures and how much from a disparity in apparent endothelial Lp's. $Lp_{media+IEL}$ for the PA ($2.82\pm0.16\times10^{-7}$ and $3.31\pm0.16\times10^{-7}$ cm/s/mmHg, the averages over the regimes 10-40 and 40-100 mmHg, respectively) and IVC ($22.53\pm2.22\times10^{-7}$ (n=8) $23.30\pm3.14\times10^{-7}$ (n=6) cm/s/mmHg), averaged over 10-60 mmHg are 6.6 (40-100 mmHg) and 45.0 (n=8), 46.5 (n=6) times that for the aorta ($5.01\pm0.22\times10^{-8}$ cm/s/mmHg, averaged over 60-140 mmHg) or the aortic resistance is 6.6 and 45.0 (n=8), 46.5 (n=6) times larger than the PA and IVC's. These differences are roughly 1.4 and 2.9 (n=8), 2.96 (n=6) times the ratios of $Lp_{overall}$ for the intact vessels and the resistance ratios are similar (PA) to or larger (IVC) than the ratios, 1.8 and 2.2, of their media thicknesses. Thus the large differences in media resistance between the arteries and

the IVC must be the result of the different media structures and are consistent with the higher medial concentrations observed by Tompkins in the PA (higher $Lp_{overall}$) and especially in the IVC vs. the aorta. It is also consistent with Lever *et al*.'s (Lever 1990) data showing that the PA and IVC have significantly higher albumin porosities than the large arteries.

In contrast to the large disparity of $Lp_{overall}$ and $Lp_{media+IEL}$ between vessels, the average calculated $Lp_{endothelium+intima}$ for the PA and IVC, 5.4 x 10^{-7} and 6.18 x 10^{-7} (n=8), 6.28 x 10^{-7} (n=6) cm/s/mmHg, respectively, are very similar, although its average value for the aorta, 8.52 x 10^{-8}, is somewhat smaller. It accounts for 34% (PA average over 10-40 mmHg), 55% (PA average over 40-100 mmHg), 78.4% (n=8), 78.8% (n=6) (IVC average 10-60 mmHg) and 37% (Aorta average 60-140 mmHg) of their total wall resistances. Since the medial resistance falls sharply from aorta to PA to IVC, the endothelium's fractional contribution to the vessel's total resistance increases accordingly, dominating for the IVC. McCandless *et al*. (McCandless 1991) measured a value of 20.1±5.2 x10^{-5} cm/s/mmHg for the Lp of confluent monolayers of cultured sheep pulmonary artery endothelial cells. As noted in the introduction, these high values may be the result of leaks. Our calculated aortic $Lp_{endothelium+intima}$ (16.0±7.3 x10^{-8} cm/s/mmHg at 60 mmHg) is consistent with Tedgui and Lever's value 15.76 x 10^{-8} cm/s/mmHg at 70 mmHg ((Tedgui 1984)), with Vargas *et al*.'s of 11.9 x 10^{-8} cm/s/mmHg at 100 cm H_2O ((Vargas 1979)) and with measurements on cultured human umbilical venous endothelial cells (HUVEC) (6.57±0.72 x 10^{-7} cm/s/mmHg) at 10 cm H_2O (Chang 2000) and dog vena cava (1.27±0.06 x 10^{-7} cm/s/mmHg) up to 120 cm H_2O (Vargas 1986).

The slightly lower value of the aorta's $Lp_{endothelium+intima}$ relative to the PA and IVC may suggest that $Lp_{endothelium+intima}$ depends on the long-term pressure in the vessel. More likely, the smaller value of $Lp_{endothelium+intima}$ for the aorta may reflect the fact that its measurement by

difference means it includes not only the conductance/resistance of the endothelium, but also contributions from the intima. Whereas the sparse intima normally contributes negligible resistance to water flow, Huang *et al*. (Huang 1997) suggest that intimal compaction by transmural pressure loading can force the endothelium to block IEL fenestrae, thereby drastically increasing wall resistance to water flow and causing the measured $Lp_{endothelium+intima}$ to be significantly smaller than just $Lp_{endothelium}$. Since the aorta has a complete and thick IEL, this effect would be strongest in the aorta. They show that with the intimal compactions and other parameters typical of the aorta (Huang 1994) $Lp_{endothelium+intima}$ will be on the order 1/3-1/5 $Lp_{endothelium}$ at 100 mmHg, thereby bringing our aortic $Lp_{endothelium}$ in line with that of the other vessels. In addition, this line of reasoning would explain why Lp at the lowest pressure, where the intima is not fully compressed and its IEL fenestrae are not blocked, for the aorta and PA experience hardly change upon denudation: without fenestral blockage the endothelium contributes far less resistance than the artery's media and thus denudation hardly changes $Lp_{overall}$. In addition, John Lever [private communication] has noted that endothelial removal likely leads to medial hydration and consequent expansion. Since the media comprises almost all of the vessel wall, even a small percentage hydration can lead to a measured $Lp_{media+IEL}$ higher than its intact vessel value. This effect is larger for thicker media. Thus the true endothelial Lp in intact aorta may indeed be consistent with our PA and IVC measurements, and it is wise to treat $Lp_{endothelium+intima}$ (resistance) calculated in this way as lower (upper) bounds, rather than as precise values.

4.7 Transmural water flux in the aorta, PA and IVC.

Typical transmural pressures in these vessels are 100, 16 and 5 mmHg, respectively. The products of the Lp values above and the corresponding pressures yields estimates of 31.6, 29.6

and 24.3 x10^{-7} (n=8 and n=6) $cm^3/(cm^2\text{-}s)$, respectively, for the transmural water fluxes in the aorta, PA and IVC, a quantitative, not qualitative, difference. Interestingly, despite the very different pressure driving forces in these vessels, the water fluxes seem to be surprisingly similar. It is hard to imagine that these small differences by themselves determine susceptibility; rather, if convective tracer transport is significant in the aorta, it ought to have the potential to be significant in these other vessels as well. However, the very different medial structures, and consequent $Lp_{media+IEL}$, of these vessels suggests that tracer (in particular, LDL) convected across the vessel endothelium may distribute more readily between the intima and media and even more efficiently drain out of the PA and IVC than in the aorta. As a result, the *local* concentration of LDL in the intima, which presumably controls the rate of the triggering event of binding to extracellular intimal matrix, in the PA and IVC may still be much lower than that in the aorta. A future publication will test this hypothesis both experimentally via confocal microscopy and theoretically, via a full theory of filtration and mass transport in the PA and IVC, using parameters measured in this study.

5. Summary

To understand LDL transport into and accumulation in vessel walls, the putative triggering events in atherogenesis, it is necessary to first investigate transmural water transport to assess the potential importance of convective LDL transport. Here we measure and compare the hydraulic conductivities Lp of the aorta, where convective LDL transport is dominant, the pulmonary artery and the inferior vena cava. The pulmonary artery's wall structure is similar to the aorta's but has a thinner wall and fewer and thinner elastin layers. The vena cava has a much different structure from either of these arteries, with only sparse bits of elastin and a thinner wall.

The aorta and pulmonary artery show a high Lp at low transmural pressure with a sharp drop followed by a plateau as the transmural pressure increases. Removal of the endothelium increases Lp significantly in all vessels and renders it independent of the transmural pressure. The medial resistance is largest for the aorta, is significantly lower for the PA and is lower again for the IVC. In contrast, the endothelial Lps of all the three vessels are similar in magnitude at their lowest pressures (which is consistent with studies of cultured endothelial cells), with that of the aorta appearing to be slightly smaller than the others. We argue that this difference may be an artifact of the measurement technique. Otherwise, it may suggest that the endothelial Lp is pressure-dependent. No studies have been done to measure the Lp of the cell monolayers as a function of the transmural pressure under which the cells were cultured. A future experiment will examine this hypothesis.

The PA experiences a smaller driving force than the aorta (16 vs. 100 mmHg) and the vein is under an even lower physiological pressure (5 mmHg). The data suggest that the balance between a lower driving force and a higher Lp leads to surprisingly similar transmural water fluxes in these vessels. This similarity seems consistent with the similar magnitudes of Tompkins' 30-minute LDL profiles across the walls of the three vessels. It begs the question of why the susceptibilities of these vessels to disease differ so greatly. One possibility may be that the higher porosity (Lever 1990) and larger Lp of the PA and IVC media relative to the aortic media may permit easy drainage of the macromolecules and prevent their accumulation in the intimas of the former vessels. Measurements of the rates of tracer spot growth in the PA and IVC, and a detailed, quantitative convection-diffusion model incorporating the present measurements of transport parameters to explain those future measurements should allow us to

quantitatively assess the difference in tissue delivery and concentration of LDL amongst these vessels. Therein may lie the potential resolution.

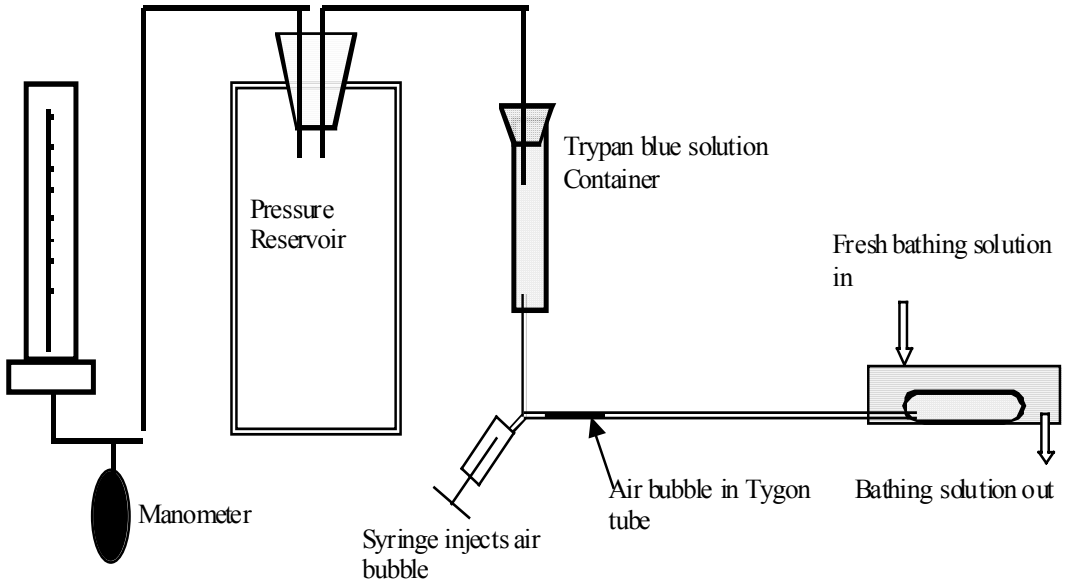

Figure 1a. Experimental setup for hydraulic conductivity Lp measurement of an isolated vessel. A sphygmomanometer controls the pressure in a large reservoir. The reservoir exerts pressure on a solution container containing a solution of 4% BSA, 1.0 mM $NaNO_3$ and 0.03% Trypan blue. A Tygon tube connects this solution container to the isolated vessel, which is bathed in the identical solution minus the Trypan blue. A long section of the connecting tubing is kept straight and horizontal and fixed to a finely calibrated ruler. The motion of an air bubble injected into the beginning of the horizontal part of this tubing determines the solution flow rate into the isolated vessel and, by incompressibility, the flow rate through its walls. This apparatus is a slight modification of that used in all previous Lp measurements on isolated vessels ((Tedgui 1984), (Baldwin 1993)).

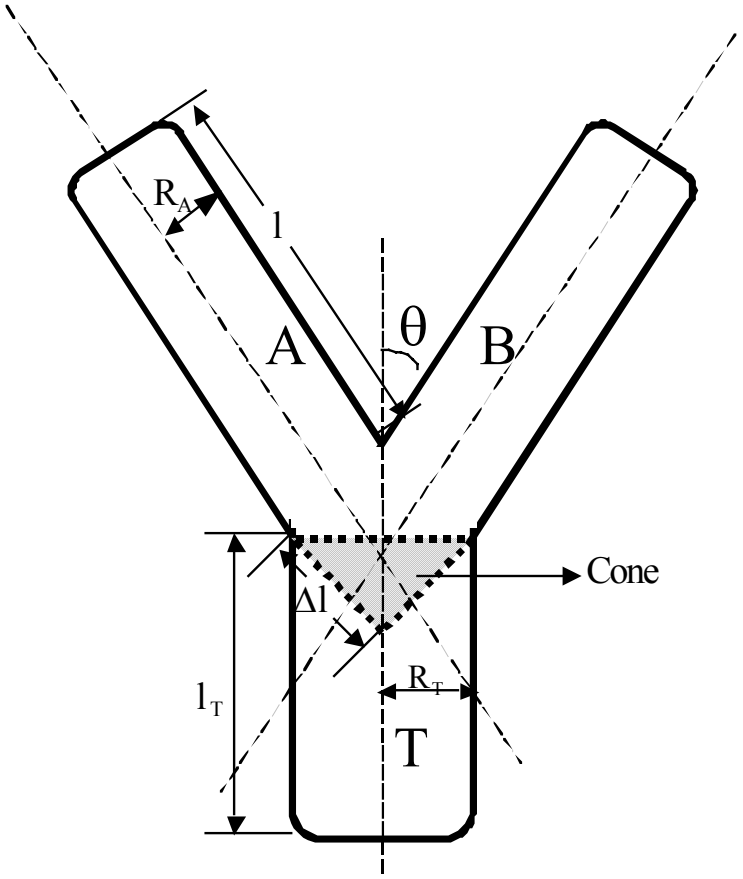

Figure 1b. Illustration of calculation of the Y-shape surface area (AS) of the pulmonary artery. AS_A, AS_B and AS_T are assumed in tube shape. Since the branches A and B has met as a V-shape joint, each AS of branches A and B is calculated as $AS=\pi OD(l+l+\Delta l)/2$. The AS of the cone is calculated as $AS=\pi R_T^2/\sin\theta$, where θ is the half angle of the bifurcation. The total AS is the sum of AS from A, B and T subtracting AS of the cone.

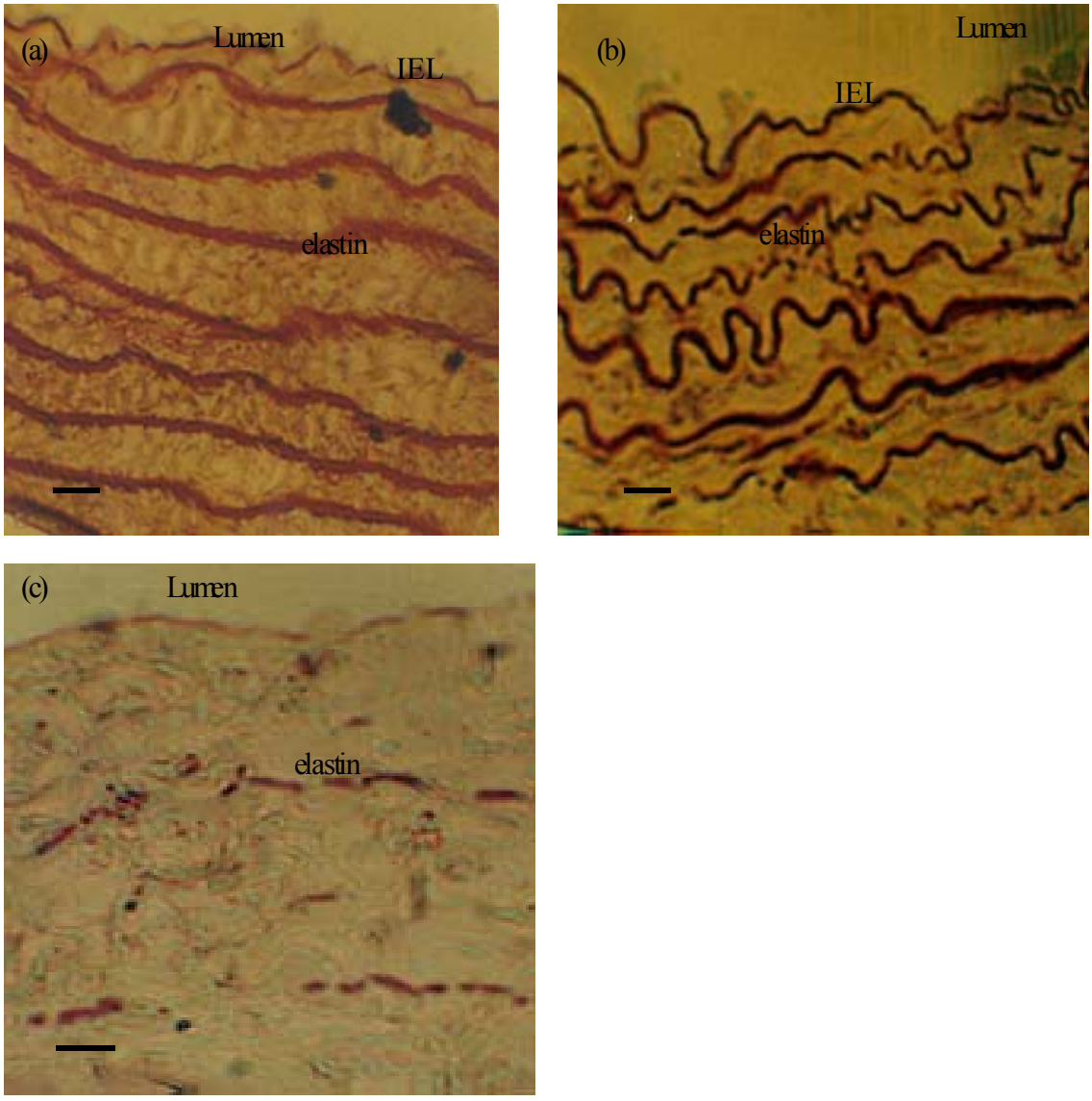

Figure 2. Vessel wall structure: Light microscopic views of100 nm thick sections stained with orcein, which specifically highlights elastin in red. (a) The aorta has a wall thickness of 107μm at zero pressure ((Huang 1998)). It has a complete IEL (4.6±1.6 μm) and continuous layers of elastin (0.4% orcein stain). (b) The pulmonary artery has a wall thickness of 78.9±3.3 μm (mean± SD) at zero pressure. It has a complete internal elastic lamina (IEL) (3.2±0.7 μm thick) and continuous wavy layers of elastin (0.4% orcein stain). (c) The inferior vena cava has a wall thickness of 66.1±4.1 μm at zero pressure. It has an incomplete IEL (the broken red line just below the lumen) and only sparse bits of elastin throughout (1.0% orcein stain). Bar=10 μm.

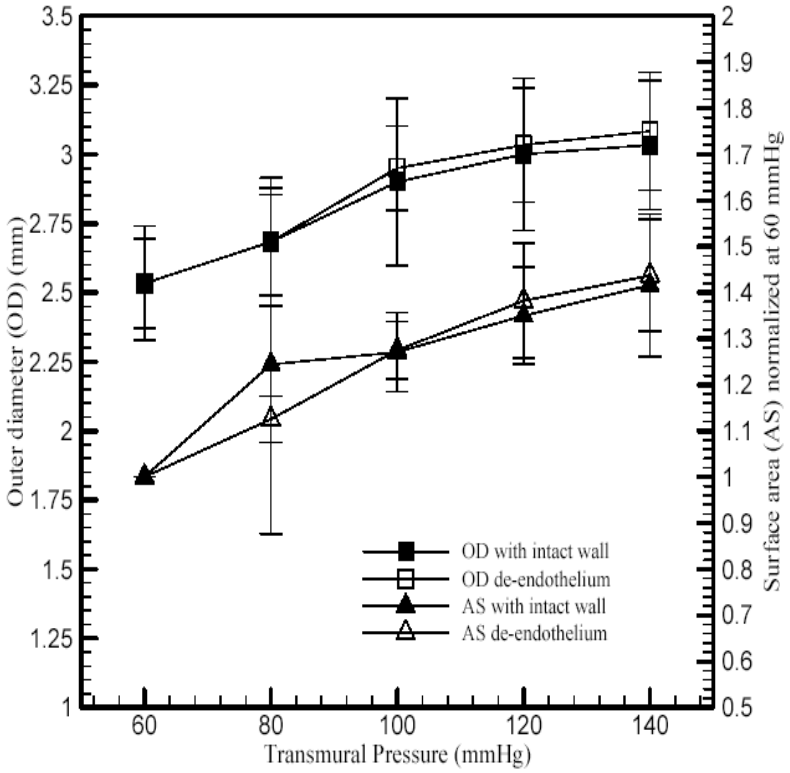

Figure 3a. The absolute outer diameter (OD) and the surface area (AS) normalized to its value AS(60) on the same vessel at 60 mmHg as functions of the transmural pressure, both with and without endothelium. The OD of the intact wall increases 20% from 60 to 140 mmHg ($P<0.05$). The OD of the deendothelialized vessel is within the error bars of the intact wall ($P>0.05$) and it increases 22% within the pressure range ($P<0.05$). The overall surface area (AS) normalized at 60 mmHg increases 42% over the pressure range ($P<0.05$). The de-endothelial and intact AS follow a similar trend ($P>0.05$); the denuded AS increases about 44% from 60 to 140 mmHg ($P<0.05$). (n=6, n is number of rats)

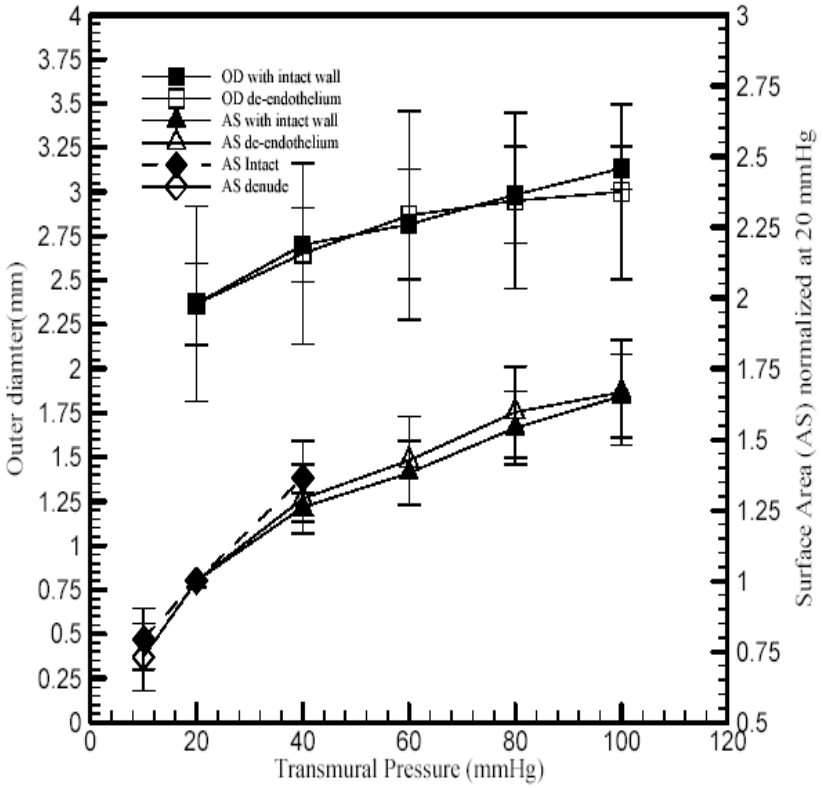

Figure 3b. Absolute outer diameter (OD) and outer surface area (AS) normalized to its value AS(20) on the same vessel at 20 mmHg for the isolated pulmonary artery as a function of transmural pressure, both with and without endothelium. The OD of the intact wall increases 32.4% from pressure 20 to 100 mmHg ($P<0.05$). The value of deendothelialized OD varies little from the OD of the intact wall ($P>0.05$). The average OD of the deendothelialized vein increases 26.7% over the pressure range ($P<0.05$). The average surface area of its intact wall increases by 65.3% ($P<0.05$) from 20 to 100 mmHg and, similarly, the average surface area of the deendothelialized vein increases 66.7% over the same pressure range ($P<0.05$). The difference between in AS between intact and denuded vein is insignificant ($P>0.05$). (n=6, n is the number of rats). The normalized AS increases 71% from 10 to 40 mmHg with the extra six rats ($P<0.05$). The difference between the two groups of rats is insignificant ($P>0.05$).

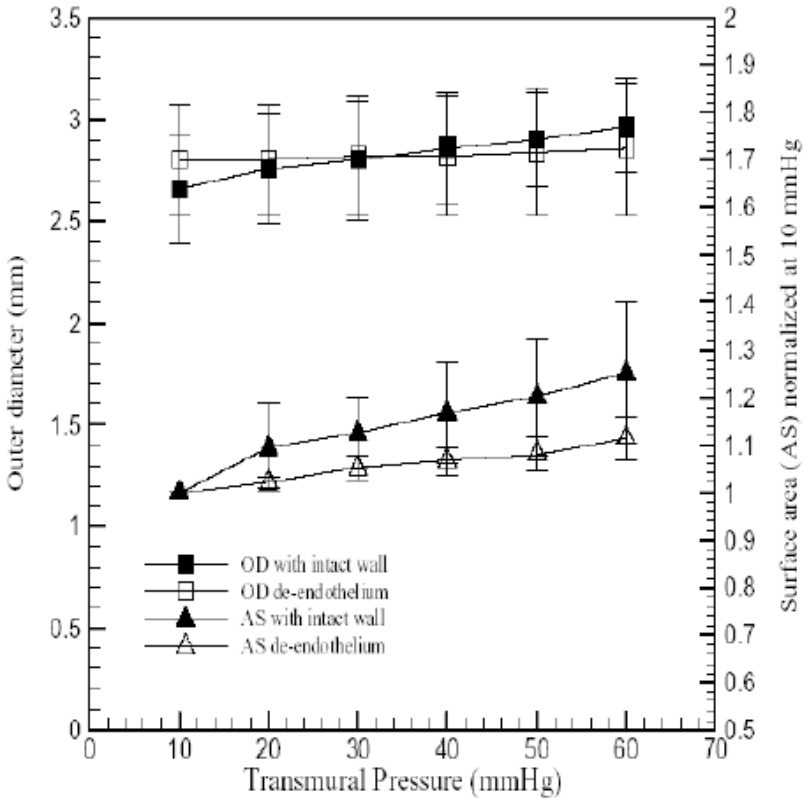

Figure 3c. Absolute outer diameter (OD) and outer surface area (AS) normalized relative to its value at 10 mmHg on the same vessel for the inferior vena cava as a function of the transmural pressure, both with and without endothelium. The average OD with wall intact increases 11.3% from pressure 10 to 60 mmHg ($P<0.05$). The average value of the deendothelialized OD varies little from that of the intact wall ($P>0.05$). The average OD of the deendothelialized vein increases 2.1% over the pressure range ($P<0.05$). The average surface area of its intact wall increases monotonically by 20% ($P>0.05$) and, that of the deendothelialized vein increases similarly (11.5%) ($P<0.05$) over this pressure range. The distinction in AS between intact and denuded vein is insignificant ($P>0.05$). (n=4)

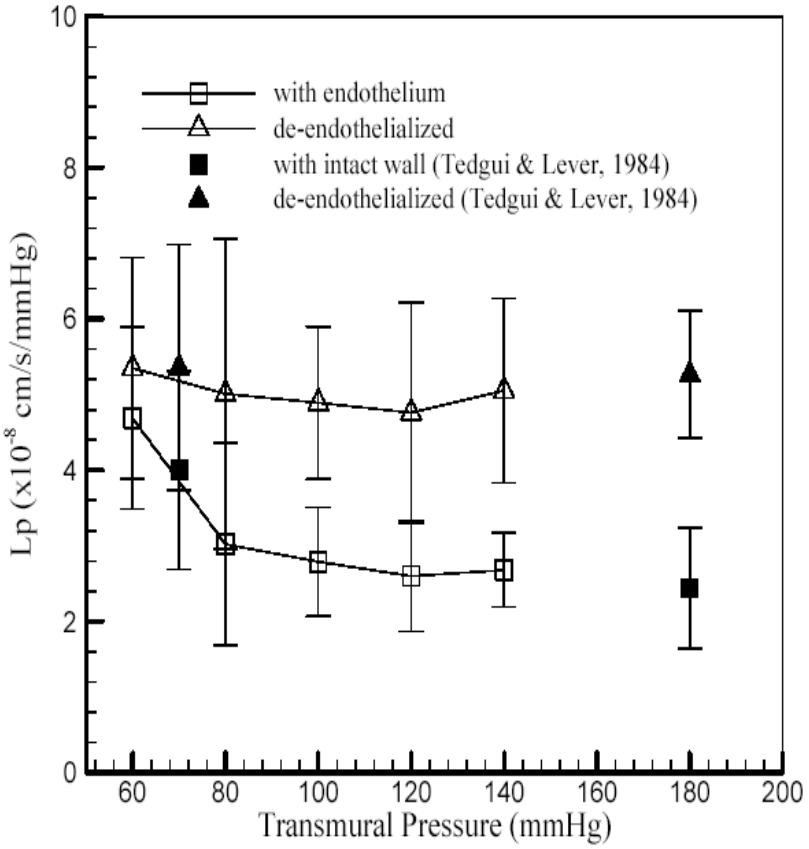

Figure 4a. The hydraulic conductivity (Lp) of rat aorta, measured both with and without endothelium on the same vessel, as function of the transmural pressure, plotted with some of the historic rabbit data from Figure 5. Each point is mean ±SD. The overall Lp drops about 40% from 60 to 100 mmHg ($P<0.05$) and remains constant with further increasing pressure ($P>0.05$). Deendothelialization increased Lp by about 3/4 relative to that of the intact vessel ($P<0.05$) and it is independent of the pressure ($P>0.05$). (n=6) Figure compares Lp of rat aorta with that of rabbit aorta ((Tedgui 1984)). The rat aorta data quantitatively agreed with the rabbit aorta both with and without endothelium.

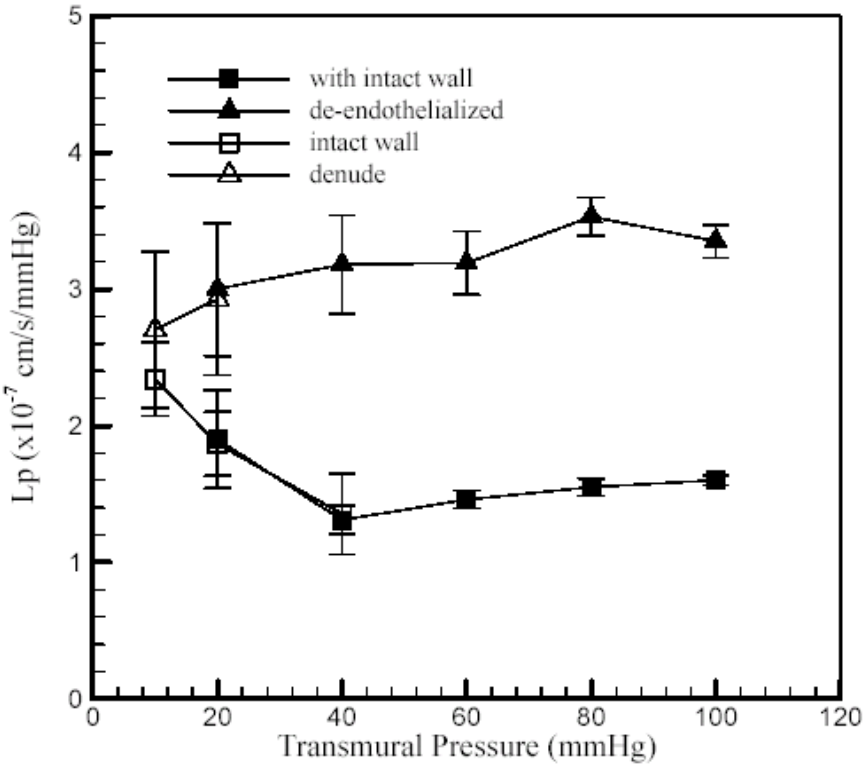

Figure 4b. Lp data for the pulmonary artery, both with and without endothelium Lp of each vessel was measured with intact endothelium and endothelial denudation at each transmural pressure. Each point represents the mean and the error bars represent the SD (n=6). The Lp of the intact vessel drops about circa 30% from 20 to 40 mmHg ($P<0.05$) and remains constant with increasing pressure (P for variation >0.05). The Lp of the deendothelialized vessel is about double of its intact value ($P<0.05$) and is independent of transmural pressure ($P>0.05$) over the values investigated. (n=6) From pressure range of 10 to 40 mmHg (n=6), the Lp intact drops 42% ($P<0.05$) and denuded Lp is independent of pressure ($P>0.05$). The difference between the two groups of rats is insignificant ($P>0.05$).

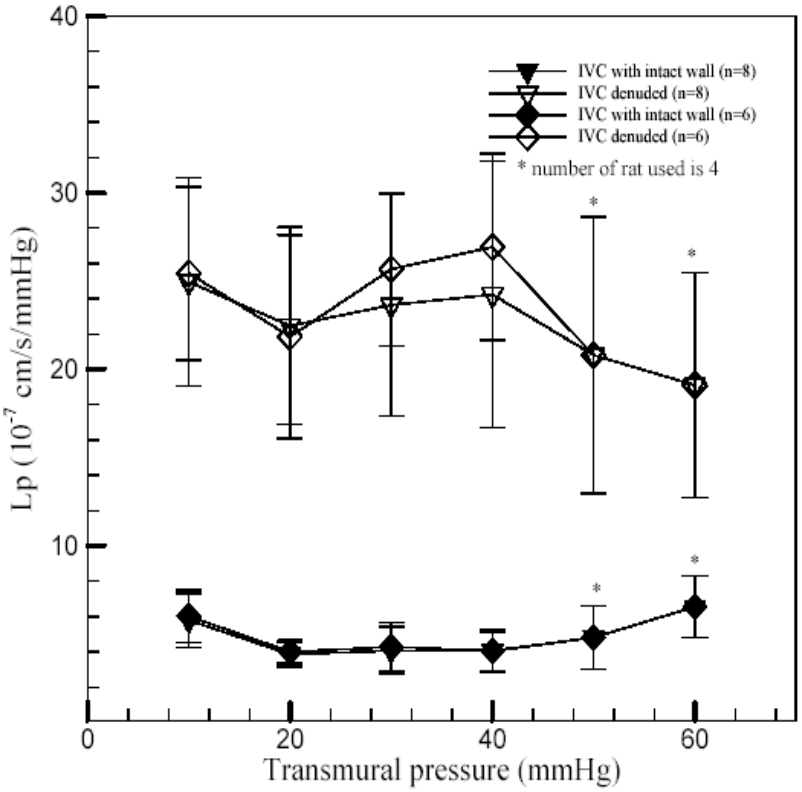

Figure 4c. Lp of the inferior vena cava both with and without intact endothelium. Lps of six vessels were measured with intact endothelium and after endothelial denudation at each transmural pressure, four from 10 to 60 mHg, and two from 10 to 40 mmHg. In addition, a second set of curves includes two animals measured only with intact endothelium and two measured only with denuded endothelium, each from 10 to 40 mmHg. Each point represents the mean and the error bars represent the SD. The Lp of the intact vein appears to drop about ~33% from 10 to 20 mmHg ($P<0.05$) and then to remain constant until rising, with larger error bars, at 50-60 mmHg. Lp of the deendothelialized vein is about 4 times Lp with intact wall ($P<0.05$) and is independent of the transmural pressure ($P>0.05$) over the values investigated.

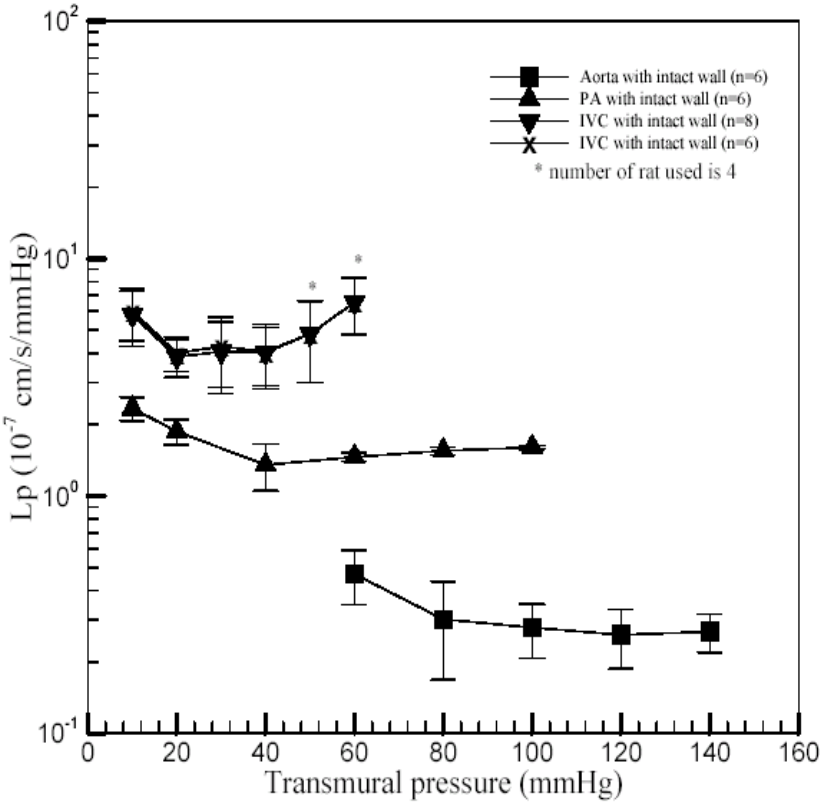

Figure 5a. Semi-log plot of the Lp vs. transmural pressure (ΔP) of the aorta, pulmonary artery and inferior vena cava, all measured with endothelium intact. The three vessels exhibit similar trends for Lp vs ΔP in that the Lp is high at the lowest transmural pressure, drops precipitously by the next highest pressure and then remains flat for all further pressure increases investigated. The Lps of the three vessels differ in size, increasing significantly from aorta (n=5) to pulmonary artery (n=6) to vena cava. Again error bars represent SD.

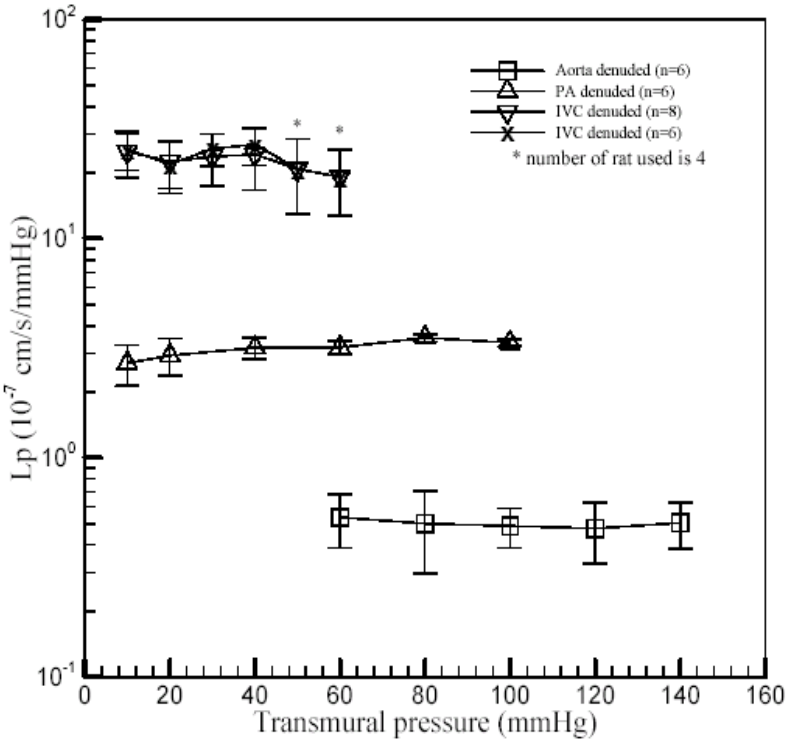

Figure 5b. Semi-log plot of the Lp vs. transmural pressure (ΔP) of the aorta, pulmonary artery and inferior vena cava, all measured with denuded endothelium. The three vessels all exhibit a similar trend in that Lp appears to be independent of transmural pressure over the values investigated. The magnitudes of Lp for the three vessels are quite disparate increasing in the order aorta (n=5), pulmonary artery (n=6) and vena cava. In all cases Lp of the deendothelialized vessel is significantly larger than Lp of the intact vessel.

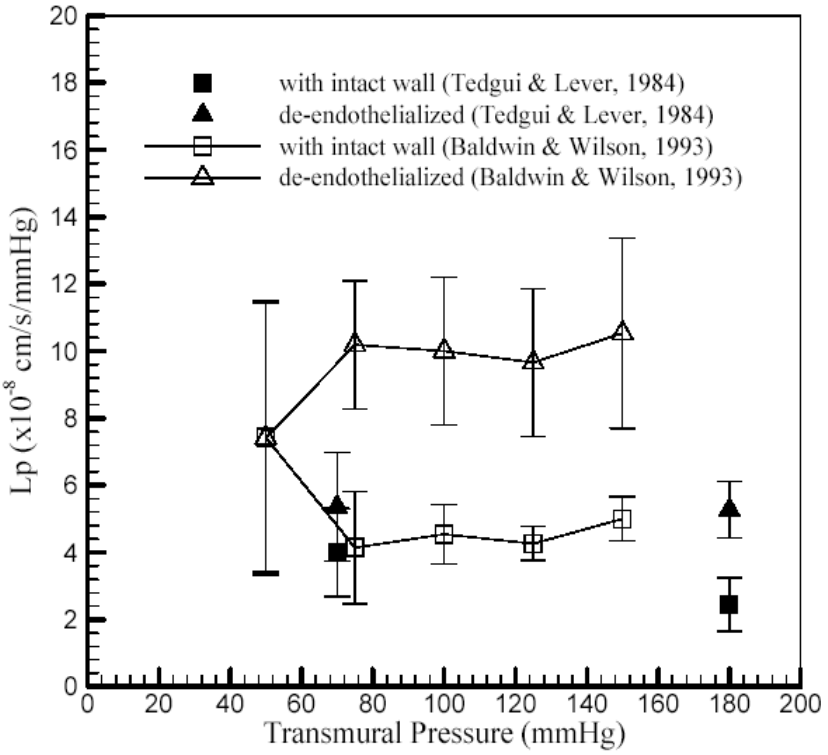

Figure 6. Historic data for Lp of rabbit aorta as a function of transmural pressure, both with and without endothelium. Baldwin and Wilson's ((Baldwin 1993)) data were uniformly about double the magnitude of Tedgui and Lever's ((Tedgui 1984)). The overall Lp drops about 40% from 50 to 75 mmHg ((Baldwin 1993)) and remains constant with increasing pressure. Lp of the deendothelialized vessel is independent of pressure. Tedgui and Lever ((Tedgui 1984)) only measured Lp at two pressure values. Deendothelialization roughly doubled their Lp relative to that of the intact wall.

Chapter 4

Macromolecular leakage and focal spot size growth in arteries and veins

1. Introduction

Atherosclerosis is a disease mainly of large arteries and the aortic valve ((Ross 1986), (Selzer 1987)). It is the leading cause of death for individuals both above and below age 65 in the United States and in all western countries. Atherosclerosis appears to begin with the delivery of low-density lipoprotein (LDL) from the blood into the vessel wall, where it spreads and accumulates (Vander 2001). Blood-borne monocytes enter the arterial intima in regions with high subendothelial lipid concentration, becoming macrophages that attempt to scavenge the extracellular cholesterol. When overwhelmed, they progress to form foam cells, and this accumulation of lipid and necrotic cells appears to comprise the earliest lesions. Eventually, such lesions lead to stenoses that compromise the cross section for flow, causing the heart ischemia, or they may rupture and release large particles into the blood.

Large arteries, such as the aorta and the coronary arteries, are susceptible to atherosclerosis when exposed to prolonged high blood cholesterol. Smaller, lower pressure arteries, such as the pulmonary artery (PA), and veins, such as the inferior vena cava (IVC), are generally spared. The human PA is only vulnerable under pulmonary hypertension. Interestingly, Schwenke reported that, unlike in humans, the rabbit PA under normal pressures is as susceptible as rabbit aorta (Schwenke 1997). Veins normally do not develop atherosclerosis. However, when veins are placed in arterial condition, i.e., high pressure, as in coronary bypass procedures,

atherosclerosis often develops. The saphenous vein is often used in the bypass surgery. After 6 to 12 years, about 71% developed atherosclerosis and their structure resemble arterial fatty streaks (Lever 1996).

To understand the transport of large molecules into susceptible vessels, work has focused on the aorta. The aorta has a continuous endothelial monolayer between the lumen and the thin, sparse subendothelial intima. A complete internal elastic lamina (IEL) with fenestrae (spaced ~20-25 μm apart, (Huang 1998)) separates the intima and the media, the latter of which consists mainly of continuous layers of elastin, extracellular matrix and smooth muscle cells (SMC). Frank and Fogelman's ultra-rapid freeze/rotary shadow etchings showed the detailed structure of the inima's matrix and how LDL molecules bind to the intima matrix and accumulate there.

Endothelial cells (EC) have junctions that are tight enough to severely restrict the transendothelial migration of molecules of albumin's size (~8 nm diameter). How a molecule such as LDL, with the size of 22 nm, can pass through these cellular junctions is an obvious question. Chien and coworkers ((Lin 1988), (Lin 1989)) used Evans blue albumin conjugate (EBA) to demonstrate the association between macromolecular leakage and the junctions of dying or dividing endothelial cells. The result showed that 99% of the cells in mitotic (M) phase were associated with EBA leakage and that 80% of cells in M phase were to Lucifer yellow-LDL (LY-LDL). Conversely, using autoradiography of the ^{125}I-LDL, Truskey (Truskey 1992) found that about 25% of the leakage sites found were associated with mitosis. Stemerman *et al*. (Stemerman 1986) and Chuang *et al*. (Chuang 1990) performed similar experiments, injecting horseradish peroxidase (HRP) as a tracer into rats and measuring the growth of HRP leakage spots in the aorta's subendothelial space as a function of circulation time between injection and

sacrifice. Stemerman *et al*. found that the HRP crossed the endothelium in isolated spots, rather than uniformly and Chuang *et al*. found that these spots grew extremely fast, reaching ~200 μm diameter in only 2 min. Such rapid spot growth seemed incompatible with a diffusion-dominated process for any reasonable diffusivity.

These results motivated our group's two-dimension, convection/diffusion model for tracer transport into the arterial wall (Huang 1994). The key ingredients of this model were the use of Frank & Folegman's (Frank 1989) ultra-rapid freezing and rotary shadow etchings that revealed the extremely loose intimal matrix structure and Lark *et al*.'s (Lark 1988) results showing that the intima had a radically different proteoglycan structure than the adjoining media. A structure-base, *ab initio* theory for the intima's transport parameters yielded values one to two orders of magnitude higher than the media's values. With these ingredients, the model yielded a convection-dominated rapid tracer spread in the intima that accounted for the large observed spots (Huang 1994).

We now ask, what parts of this transport picture in the large arteries changes when one shifts to less susceptible or immune vessels? The typical pressure drop the aorta suffers far exceeds the PA's, which again far exceeds the IVC's (100 vs. 16 vs. 5 mmHg). As such, one might expect HRP tracer spots to grow much more slowly in the lower-pressure vessels. However, in Chapter 3, we found that, the hydraulic conductivities Lp of the vessels follow a very similar trend to the pressure drops. This might suggest similar tracer growths. The combination of Lp and Δp is such that the overall water flows through these three types of vessel walls is surprisingly similar. The endothelial layers of all three of these vessel types appear to have similar conductivities; thus the difference in wall values derives from very different medial conductivities, likely a combination of their thicknesses and porosities. Thus easier drainage into

the vessel's media for the lower pressure vessels might then again suggest slower spot growth than in the aorta. Below we carry out these measurements and experimentally resolve these issues. The specific questions that we ask are: Is macromolecular leakage into the vessel wall uniform or localized? How quickly do tracer leakage spots grow? Is such growth convection or diffusion dominated? The results will be the basis of a crude theory here and will motivate detailed theories for tracer transport into these vessel walls and, hopefully, provide some consequent insight into their differing disease susceptibilities.

Before proceeding, we note that the pulmonary artery's basic structure is similar to the aorta's, with an endothelium, continuous IEL, and a media comprised of continuous elastin sheets, extracellular matrix and SMCs, but the PA has a thinner vessel wall (78.9±3.3 μm) than the aorta (145±9.7 μm, Chapter 2). The vein has a different structure. Since it is usually exposed to low pressures (~5 mmHg), it is not as elastic as the other two vessels. Hence, the vein has an incomplete IEL, only scattered, discontinuous elastin and less SMCs. Instead, the vein contains a large amount of collagen fibers (Chapter 2).

2. Methods

To measure the rate of leakage spot growth, we follow the protocols used by Stemerman *et al*. (Stemerman 1986) and Chuang *et al*. (Chuang 1990), repeated in brief below, applied to these other vessels. All protocols below were IACUC-approved.

2.1. HRP tracer spot experiment

We anesthestized 16 healthy male Sprague-Dawley (SD) rats, weighing 250-300g, were with 1% (w/v) Pentobarbital sodium (30mg Pentobarbital/kg body weight of rat, Sigma, MO) by intraperitoneal injection. After 0.5ml of HRP (type II; 30mg/500 g of rat weight dissolved in

0.5ml 0.15M NaCl, Sigma, MO) intravenous injection through a femoral vein cannulation, four rats were sacrificed after each circulation time 0.5, 1, 2, or 4 min with overdose of pentobarbital sodium. Prior to the sacrifice, 0.5 ml heparin (1000 units/1ml, Elkins-Sinn Inc. NJ) was injected prevented blood clotting. We excised the aorta, PA, and IVC fixed them in 1% and 2% (v/v) glutaraldehyde (Sigma, MO) for 1hr each and incubated the tissues in 3,3'-diaminobenzidine (DAB, Sigma, MO) and 0.02% H_2O_2 in Tris buffer (pH 7.4) at 37^oC for 60 min. The time between rat sacrifice and vessel fixation was 10-20 minutes. After preparing the tissues for *en face* examination, we counted the brown spots of the DAB reaction product under the microscope (Olympus BX51, Japan) and measured the spot areas using Image-Pro Plus. We then calculated the radius of the circle with the same area.

An additional 16 rats (four for each circulation time) underwent the identical procedure, but with HRP injected through a carotid artery (CA), rather than a femoral vein (FV), cannulation and only the IVC was excised.

2.2. Transmission Electron Microscopy (TEM)

Eight SD rats weighing 250 to 350 g were FV cannulated as described above. Six rats received HRP as above and two each were sacrificed after 7, 10 and 13 min HRP circulation; two rats were sacrificed without having received HRP. After the DAB reaction on vessels excised from the HRP-injected rats, the tissues were post-fixed in 2% (v/v) osmium tetroxide (OsO_4, Ted Pella, CA) for 90 min. The specimens were *en block*-stained with 2% (w/v) uranyl actate (EMS, PA) for 15 hr. at 60^oC. The specimens were rinsed and dehydrated in a series of ethanol and propylene oxide. The dehydrated specimens were embedded in Epon 12 (Ted Pella, CA). Pale gold to silver sections were cut with a diamond knife on a LKB III ultramicrotome and

stained with lead citrate for examination under the electron microscope (Zeiss model 902, Germany).

2.3. Light microscopy with orcein stain

An overdose of 1% pentobarbital sodium was injected to sacrifice the rat. The blood vessels of interest, i.e., the PA, the IVC and the aorta, were removed and fixed with 1% and 2% (v/v) gluteraldehyde solution for 1 hr each, followed by PBS solution to wash out the fixative. The tissue was post-fixed with 2% (v/v) osmium tetroxide (Ted Pella, CA) for 90 min. After fixation, the tissue was rinsed with distilled water 3 times (about 1 min. each), dehydrated with ethanol in the series 30%, 50%, 75%, 85%, 95%, and 100%, (v/v) and propylene oxide (Ted Pella, CA) and finally, after infiltration, embedded in Epon 12 (Ted Pella, CA).

We sectioned the Epon blocks to a thickness of around 200 nm (purple reflection ((Bozzola 1992), (Huang 1998)) using a glass knife with an MT-1 ultramicrotome (Dupont) and glued the sections to a glass slide with 2% (w/v) gelatin (Ted Pella, CA). We then applied orcein stain to specifically highlight the elastic fibers in the vessel walls (Huang 1998). The slides were dried and observed under light microscopy (Olympus BX51, Japan). The vessel wall thicknesses were measured by using NIH ImageJ. For the aorta and the PA, which contain large amounts of elastin, we used a 0.4% (w/v) orcein solution (0.4 g, of orcein, dissolved in 100 ml 70% ethanol, with 0.6 ml of concentrated HCl then added), whereas for the IVC, which contains much less elastin, we used a 1% orcein solution.

2.4. Silver Stain

We anaesthesized three healthy male SD rats, weighing 250-300g, with 1% (w/v) pentobarbital sodium (30 mg/kg body weight of rat, Sigma, MO) by intraperitoneal injection and cannulated their right carotid artery and jugular vein. After a 0.5 ml Heparin injection into the

left femoral vein, an overdose of pentobarbital sacrificed the rats. The aorta was perfused through the cannulated carotid artery with heparinized 1% (v/v) gluteraldehyde at 100 mmHg, and then the perfusate was changed to 5% glucose for 2 min, and a 1:1 mixture of 3% CoBr and 1% NH_4Br for 1 min. The aorta was removed, its adventitia carefully peeled with a fine forceps and its aorta cut longitudinally and mounted onto a glass slide for *en face* observation.

The IVC was perfused through the jugular vein with the same solutions at 10 mmHg, but with a perfusion time 5 times longer than the aorta. The PA was excised and fixed in heparinized 1% (v/v) gluteraldehyde for 2 hr. We then incubated it with 5% glucose for 2 min, and a 1:1 mixture of 3% CoBr and 1% NH_4Br for 1 min. We carefully removed the adventitia of the IVC and the PA and prepared the tissues as described above. All vessels were observed under the light microscope (Olympus BX51, Japan). The sizes of the endothelia were measured by using NIH ImageJ.

2.5. Crude model for spot growth

In order to analyze the data we propose a very crude model. It assumes an idealized geometry of a flat endothelium that is parallel to a flat IEL. The tracer is convected into the subendothelial intima only through a localized leak, e.g., a leaky circular junction around an endothelial cell, centered at the origin and spreads in the intima purely passively by virtue of the advancement of the convective front, without diffusion. Water enters the subendothelial intima through all of the cell-cell junctions and exits through the IEL, both of which are characterized by a hydraulic conductivity. Since the aortic intima is significantly more porous than the media, the model guesses that the other vessels are somewhat similar in this respect, even if the mismatch is not as extreme. As such, the spot grows because there is far less (intimal) resistance

to lateral flow away from the leak than for normal flow into the denser IEL/media. Below is a simple conservation of mass argument for the incompressible water flow that expands the spot.

The volume of an assumed circular tracer spot in the intima layer is $V_{spot} = \pi R^2 l$, where R is the radius of a spot and l is the thickness of the intima. The rate dV_{spot}/dt that the spot size changes arises from an imbalance between the inflow Q_{leak} of water through the leak, the inflow across the endothelial surface Q_E, and the outflow Q_M to the media below:

$$2\pi R l \frac{dR}{dt} = Q_{leak} + Q_E - Q_M , \qquad (1)$$

with Starling's law $Q_E = Lp_E \Delta P_E (\pi R^2 - A_{leak})$ and $Q_M = Lp_M \Delta P_M \pi R^2$ relating Q_E and Q_M to the product of their respective driving forces, ΔP_E and ΔP_M, and hydraulic conductivities, Lp_E and Lp_M, much of which is accessible to experimental measurements (see Part I). l is the intimal thickness and A_{leak} is the area of a leak which, if only the junctional area, is quite small. We shall estimate $Q_{leak} = Lp_{leak}\, \Delta P_{E\text{-}leak}$ from fitting the experimental data below, since the intimal pressure (and thus $\Delta P_{E\text{-}leak}$) at the leak is, as yet, unknown. Equation (1) assumes that there are no osmotic differences across the endothelium or the IEL and that the radial velocity in the intima is one-dimensional, i.e., depends only on R. This latter assumption is reasonable for a porous media (Darcy) flow, which satisfies potential flow equations (Happel 1965). Far from the leakage site, a steady-state balance implies that the filtration flux across each sublayer is equal to that across the entire wall, vis., $Lp_E \Delta P_E = Lp_M \Delta P_M = Lp \Delta P$, the latter whole wall quantities. (Part I uses this to calculate the average intimal pressure.) If one (crudely) neglects the variation in ΔP_E with radial position (the present model is just a mass balance, without a force balance, and is therefore too simple to include this variation) and applies this relation everywhere, one gets

$$\pi l \frac{dR^2}{dt} = Q_{leak} - Lp\Delta P A_{leak} = K', \qquad (2)$$

K' a constant. In reality, since Lp_{leak} is so much larger than Lp_E (Huang 1994), ΔP_E is smaller (and ΔP_M is larger) near the leak and its radial variation is what drives the radial flow in the intima. Thus this model underestimates the outflow Q_M across the IEL in the leak region and thus leads to either an underestimated Q_{leak} or an overestimated spot growth, with the former the case for a fitting of R vs. t to data as below. Clearly it will be best far from the leak. Nevertheless, Q_M still slightly exceeds Q_E due to the differences in area. Equation (2) attributes tracer spot growth to the excess fluid that enters through the leaky junction over what would have entered had the junction been normally permeable: the larger this mismatch, the faster the spot grows.

The solution to Eq. (2) is:

$$R = \sqrt{K(t - t_0) + R^2(t = t_0)}, \qquad (3)$$

where $K = \frac{K'}{\pi l}$, and the initial spot size is $R^2(t_0)$ is the radius of an endothelial cell (slightly different for each vessel) when the spot results from the junctions around a single leaking cell. The circulation time t_0 then represents the time at which the tracer arrives from the point of injection to the vessel in question. By doing a least-square fit of $R^2(t) - R^2(t=t_0)$ vs. t, we get values for t_0 and for K which, with values for Lp, ΔP and A_{leak}, yields Q_{leak}. Because, as noted in the previous paragraph, this fitting just gives a lower bound on Q_{leak}, and because the spot radius is most sensitive to Q_{leak} initially, the fitting procedure also underestimates the initial growth. As a consequence, this crude model should therefore lead to spurious negative values of t_0. At later times, though, one expects the model to fit reasonably well.

2.6. Statistics Analysis

Paired Student' *t*-tests are used for comparison between tracer spot sizes for one vessel type at different times or between vessel types. ($P<0.05$, statistically significant)

3. Results:

3.1. Ultrastructures of pulmonary artery and inferior vena cava

The ultrastructure of the PA is shown in Figures 1A, without stain on the left and with orcein stain, specific for elastin, on the right. It consists of continuous endothelium, intima, IEL and SMC. The intima is confined to a thin space between the endothelial cell and IEL. It contains some collagen fibers (Frank 1989). The orcein stain in Figure 1B confirmed the continuous elastin in the PA's media. Figures 1C shows the ultrastructure of the IVC. It has an abundance of collagen fibers. Figure 1D shows it has almost no, i.e., a very discontinuous, IEL and only sparse elastin. Figure 1E and F present the ultrastructure and light microscopy of the aorta for later comparison.

3.2. EM cross-sections of the pulmonary artery and inferior vena cava with HRP

With 7-13 min HRP circulation before sacrifice, Figure 2a shows how HRP reaction product distributes in the extracellular space of the PA in transverse sections. For such long circulation times, HRP also passes through the normal endothelial cell junctions, as seen in the figure. There are a few indications of cell vesicles (v) near the junction. HRP reaction product forms a thin, discrete, dark layer (~200nm) between the endothelium and the IEL, concentrating in and outlining the existence of the intima layer. A noticeable amount of tracer leaks through the IEL's fenestrae and appears beneath the IEL as well. Figure 2b shows the corresponding tracer-product distribution in the IVC. In addition to appearing in the normal junction and cell

vesicles, a thin, dark layer of the tracer product aligns beneath the endothelial cell despite the absence of a continuous IEL. The line has the thickness of ~135nm.

3.3. Endothelial cell radii measurement

The endothelial cell area (A) was measured from silver nitrate staining by dividing the total area examined by the number of assumed circular cell of area $A=\pi R^2$, where R is the radius of the cell. The PA endothelial cell has a radius of ~12 μm. The IVC has the radius of ~11 μm.

3.4. Discrete HRP spots and their growth with increasing circulation time

Figures 3 are *en face* views of the PA and IVC endothelia after 120s HRP circulation. The isolated brown spots, surrounded by much lighter yellow background, indicate focal leakage of HRP at these short circulation times. This indicates that molecules (e.g., LDL) larger than HRP likely traverse the endothelium only through rare leaky spots as well.

We now examine how focal tracer spots grow at 0.5, 1, 2 and 4 min circulation times for both the PA and the IVC. Each data point represents the average of ~3-4 spots per rat vessel times 4 rats. Figure 4b shows the result for the PA. At 30s, the spot size is 53.2±10.4 μm. It grow 40% ($P<0.05$) to 74.7±8.6 μm at 1 min and then slows down gradually. The spot sizes become 85.8±11.0 μm and 109.5±8.7 μm at 2min and 4 min, respectively; the increase in the spot size in this period is only 28% ($P<0.05$). The PA exhibits spot size growth that is surprisingly similar to the aorta's (see Figure 4a for our results and those of Chuang *et al* (Chuang 1990)). The next section focuses on this result in more detail.

Figure 4c shows the growth of tracer spots in the IVC for both FV and CA cannulations. Both curves exhibit focal spots that are uniformly much larger than in the aorta. The FV-cannulation, which was used for the aorta and PA spot size growth measurements, is far upstream from these arteries, but adjacent to the IVC. As such, there is almost not time delay or

tracer dilution due to circulation from the point of tracer introduction until its appearance in the IVC. The spot size is very large (192.56±62.8 μm) even at 30s and increases only slightly at later times to 206.59±80.03μm, 210.96±10.45 μm and 214.32±69.09 μm; spot size growth with circulation time does not appear significant (P>0.05). With CA-cannulation, the tracer is introduced upstream from the IVC and there is a time delay between tracer introduction and its appearance in the IVC. At 30s, the radius of the spot is about 132.86±37.32 μm. The spot size increased 28% (P<0.05) at 60s to 170.09±51.8μm. At the later times, the spot grows more slowly to 158.23±15.77μm (P>0.05) and 184.78±30.1μm (P>0.05).

3.5. Model results

We choose l = 100 nm (Huang 1994). Our observation, is that these radii are similar in all three vessels and we therefore use R_{leak} = 15 μm throughout. Lp and ΔP are available for each vessel from Part I. Despite the crudeness of the model, its root-t dependence fits the data adequately for all three vessels although, as noted in the methods section, not at short times. This underestimated short time growth is expected to lead to spurious negative values for the time t_0 at which the tracer arrives in the vessel. For the historic aorta data it yields t_0=-55 s, as compared with Huang *et al*'s much more thorough theory's value of ~+25s. For the PA, the arrival time t_0 comes out to -52s, very slightly less than the aorta's, as one would expect. For the IVC, however, if one assumes that the spot originated from the junctions around a single endothelial cell, one finds t_0=-321 s. Extrapolating the curve back to various assumed t_0 yields different initial spot radii. For t_0~+25s the radius is 9 cell radii; a similar underestimate t_0~-56s as in the arteries yields an initial radius of ~8.5 cell radii.

From the model's fit, the PA has K = 40.8 μm^2/s, Q_{leak} = 37.3 μm^3/s and $Lp\Delta PA_{leak}$= 24.52 μm^3/s, the aorta has K = 43.8 μm^2/s, Q_{leak} = 33.6 μm^3/s and $Lp\Delta PA_{leak}$= 19.8 μm^3/s and the IVC has K = 60.5 μm^2/s, Q_{leak} = 40.3 μm^3/s and $Lp\Delta PA_{leak}$= 21.2 μm^3/s.

4. Discussion

The goal of this paper is to study the transport of macromolecules from the lumen into the walls of PA and the IVC and to see how it differs from that into large, atherosclerosis-susceptible vessels such as the aorta. Specifically, we investigate whether this transport is focal or uniform and, if focal, how quickly the localized spots spread. This may indicate whether or not such spread is convection dominated, as in the large arteries. It may also shed light on whether and how the critical transport processes in these vessels distinguish benign transport from those that may trigger atherosclerosis. We interpret vessel-vessel differences in terms of differences in vessel structures and filtration properties such as Lp, measured in Part I.

4.1. Ultrastructures

Large arteries such as the aorta typically suffer time-averaged transmural pressures of ~100 mmHg and have a low hydraulic conductivity, leading to a transmural water flow that is orders of magnitude slower than the downstream flow (Chapter 3). As noted in the introduction, focal endothelial leakage allows macromolecules such as LDL or HRP to enter the vessel wall via a convection-dominated process. The vessel ultrastructure of a thin, ultra-porous intima and a thick, dense media facilitates the rapid spread of these molecules in the intima ((Stemerman 1986), (Chuang 1990), (Chen 1995)) and allows them to remain there at high concentrations long enough to bind to intimal extracellular matrix. (Huang *et al*.'s (Huang 1994)) structure-based (Frank 1989) *ab initio* transport parameter theory found that the filtration resistance of the intima

is one to two orders of magnitude smaller than that of media.) These are believed to be the earliest in a cascade of events leading to lesion formation. We begin by examining if any of the structural features carry over to less susceptible or immune vessels.

The PA has a physiological pressure of ~16 mmHg, with a hydraulic conductivity ($2.34 \cdot 10^{-7}$cm/s/mmHg) that is roughly proportionally lower than that of the aorta ($2.8 \cdot 10^{-8}$cm/s/mmHg), thereby leading to a comparable transmural water flow. ($Lp\Delta P$ for the PA is ~$29.6 \cdot 10^{-7}$cm/s vs. $29 \cdot 10^{-7}$cm/s for the aorta.) The structure of the PA resembles that of the aorta. It consists of continuous endothelium, intima, and IEL (which serves as an additional filtration barrier (Chen 1995)), with a thick media consisting of continuous strips of elastin separated by SMCs and extracellular matrix. See Figures 1A & 1E (tracer free) and Figures 2a & 2b (with tracer). The intensity of the immediately subendothelial HRP accumulation, a ~200nm stripe, in Figure 2a suggests that the PA's intima is also much sparser than its media and of comparable size to the aorta's. Tompkins (Tompkins 1989) measured the ^{125}I-LDL (30min circulation) and HRP (1min circulation) concentration distributions resolved in ~10 sections across the vessel wall for various vessels, including the PA, of squirrel monkey. He found a much higher tracer concentration in the first layer near the lumen that falls dramatically with the depth concurs, which is consistent with the PA having a sparse intima. This will be important to the interpretation of the observed spot sizes below.

The IVC is the largest and most accessible vein in this small animal model. It has a low physiological pressure of 5 mmHg, but also the lowest Lp, thereby resulting in a similar transmural water flow to the other two vessels. Its structure, however, is much looser and less compact than the other vessels (Figures 1), consistent with its much higher Lp. Its media's elastins are very sparse - they can only be seen with a much higher concentration of the elastin-

specific stain orcein than needed for the arteries - and discontinuous and only rare fragments of an IEL. Its media is the thinnest and has an abundance of collagen fibers (Figure 1C), which accounts for its much lower distensibility (Figure 1D). Consequently, the IVC lacks a definite boundary that highlights an intima layer (Figure 2c). Our finding of intense HRP staining just beneath the endothelium with a sharp drop in intensity below argues that the IVC appears, despite the lack of an IEL, to have an intima layer that is similarly sparse and similar in thickness to those in the arteries. This would explain Tompkins' (Tompkins 1989) high LDL concentration in the first decile of the IVC wall near the endothelium. This is consistent with the fact that endothelial cells synthesize an intimal extracellular matrix that is very different from that made by the SMCs in the media, and these syntheses do not appear dependent on an IEL ((Lark 1988)).

4.2. Tracer spots and their growth

In both vessels the tracer HRP (~5 nm diameter (Chen 1995)) crosses the endothelium at rare, isolated leaks, rather than uniformly, at short circulation times of <5min. It follows that the much larger LDL (~22nm diameter) should follow the same trend, potentially even at longer times. Figure 4a shows that, despite the lower transmural pressure driving force ΔP in the PA, the spot growth with tracer circulation time in the PA and in the aorta taken in our lab (Figure 4(b)) are very similar in both the trend exhibited and in the actual spot sizes at the same circulation times (P>0.1). (Figure 4a shows that our aortic spot sizes compare well with Chuang *et al*. (Chuang 1990); they are slightly lower, but with overlapping error bars. The slight difference may be due to the judgment used to define the precise spot border.) Given the similarity in the ultrastructures and in the sizes of the transmural water flows in these two vessels, this suggests that tracer entry into the PA's wall and its intimal spread are likely

convection-dominated, as in the large arteries. These similarities also render the result less baffling than one might have thought based solely on their transmural pressures.

The crude model proposed above allows for some quantitative comparisons. First, the adequate fit of the root-t model is consistent with the spot growth being convection-dominated, as is its similarity to the growth in the aorta, which was shown to be too fast to be consistent with pure diffusion for any reasonable diffusivity (Huang 1994). Because the root-t model underestimates Q_{leak}, it gives a curve that is *initially* flatter than the data and, consequently as already noted, a spuriously negative/meaningless time of tracer arrival in the vessel of -52s for the PA and -55s for the aorta. Finally, from the model's fit, the PA has K = 40.8 μm^2/s, Q_{leak} = 37.3 μm^3/s and $Lp\Delta PA_{leak}$= 24.5 μm^3/s while the aorta has K = 43.8 μm^2/s, Q_{leak} = 33.6 μm^3/s and $Lp\Delta PA_{leak}$= 20.0 μm^3/s. This suggests that comparable spot sizes means the convective flows through isolated aortic and PA endothelial leaks are comparable as are the areas of the leaks.

We now turn our attention to the IVC. Figure 4c shows the experimental spot-size curves for both FV and CA cannulations. We measured the spot growth for the aorta, the PA and initially for the IVC using FV cannulations. However, unlike for the arteries that were far downstream of the FV, the IVC's proximity to the FV left essentially zero time delay between tracer injection and its arrival in the target vessel and the HRP tracer was not yet diluted in the surrounding blood when it arrived there. As such, the time points for the IVC curve with FV cannulation were shifted by circa 25s from those of the other vessels and the spots appear larger because the local lumen concentration feeding the spot is higher in the FV cannulation. Since, even if convection is important, diffusion may not be negligible in IVC transport and since the measured size of the spot depends on the concentration level of detectability of the HRP reaction product, a higher local lumen HRP concentration makes the spots look larger (see figure). To

correct this problem and to access earlier circulation times, we performed CA cannulation experiments.

The FV-cannulated IVC spot size curve in Figure 4c is relatively flat, with only a slightly lower 30s value and it is uniformly much larger than the aortic and PA curves. The CA-cannulation curve is, as expected, a bit lower and shifted ~25s to the right relative to the FV-cannulated curve. It is also essentially flat, except for a lower value at 30s that differs from the 4 min value by a far smaller percentage than in the arteries. The much larger magnitude relative to the aorta is consistent with Chuang *et al*'s (Chuang 1990) finding that veins tend to have clusters of dying cells, rather than single cells that leak. When a cell is dying, a cluster of neighboring cells might burrow underneath the dying cell in order to slough it off without leaving a large hole. This might stretch their junctions temporarily and lead to leakage of the cluster of cells, rather than just a single cell ((Takahashi 1983), (Weinbaum 1985)). In any case, although the root-t model gives a spurious negative t_0 values, t_0's large size relative to the arteries suggests a much larger initial leak radius (The model suggests a clearly too large radius of ~127.5 μm≈8.5 cell radii) than one EC radius, which is consistent with this explanation.

What appears to be the asymptotic spot size for the IVC is 39% larger than its 30s value, as opposed to 105% and 106% for the aorta and PA. The contrast is even larger when one compares the apparent asymptotic spot sizes with the estimated sizes of the leaks themselves in the form R(t)-R(0) or normalized as (R(t)-R(0))/R(0), equal to 6.5 for the aorta, 6.3 for the PA and 0.45 for the IVC, all for the same t_0. Whereas these precise values are not significant due to the inaccuracy of the model at short times, but they illustrate that the IVC curve is nearly flat relative to the aorta and PA curves. That the IVC spots grow neither nearly as fast nor as far as in the other vessels, despite its apparent thin, very porous subendothelial intima and overall

transmural water flow that appears comparable to those of the arteries requires discussion. The first piece of relevant information is that, even though Tompkins found higher tracer concentrations in the decile of IVC wall nearest the lumen than in the subsequent deciles, the mismatch was not as stark, since the IVC's media's concentration was higher than the aorta's. Moreover, Part I found that the Lp of the IVC media was substantially larger than in either of the arteries in question (45 times the aorta, 10 times the PA), both as a result of the much thinner and evidently much more porous IVC media, consistent with the much higher water content (81%) of the IVC relative to the PA (76%) and the aorta (64-69%). As a result, it would seem likely then that, despite the large transmural water flow, the overriding water flow direction in the IVC's intima is normal, rather than parallel, to the endothelium. This dictates more modest spot growth. Moreover, the IVC media had a greater distribution volume (0.051for albumin) than that of the aorta (0.009) (Lever 1990). Since this mismatch in intima/media void spaces is not as stark as in the arteries, it suggests that the tracer can more easily distribute between the two regions and even efflux from the tissue into the extravascular space, and thus not build up to as high concentrations in the IVC's intima.

This may, indeed, be the reason why, despite the similarity in overall water flow between the three vessel types and despite the large spots in the PA and in the IVC, only the large, high-pressure arteries are susceptible to lesions under normal conditions. This line of argument has motivated our current development of more detailed convection/diffusion theories for tracer transport into the PA and IVC walls and to confocal microscopy studies of tracer spots. These theoretical and experimental studies seek to determine the spatially distributed (as a function of radial distance from the leak and of depth into the wall) intima tracer concentrations in these

vessels, as opposed to the spot size measurements that correspond to (projections) integrals of the tracer concentration over the direction normal to the endothelium.

Applying Eq. (3) to the CA-cannulation data gave K = 60.53 μm^2/s, Q_{leak} = 40.26 μm^3/s and $Lp\Delta PA_{leak}$ = 21.24 μm^3/s. K and Q_{leak} through the IVC's leaky site are double that of the other vessels. However, if the IVC leak is due to a cluster of dying/leaking cells, it is more appropriate to calculate the flow per leaking cell $q_{lea} = Q_{leak}/N_{leak}$ where N_{leak} is the number of leaking cells. For the aorta q_{leak}= 0.047 μm/s and for the PA, q_{leak}= 0.057 μm/s. We know that the IVC has a leak radius that is larger than one (the root t model's leak radius of 8.5 cell radii is clearly far too large), and thus its leak q_{leak} per cell will certainly be smaller than for the arteries.

5. Concluding remarks

This paper has reported HRP tracer transport experiments to gain insight into the way in which macromolecules enter into the walls of blood vessel, as occurs in the early stages of LDL accumulation processes. We examine the growth of tracer spots with tracer circulation time in the rarely atherosclerotic pulmonary artery and in the resistant inferior vena cava and compare to growth in the susceptible aorta. The goal is to see what differences in such processes tell us about vessel disease susceptibility. This paper discusses the results in conjunction with the differences in ultrastructures and hydraulic conductivities among these vessels.

Although the pulmonary artery experiences a lower transmural pressure (16 mmHg) than the aorta (100 mmHg), the rapid convection-driven growth in the PA of a tracer spot from a radius corresponding to a single leaky endothelial cell to roughly nine cell radii in ~4min is similar to that in the aorta. The two vessels' similar ultrastructures suggest a similar line of reasoning. In the aorta, the tracer spreads in the sub-endothelium intima layer that is bordered by

a continuous, presumably less permeable IEL. The similarity in spot growth at 1/6 the pressure driving force indicates that the PA must be more permeable than the aorta. This is consistent with measurements in Part I showing that the Lp of the PA is nearly an order magnitude larger than that of the aorta. The combination of Lp and transmural pressure data lead to similar overall transmural water flows and thus to the plausibility of similar rates of tracer spot growth. A crude root-t model infers from the similar spot growths that the flow through the leak into the intima is similar in both vessels.

The inferior vena cava (IVC) suffers a very low transmural pressure of ~5 mmHg. Its spot growth is quite different from those in the arteries. The spots appear to originate from a cluster of leaking cells, as Chuang (Chuang 1990) noticed, and to grow only a small percentage in 4min. Despite its absence of a continuous IEL or, in fact, much elastin, we have found evidence of a sparse, subendothelial intima in the IVC, as in the arteries. Chapter 3 found that the balance between a much higher Lp and a lower Δp in the IVC nevertheless leads to an overall transmural flow that is comparable to those in the arteries. However, probably because its media is much more porous (Lever 1990) (and thus has this much higher (Chapter 3)) than the arteries' media, the water flow in the intima is likely directed differently, being predominantly in the direction normal to the endothelium. This contrasts with the situation in the arteries' subendothelial intimas that drives the rapid formation of large spots there. The crude root-t model infers from the data that the total water flow through the leak into the intima in the vein is roughly double that into the arteries, but the flow per leaking cell is smaller. The combination of this and the IVC's larger media porosity suggests that even though there seems to be more tracer swept into the IVC than into the arteries' walls in each leak, the macromolecules swept in would have a much easier time escaping/effluxing before being detained.

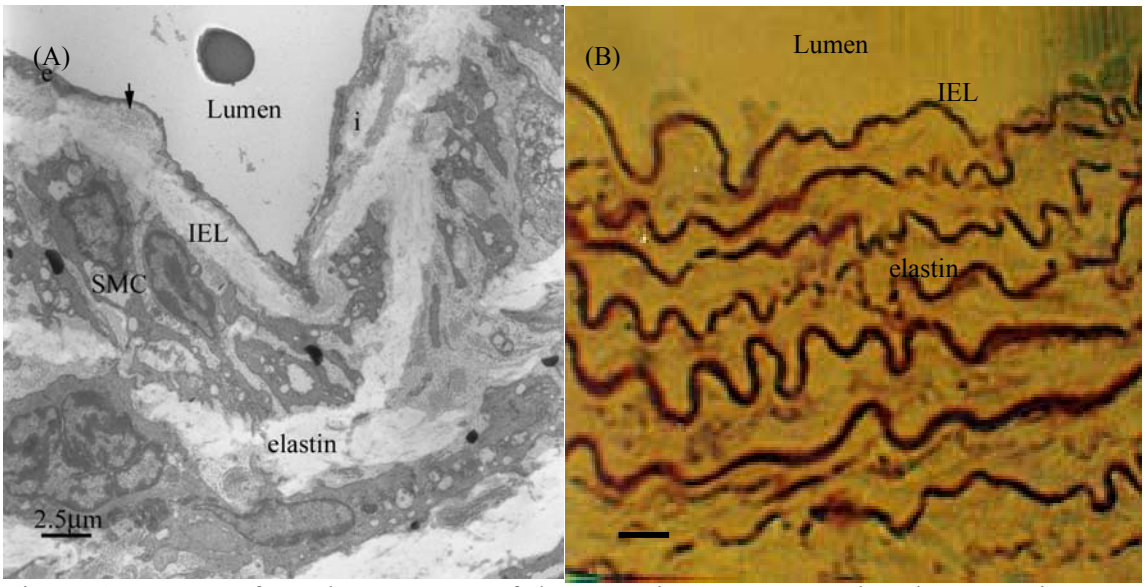

Figure 1A. Tracer-free ultrastructure of the rat pulmonary artery by electron micrograph shows continuous endothelium (e), intima (i) internal elastic lamina (IEL) and smooth muscle cell (SMC). The arrow points to the collagen fiber in the sub-endothelial intima (bar represents 2.5 µm). B. Orcein stain of the PA elastin. (bar represents 10 µm)

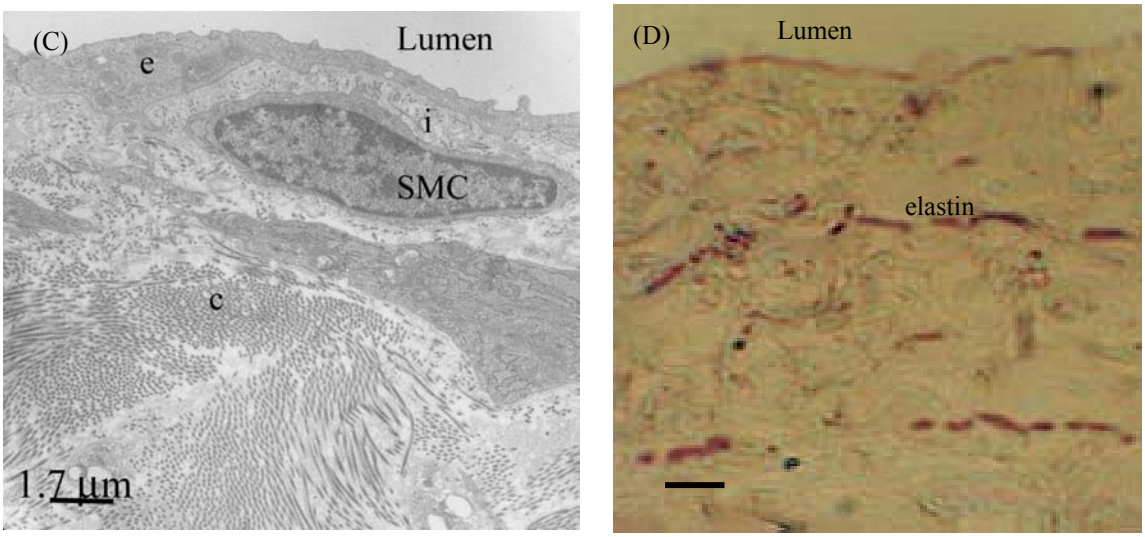

Figure 1C. Tracer-free structure of the inferior vena cava shows a monolayer of endothelium (e), smooth muscle cell (SMC) and cross-section of abundance of collagen fibers (c). The space between the endothelium and SMC is the sub-endothelial intima (i). (bar represents 1.7 µm). D. Orcein stain of the IVC elastin. (bar represents 10 µm)

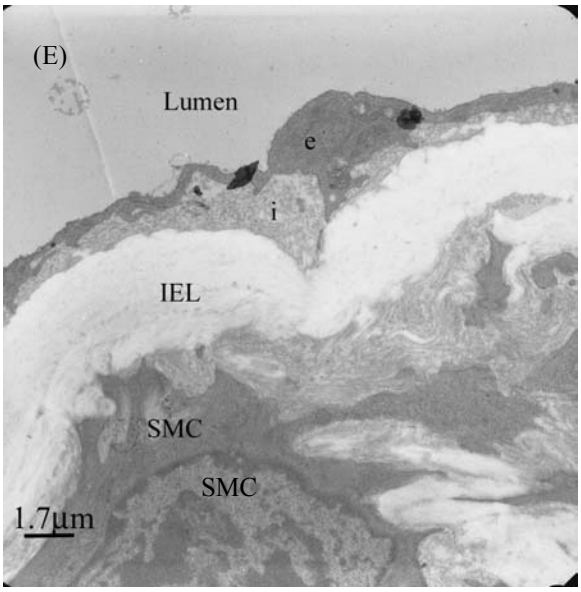

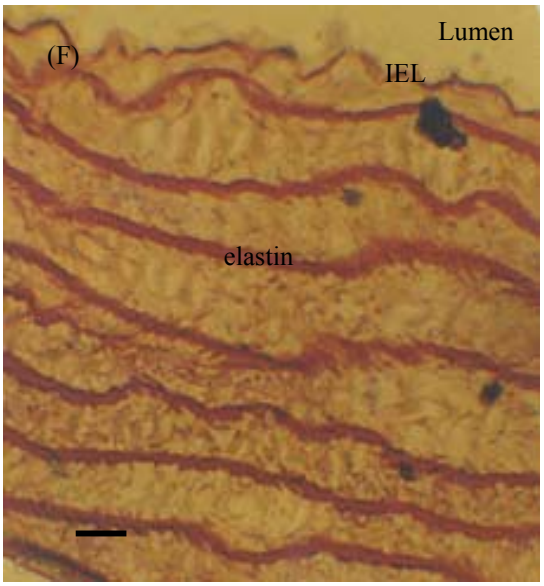

Figure 1E. Tracer-free electron micrograph of the rat aorta shows a monolayer of endothelium (e), internal elastic lamina (IEL) and smooth muscle cell (SMC). Between the endothelium and IEL, there is the intima (i). (bar represents 1.7 μm). F. Orcein stain of the aortic elastin. (bar represents 10 μm)

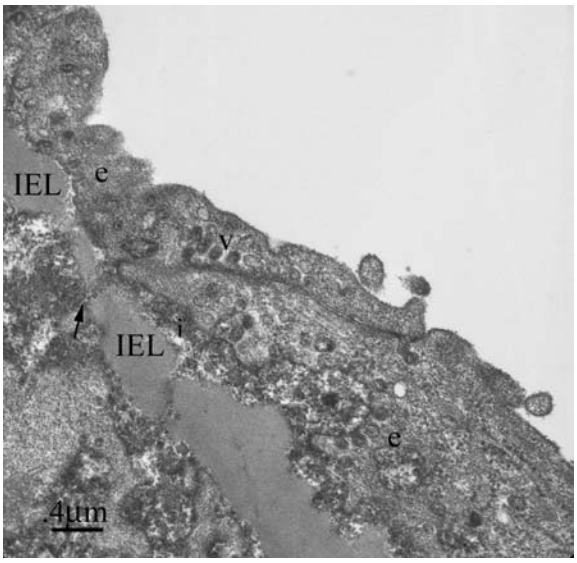

Figure 2a. Ultrastructure of the rat pulmonary artery with HRP tracer (7 min). The arrow points the fenestra with HRP tracer (e: endothelium; i: intima; v: vesicle; IEL: internal elastic lamina). (The bar represents 0.4 μm)

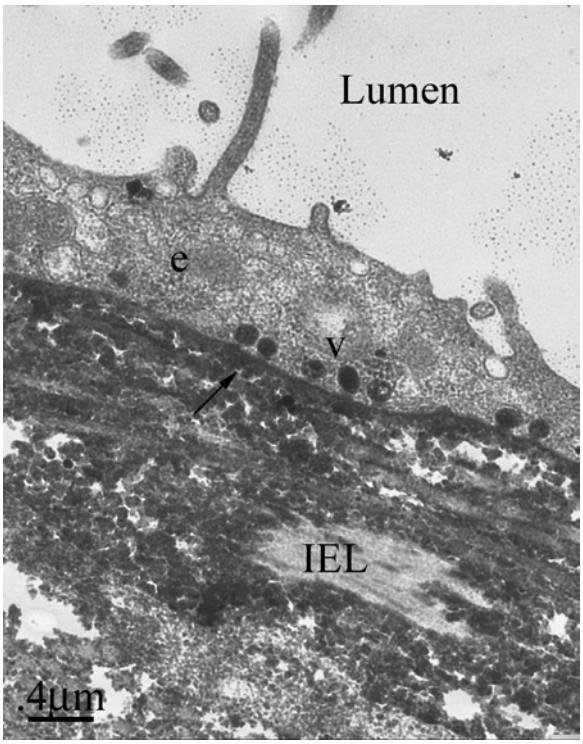

Figure 2b. Transmission electron microscopy of rat inferior vena cava with HRP tracer (7 min). The arrow point is the outline of the HRP tracer in the subendothelial intima region. (e: endothelium; v: vesicle; IEL: internal elastic lamina) (The bar represents 0.4 μm)

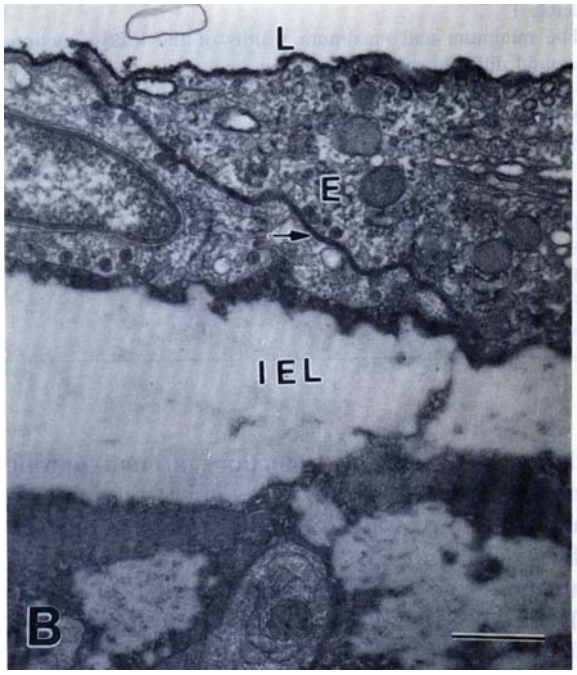

Figure 2c. Transverse section of aorta electron micrograph. The arrow points the normal cellular junction with HRP tracer (5 min). The tracer outlines the sub-endothelial intima. (E: endothelium; IEL: internal elastic lamina) The bar represents 0.5 μm. (Courtesy of Chen *et al*., (Chen 1995))

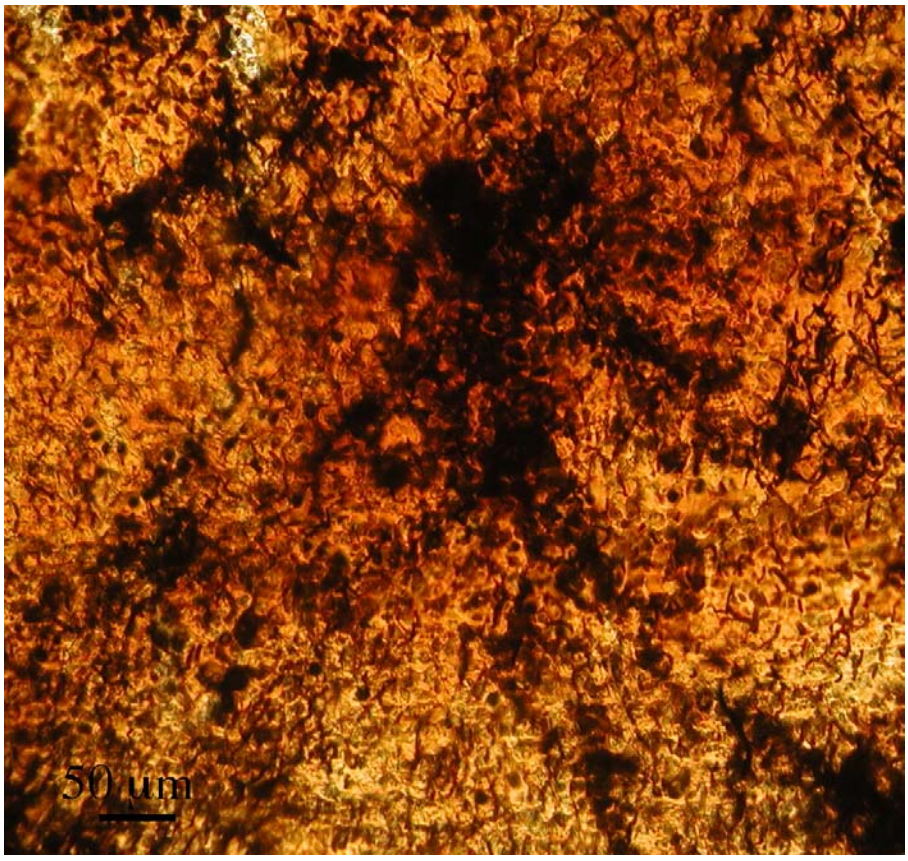

Figure 3a. *en face* view of the pulmonary artery endothelia with 120s HRP circulation. The dark brown spot indicates the focal HRP leakage. Bar=50 μm

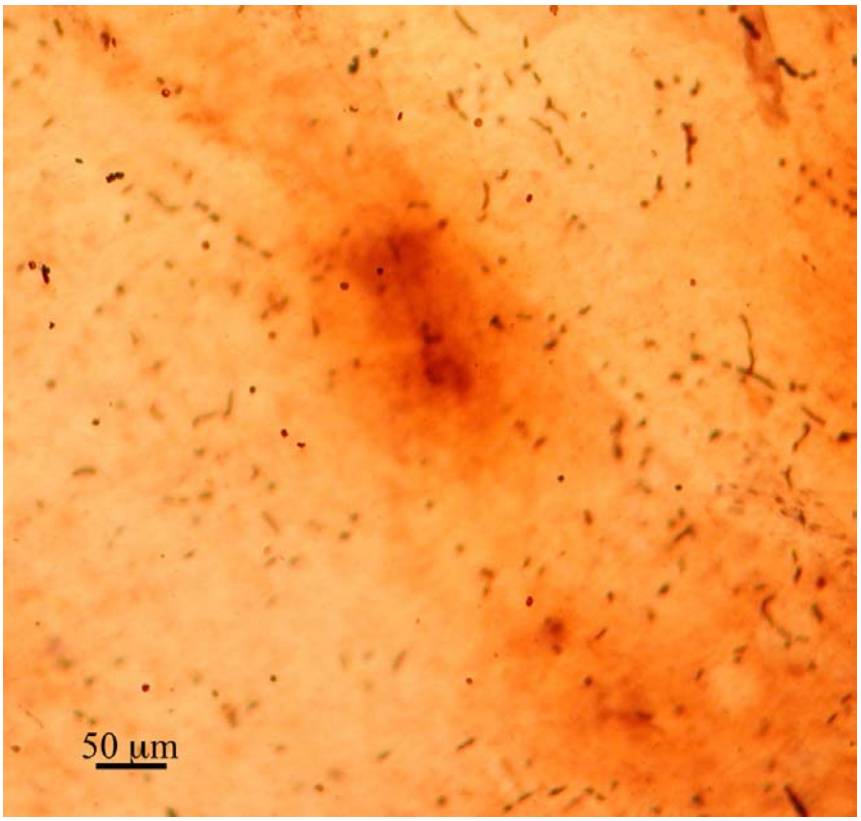

Figure 3b. *en face* view of the IVC endothelia with 120s HRP circulation. The brown spot indicates the focal leakage against the light yellow background. Bar=50 μm

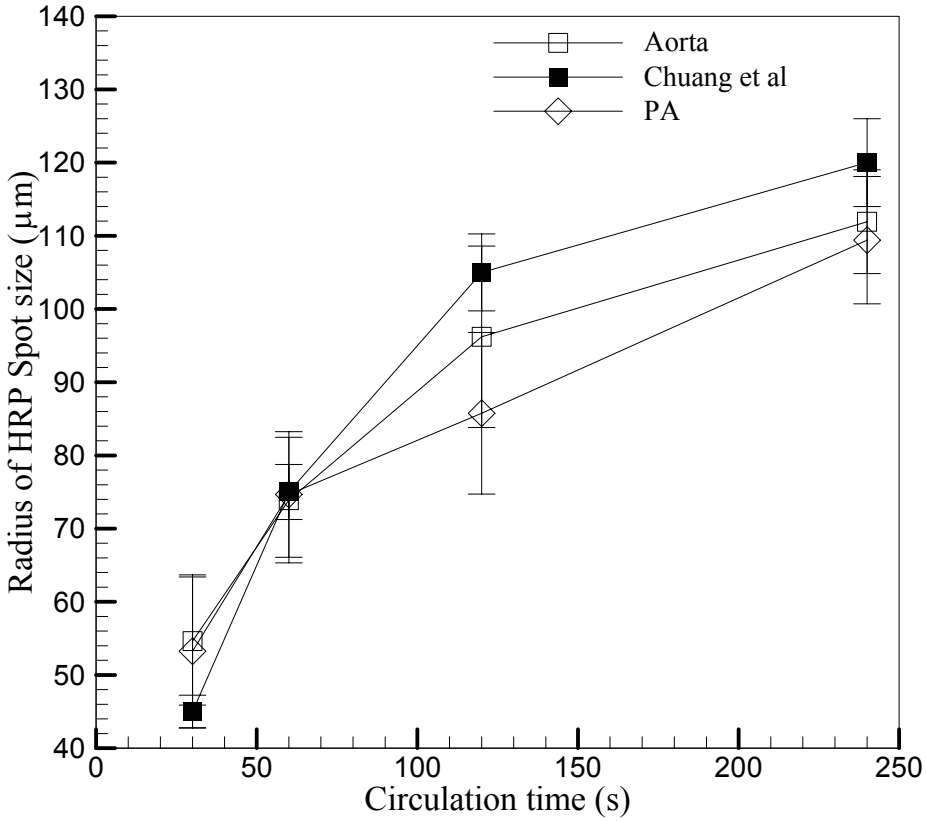

Figure 4a. Spot size of the rat aorta and PA. The tracer spot grows about 35% from 30 to 60 s for the aorta ($P<0.1$) and the growth slows down afterwards. Compared with Chuang *et al*. (Chuang 1990), the results were in reasonable agreement. The PA follows similar trend ($P>0.1$) and increases 40% from 30 to 60 s ($P<0.1$). Number of rats (n) is 4.

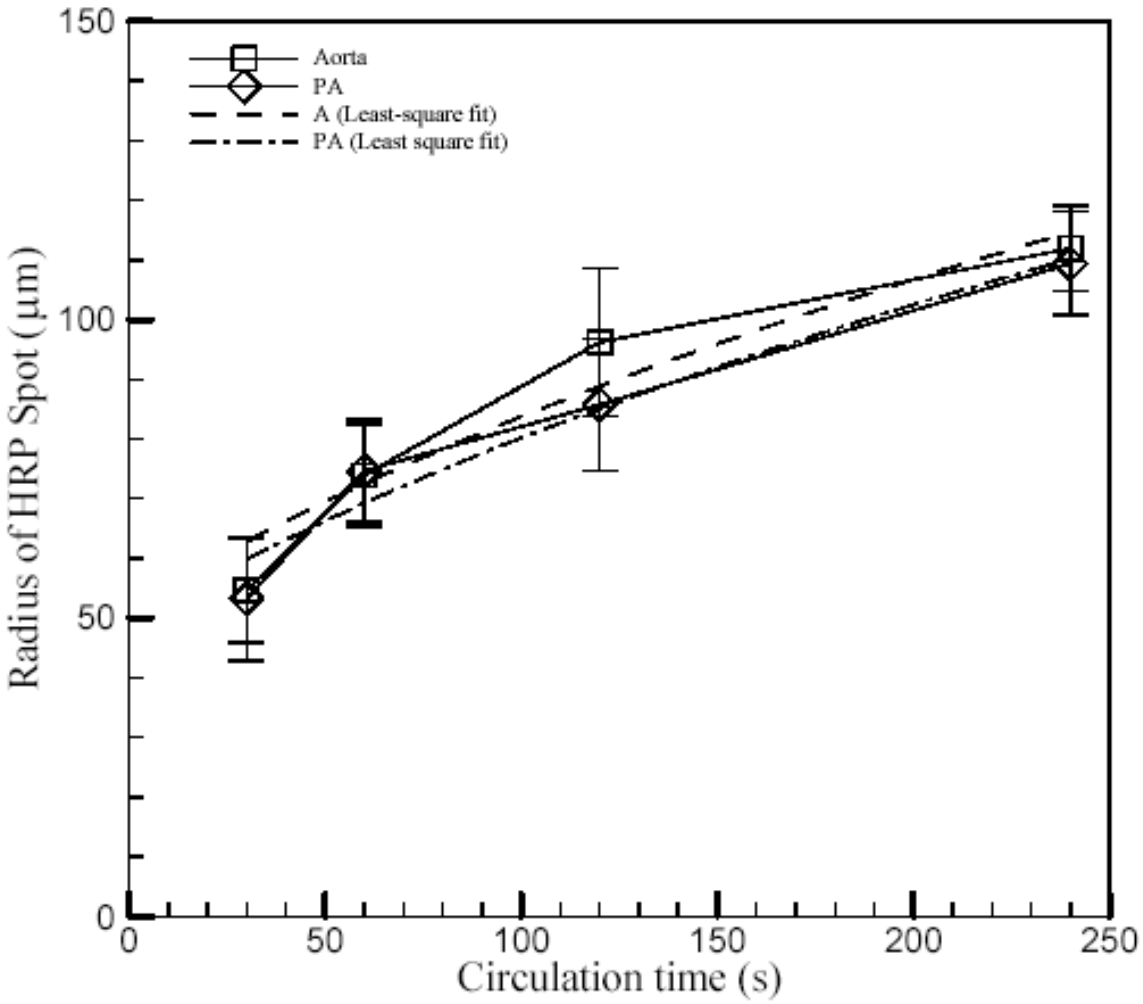

Figure 4b. Spot size of the rat aorta and PA comparing to the root-t model. The model (dash-dot line) underestimates the growth of the aorta (K = 45.5 μm^2/s, Q_{leaky} = 34.1 μm^3/s). K = 43.2 μm^2/s, Q_{leaky} = 38.07 μm^3/s for the PA.

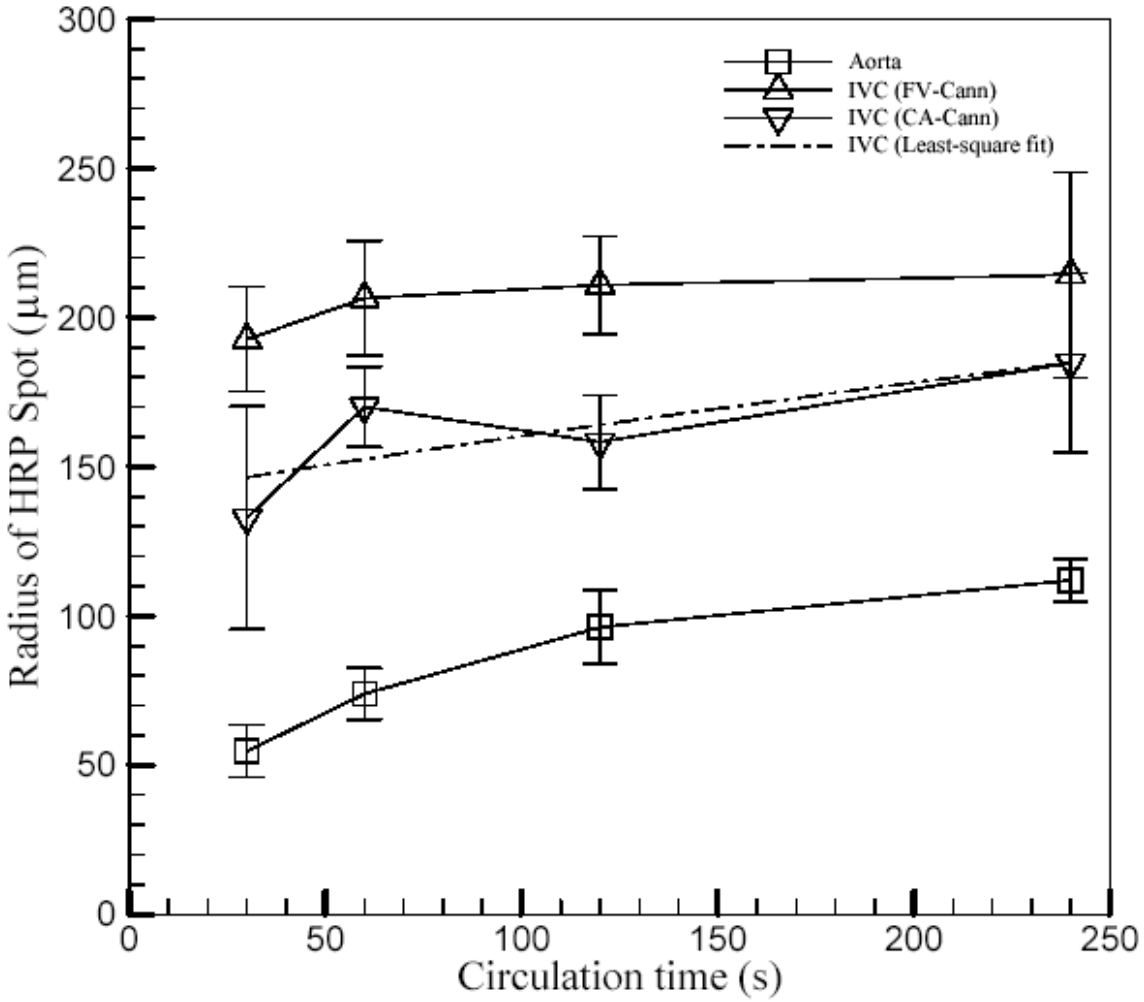

Figure 4c. Spot size comparison of the aorta and IVC. The IVC of both femoral vein (FV-cannulation) (n = 4) and carotid artery (CA-cannulation) (n = 4) cannulation have relatively flat trend (P>0.1). The CA-cannulation shows about 28% of the spot size growth from 30 to 60 s (P>0.1). The 30-s spot of the IVC is about 1.7 times that of the aorta (P<0.1). The model (Dash line) predicts the spot growth K=78.53 $\mu m^2/s$ and Q_{leaky} = 45.91 $\mu m^3/s$ of the IVC.

Chapter 5

Preliminary studies of the role of aquaporin 1 to the hydraulic conductivity of the rat aortic wall and its endothelium

1. Introduction

Atherosclerosis is the leading cause of death in Western countries both above and below age 65. It afflicts large arteries such as the aorta (Vander 2001) and is triggered by low-density lipoprotein (LDL) transport from the blood into the arterial wall where it accumulates. Blood-borne monocytes enter lipid-laden subendothelial intimal arterial regions and transform into macrophages as they and media-derived smooth muscle cells scavenge extracellular cholesterol ((Ross 1986), (Selzer 1987)). When overwhelmed, they form foam cells, which appear to start the formation of the earliest lesions. These eventually thicken the arterial wall, narrowing the cross section for blood flow, making arterial wall less complaint and increasing the risk of a lesion rupture or of blockages.

A monolayer of the endothelial cells separates the lumen from the thin, sparse subendothelial intima. An internal elastic laminar (IEL) borders the intima, followed by the dense tunica of media comprised of a repeated structure of elastin sheets separated by extracellular matrix and smooth muscle cells (SMC). Beyond the media is the loose adventitial layer. Stemerman *et al* (Stemerman 1986) showed that macromolecules rapidly cross the endothelium focally through isolated hot spots, and not uniformly. Weinbaum and co worker ((Weinbaum 1985), (Wen 1988)) suggested that such leaks correspond to dying or mitotic endothelial cells that consequently have temporarily widened or not-yet-formed intercellular

junctions, and therefore allow macromolecules too large to pass through intact junctions to leak into the arterial walls. Lin *et al*. ((Lin 1988), (Lin 1989)) showed that 99% of the cells in mitotic (M) phase are associated with Evans blue albumin conjugate (EBA) leakage and the 80% of cells in M-phase leaked Lucifer yellow-LDL (LY-LDL). Truskey *et al*. (Truskey 1992) used autoradiography to measure the permeability of ^{125}I-LDL and found approximately 25% of the leakage sites were associated with mitotic cells.

Chuang *et al*. (Chuang 1990) studied the rapid subendothelial spread of HRP with increasing tracer circulation time. They found that localized HRP spots in the aorta initially grew very rapidly and then appeared to slow down, reaching almost ~200 μm in diameter after 4 min circulation time. Such growth was not consistent with a diffusion-dominated mechanism for any reasonable diffusivity. Yuan *et al*'s (Yuan 1991) unsuccessfully tried to explain this data in terms of a mathematical model that included some ultrastructural details of the vessel wall. Huang *et al*. (Huang 1994) incorporated the observed extremely sparse subendothelial intima matrix structure into a two-dimensional convection-diffusion mathematical model and were able to explain these HRP spot data. These studies show that transendothelial convection plays a crucial role in tracer transport into the vessel wall. When there is no osmotic pressure gradient across the wall, Starling's law, $Q = Lp\mathrm{A}\Delta P$, describes the flow rate Q across a section of wall of outer surface area A, where the transmural pressure ΔP is the driving force and Lp is the hydraulic conductivity of the wall. Its reciprocal reflects the flow resistance. Lp of the wall and of its individual layers are critical transport parameters for convection that depend on the wall's ultrastructure.

Various techniques have been used to measure Lp, the best of which involves excising the vessel under pressure so as to preserve its endothelium and then hooking it up to a system

that controls the transmural pressure and measures the transmural flow and the vessel area ((Tedgui 1984), (Baldwin 1993)). In previous Chapter (Chapter 3), we modified and adapted this procedure, originally used by these investigators on rabbit aorta, to the much smaller rat vessels and found Lp as a function of ΔP that agrees qualitatively with Baldwin and Wilson's (Baldwin 1993) and quantitatively with Tedgui and Lever's (Tedgui 1984) rabbit aorta results.

Until now it has been assumed that the endothelial hydraulic conductivity corresponded to transport through inter-endothelial junctions ((Truskey 1981), (Fry 1985),(Huang 1994)), through which water is small enough (1.2 Å) to pass. Another pathway known for water transport is diffusion through pure lipid bilayers of the cells (Sidel 1957). The last decade brought the identification of the ubiquitous class of extremely specific, aquaporin (AQP)–water channel membrane proteins (Verkman 1992). Aquaporins 0-9 have so far been identified in various cell types from plant ((Fortin 1987), (Johanson 2001)) to animal tissue cells, including erythrocytes (Cho 1999), smooth muscle (Shanahan 1999) and epithelial and endothelial (Nielsen 1993) cells, among others. Endothelial cell have been observed to contain type 1 AQP (AQP-1) (Nielsen 1993), also known as CHIP28 (channel forming integral protein, 28 kDa). An AQP-1 unit is a tetramer with each of the four circa 60 Å long monomers providing a water pore (Figure 1). The AQP-1 pore has a dumbbell shape (Figure 2) with a wide opening of about 15 Å to the extracellular space. About 20 Å from the opening, the pore constricts down to 2.8 Å in diameter, hence giving rise to AQP-1's high selectivity ((Sui 2001), (Murata 2000)). The sulphhydryl group of Cysteine189 (Cys189) of AQP-1 plays a critical role in the functioning of the water channel. It is located in the pore near the extracellular side of the constriction (Figure 3) (Sui 2001)) and is sensitive to mercury (Preston 1993). A mercury ion (Hg^{2+}) (with a size of 2.2 Å) can bind to the Cys189 and block the narrow pore's neck (~2.8 Å), thereby blocking the

channel's ability to transport water. A number of studies have used mercuric chloride ($HgCl_2$) as the blocker of water permeability in isolated cells deriving from the lung (Schnitzer 1996) and the kidney (Zhang 1993). Waltz *et al*. (Waltz 1994) used a transmural osmotic gradient in the absence of a transmural pressure to swell aquaporin-containing synthetic membrane vesicles, and from the swelling rate calculated the hydraulic conductivity l_p=3.85x10^{-18} cm^5/N·s for a single water channel. Detailed molecular dynamics simulation (Zhu 2002) of single water channel also calculated l_p and found the value 2.0±0.3x10^{-17} cm^5/N·s.

J. Toussaint in our lab has used immunohistochemistry with anti-aquaporin-1 antibodies to show that rat aortic endothelial cells express this protein in their cell membrane. The aim of this study is to investigate whether and, if so, to what extent these aortic endothelial cell AQP-1 channels contribute to the aortic endothelial hydraulic conductivity, i.e., to water transport, and thus to the subsequent macromolecule tracer transport, across the endothelium. Our approach is to measure, as in Part I, Lp of rat aorta excised under pressure to again preserve its endothelium, as a function of transmural pressure in the absence of aquaporin blocker. Since measurement of Lp alone cannot distinguish contributions from different water pathways, we then introduce $HgCl_2$ into the vessel to block the AQP-1 channels in its membrane and repeat the measurement of Lp(Δp) on the same vessel for the same transmural pressures. This is the first measurement that we know of using $HgCl_2$ to modify Lp of a vessel, rather than of a single cell.

2. Methods:

2.1. Experimental setup

As in Chapter 3, we have modified Tedgui & Lever's (Tedgui 1984) experimental setup and adapted it to the rat. The pressures in two large pressure reservoirs (A & B) are each

controlled by a separate monometer. Each pressure reservoir is connected to its own solution reservoir, and the two sets of solution reservoirs are connected to opposite ends of the excised aorta (Figure 4). Reservoir A_1 & B_1 contain phosphate buffered saline (PBS) solution with 4% (w/v) bovine serum albumin (BSA, Fraction V, Fisher Scientific), 10^{-3}M of $NaNO_3$ (Sigma, MO) to reduce smooth muscle cell contraction and 0.03% (w/v) trypan blue. Reservoir B_2 contains $HgCl_2$ at the concentration of the experiment with 4% BSA in PBS solution. Reservoir A_2 is a waste container. A three-way connector connects the solution reservoirs A, a 1-ml syringe that introduces the air bubble, and the 120 mm Tygon catheter of inner diameter 0.5 mm. The trypan blue serves two purposes: If the intense blue dye appears in the adventitia against its background of clear medium, this means the vessel has a leak. We then attempt to secure the leak; otherwise we must discard the vessel. We had to discard 2 out of 10 aortas. Trypan blue is a vital stain that penetrates the cell wall of dead cells and thus can indicate if the vessel is dying ((Baldwin 1993), (Tedgui 1984)).

All protocols were IACUC-approved.

2.2. Procedure

Twenty-two healthy male Sprague-Dawley (SD) rats (Charles River, CT) on a normal diet weighing between 250 and 350 g were used for measurement as well as for $HgCl_2$ titration. Four of the rats were given 1.0 mM $HgCl_2$, five 0.5 $HgCl_2$, three 0.25 mM, three 0.1 mM, two 0.02 mM, and an additional five 0.01 mM $HgCl_2$. After anesthesia with 1% pentobarbital sodium (Sigma, St. Louis, MO, 15 mg/500g rat, i.p.), a 0.5 ml of heparin (1,000 units) intravenous injection prevented blood coagulation. A rodent respirator kept the rat ventilated. After opening the chest and carefully dissecting the fat, we exposed the aorta from the rest of the fat and connective tissue and tied the first five pairs of intercostal arteries. The aorta was cannulated

from the distal end with a catheter filled with solution from Reservoir A_1 and pressurized at 60 mmHg. The lumen of the aorta was washed with this solution. We then inserted a second cannulation from Reservoirs B right below the aortic arch, excised the vessel and placed it in a bath of PBA solution that contains 4% BSA and 10^{-3} M $NaNO_3$. Both the vessel and the bath were kept at 37^{o}C. Refreshing the solution every 30 min. kept the medium well oxygenated. By this point ~1.5hr had elapsed.

To begin the measurement, we closed the valves 2, 3 &4, introduced a bubble into the horizontal catheter leading from Reservoir A_1 at 40 mmHg, and then increased the to the desired value. Due to the incompressibility of the fluid medium, monitoring the movement of the bubble's front meniscus at the given pressure provided a measurement of the flow rate through the vessel wall. The experimental pressures ranged from 60 - 140 mmHg at 40 mmHg increments. For more detail, see Chapter 3. At each pressure, the bubble velocity was recorded when it became steady (average ~1 hr, longer at lower and shorter at higher pressures). A mechanical caliper (±0.1mm accurate) measured the outer dimensions (length and diameter) of the vessel after Lp measurement at each pressure. Chapter 3 addressed the accuracy of the caliper. After completing these reference measurements on the vessel, we close valve 1 and opened valves 2 &4, and raised the pressure of Reservoirs B above that of Reservoirs A. Reservoir B_2 perfused the vessel with $HgCl_2$-containing medium for 5 min at 100 mmHg. The vessel was washed with the trypan blue solution from Reservoir B_1 for 10 min by switching from valve 4 to 3. Reservoir A_2 collected the waste solutions. To measure Lp after inhibitor introduction, we adjusted the pressure of Reservoirs A to the desired value, again closed valves 2, 3 & 4 and retested the vessel for leaks before restarting the Lp measurements. The measurements were repeated at the same pressures as before the introduction of $HgCl_2$. To titrate

the appropriate $HgCl_2$ concentration that would be adequate, yet avoid artifacts, we carried out this procedure for concentrations from 1.0 to .01 mM, as noted.

2.3. Data analysis

As in Chapter 3, we suppose the aorta is cylindrical in shape. The outer surface area of the vessel (AS) is then $AS=\pi(OD)L$, where OD and L are the outer diameter and length of the vessel, respectively. The bubble velocity $V=l/t$, where l is the distance bubble travels in a time t. Let ID be the inner diameter of the catheter. At steady-state, the flow rate Q through the vessel wall equals that $Q=\pi(ID)^2V/4$, which is traced out by the bubble. The hydraulic conductivity $Lp=Q/(AS*\Delta P)$, where ΔP is the transmural pressure controlled in the experiment. Hence, we have the Lp as function of ΔP. The Lp of the blocker-free vessels is given both as an average over all vessels used, including this latter group, as well as only for the vessels later exposed to the $HgCl_2$ concentration in question. Paired Student's t tests compare the Lps with and without the blocker. $P<0.05$ is the choice for statistical significance. The data are presented as mean±SD. Finally, we estimated $Lp_{endothelium}$ from the relation: 1/(the whole wall Lp with intact endothelium) = 1/(the whole wall Lp with endothelium denuded) + $1/Lp_{endothelium}$ as in Tedgui and Lever (Tedgui 1984) and Chapter 3. The resistance of the media was known from Chapter 3. It is easy to estimate $Lp_{endtothelium}$ from the relation above and the two Lp values.

3. Results

We measured $Lp(\Delta p)$, first without and then with $HgCl_2$. for each aorta. Averaging over all rat aortas measured without $HgCl_2$, we found Lp at 60 mmHg to be $2.90\pm0.90\text{x}10^{-8}$ cm/s/mmHg. This value dropped ~27% at 100 mmHg to $2.19\pm0.62\text{x}10^{-8}$ cm/s/mmHg ($P<0.05$), and remained flat up to 140 mmHg ($P>0.05$) See Figure 5. These results are consistent with

those of Chapter 3 (P>0.05) and those of rabbit aorta (Tedgui 1984). A titration procedure that measured Lp(Δp) found artifacts at high transmural pressures over 100 mmHg for $HgCl_2$ concentrations of .02 mM or higher. For example, upon administration of 1.0 mM (0.5 mM) $HgCl_2$, Lp dropped 45.4% (24.5%) at 60 mmHg comparing only with measurements on the same vessels, Lp dropped 30% and 20% for 1.0 mM and 0.5 mM $HgCl_2$, respectively, comparing with the pooled data, but was statistically identical to the $HgCl_2$-free values at 100 mmHg and appeared to even exceed Lp of the same vessel in the absence of $HgCl_2$, although the P value distinguishing these two measurements is not significant. Lp after AQP inhibition with 0.1mM, 0.25mM and 0.02mM behaved similarly to those at 1.0 mM and 0.5 mM. Thus we settled on a concentration of 10 μM $HgCl_2$, the highest concentration that we tried that showed an effect at 60 mmHg without an apparent increase, even one that was not statistically significant due to small sample size, in Lp at higher pressures. After perfusion with this concentration $HgCl_2$, the Lp curve became quite flat (the variation has P>0.05 – see Figure 6c). At 60 mmHg, Lp with blocker drops 27% from the Lp values of the same vessels without $HgCl_2$ and 41% from the Lp of the pooled data without blocker. At 100 and 140 mmHg, it drops 15% and 9% from Lp of the same vessels without blocker, and 27% and 20% from Lp of the pooled data without blocker. The 15% and 9% drops had questionable statistically significance (P=0.9>0.05).

4. Discussion

AQP-1 is a highly specific transmembrane water channel protein; even single protons cannot cross through the aquaporin channel, since they associate with a molecule of water to become H_3O^+, which is too large to cross the narrow 2.8Å diameter neck of the channel ((Sui 2001)). J. Toussaint, in our group has used immunohisotchemistry with anti-AQP1 antibodies to

clearly show that AQP-1 is present in rat aortic endothelial cell membranes. It is thus reasonable to suspect that AQP1 contributes to rat endothelial water permeability and thus affects macromolecular transport (see (Huang 1994) and Chapter 3). A mercury ion of size 2.2Å can bind to the Cys189 in the water pore of the AQP-1 and block its narrow neck (Sui 2001). Here we measure Lp of an excised rat aorta as a function of pressure, introduce mercuric chloride, a common inhibitor for AQP-1 ((Schnitzer 1996), (Zhang 1993)), and measure Lp of the same vessel at the same pressures. A titration procedure is required to determine the appropriate concentration of $HgCl_2$; a too low value may not block all of the aquaporins in the membrane and a too high value may create artifacts for many reasons including the fact that $HgCl_2$ is a toxic substance to living cells (Aleo 2002).

First we briefly describe what we learn from this titration procedure. At all higher concentrations tried, e.g., 1.0 and 0.5 mM of $HgCl_2$, Lp drops (~45.4% ($P<0.05$) at 1.0 mM and 24.5% ($P<0.05$) at 0.5 mM) from their control values at 60 mmHg, confirming water transport inhibition (Figures 6a, b). At higher Δp, Lp either does not change in a statistically significant way from the blocker-free measurements, or even seems to increase. At 10μM, Lp with the blocker drops below control. At 60 mmHg, Lp with the blocker is 27% lower ($P<0.05$) than the control data on the same vessel and 41% lower than the pooled data (Figure 6c). Note the similar percentage drop in Lp at 0.5mM and 10μM at 60 mmHg, indicating that at both concentrations, all of the AQP1s seem to be blocked. As noted, at higher transmural pressures, this effect becomes statistically questionable for 10μM and seemingly reversed for higher $HgCl_2$ concentrations. One possible explanation for this is that water crosses the endothelium through both inter-cellular junctions and through AQP1 channels. At low transmural pressures and transmural flows, $HgCl_2$ can diffuse against the flow and not get forced into the junctions

whereas, at higher pressures and flows, it accumulates there and widens the junctions. Note that $HgCl_2$ is a toxic substance to cellular junctions (Aleo 2002). This increases the junctional flow and may counterbalance the closing down of the AQP1 channels. It will be useful to clarify this issue to repeat these experiments with a silver-based blocker (Niemietz 2002) that might not display this effect at higher pressures.

Chapter 3 determined from measurements of aortic Lp, both with intact and denuded endothelium on the same vessel that about 29% of the total wall resistance in the rat aorta derived from the endothelium at 60 mmHg. With this information, one can evaluate and compare the fraction of the endothelial $Lp_{endothelium}$ attributable to AQP-1 at 60 mmHg. Using the pooled data, the control value without blocker for $Lp_{endothelium} = 10.3 \times 10^{-8}$ cm/s/mmHg. For 1.0 mM, we have $Lp_{endothelium} = 13 \times 10^{-8}$ cm/s/mmHg without blocker (only same vessels) and $Lp_{endothelium} = 3.4 \times 10^{-8}$ cm/s/mmHg after the inhibition, a drop of 74% for these vessels and 67%, from the pooled control. For 0.5mM, we have $Lp_{endothelium} = 10.93 \times 10^{-8}$ cm/s/mmHg without blocker and $Lp_{endothelium} = 5.1 \times 10^{-8}$ cm/s/mmHg after the inhibition, a drop of 25.0% for these vessels and 50%, from the pooled control. For 10μM, we have $Lp_{endothelium} = 8.41 \times 10^{-8}$ cm/s/mmHg without blocker and $Lp_{endothelium} = 3.6 \times 10^{-8}$ cm/s/mmHg after the inhibition, a drop of 57% for these vessels and 64%, from the pooled control. These numbers represent the fraction of water going through AQP-1 and the fraction crossing the endothelium otherwise, presumably through the endothelial cell junctions. Note that a role for AQP-1 in transendothelial water flow would require water to pass through the endothelial cells themselves, in addition to the pathway around them. J. Toussaint in our lab has used immunohistochemistry with fluoresce-labeled antibodies and confocal microscopy to show the expression of AQP-1 on both sides of the rat aortic endothelium, which is consistent with this hypothesis.

Given the important role that these data suggest aquaporins play in endothelial hydraulic conductivity, it is intriguing to suspect that, being a membrane protein, it may be subject to active cellular control as a result, say, of chronic transmural pressures. This may be a mechanism by which the endothelium can actively regulate the transport into the vessel wall, which could be important for understanding atherogenesis. This is the subject of ongoing studies in our lab.

5. Summary and Future work

In this paper we have shown that, by administering the aquaporin blocker $HgCl_2$ to rat aorta excised under pressure so as to maintain its endothelium intact, one can lower the aorta's hydraulic conductivity Lp by 27% and its endothelial Lp by 57% at 60 mmHg with each vessel. The reduction is less and within the error bars for 100 and 140 mmHg, and we suspect that the reason for this is the disruption or widening of the endothelial cell junctions by $HgCl_2$. It appears that aquaporin accounts for a significant portion of the transendothelial water transport for a certain pressure range. As noted, Toussaint's immunofluorescence combined with confocal microscopy to get three-dimensional resolution have indeed shown that AQP-1 is present on both the luminal and abluminal sides of the endothelial membrane, although he has not yet quantified the relative amounts on the two sides of the membrane. Repeating his experiment with quantitative fluorescence should clarify the relative amounts on both sides of the membrane, and Western blot analysis should give the absolute amount of membrane aquaporin per endothelial cell. Alternately, one can modify Wen *et al.*'s (Wen 2001) immunofluorescence antibody technique to identify the AQP-1 on both side of the aortic endothelium. In brief, one can take transverse cryosections to locate the AQP-1 on both sides of the cell membrane. Using Hautchen

en face preparations (Truskey 1992) may also allow us to quantify the AQP-1 on either side of the membrane.

In order to further investigate the results at higher pressures that are hard to reconcile with those at 60 mmHg and to confirm the effect of aquaporin on vessel and on endothelial Lp, it will be useful to repeat the experiments described above using another AQP-1 blocker, such as silver (Ag^{+}, 2.5 Å) or gold (Au^{+}, 2.7 Å) ions (Niemietz 2002). These ions, given their larger ionic size, appear more effective at blocking the AQP-1, and may have fewer artifacts, e.g., may have a harder time entering the interendothelial cell junctions, than Hg^{++} at higher pressure.

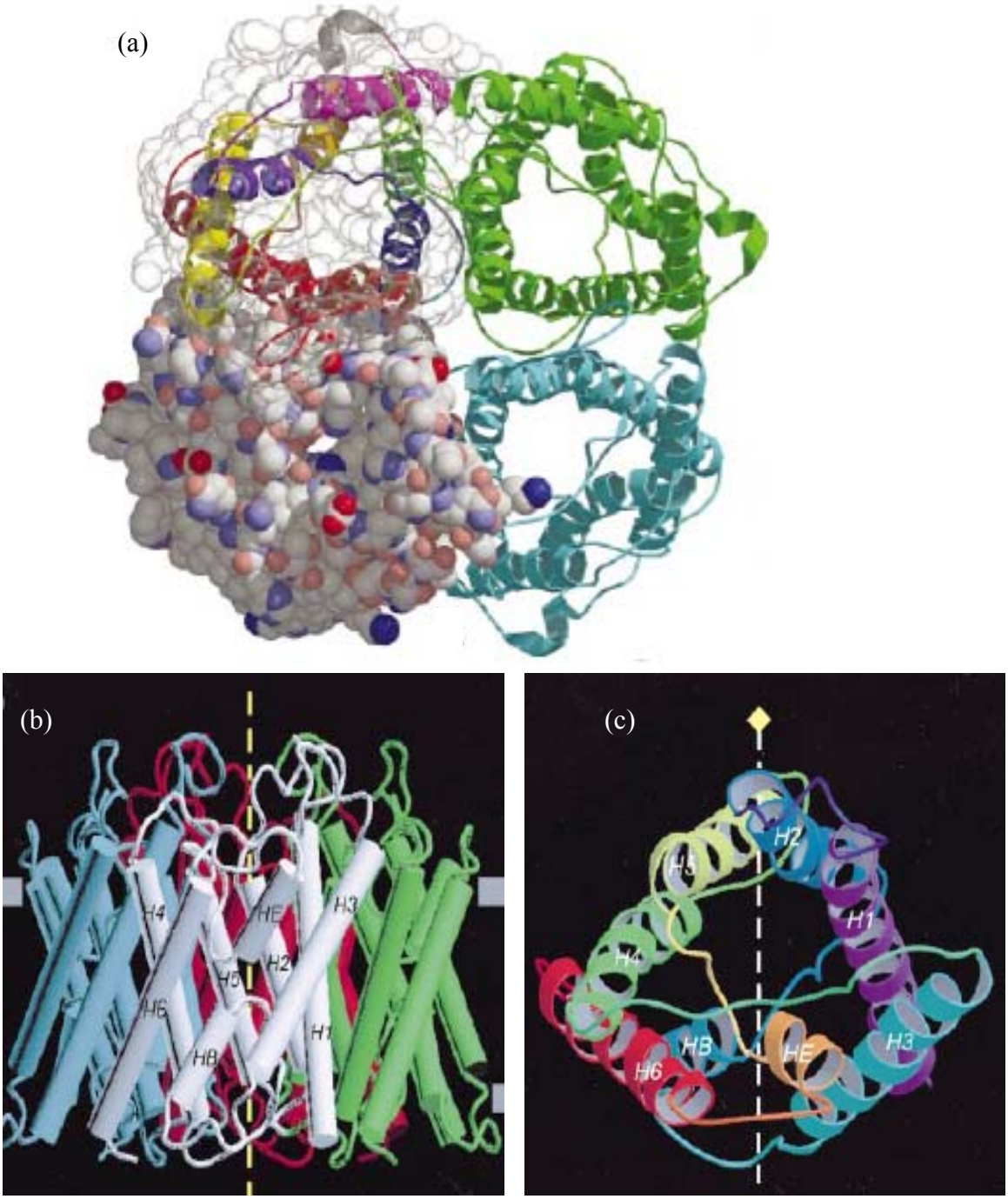

Figure 1. (a) Top view of unit AQP-1. The AQP-1 is formed by four monomers represent with 4 colors (Sui 2001). (b) Side view of a unit AQP-1. Each color represents a monomer. The top side is the extracellular space (Murata 2000). (c) Top view of a monomer. The monomer is formed by 6 helices (Murata 2000).

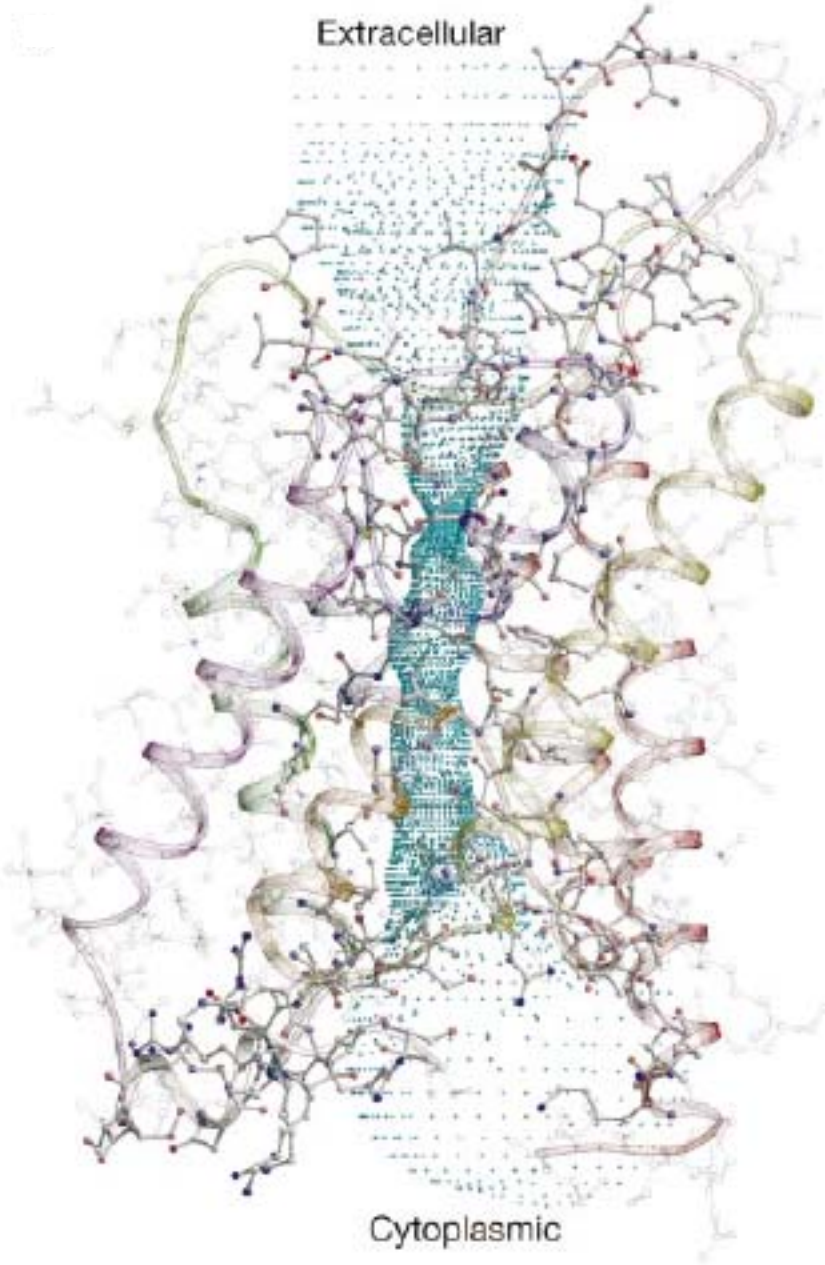

Figure 2. Side view of the dumbbell shape of the water pore. The blue region is the water pore (Sui 2001).

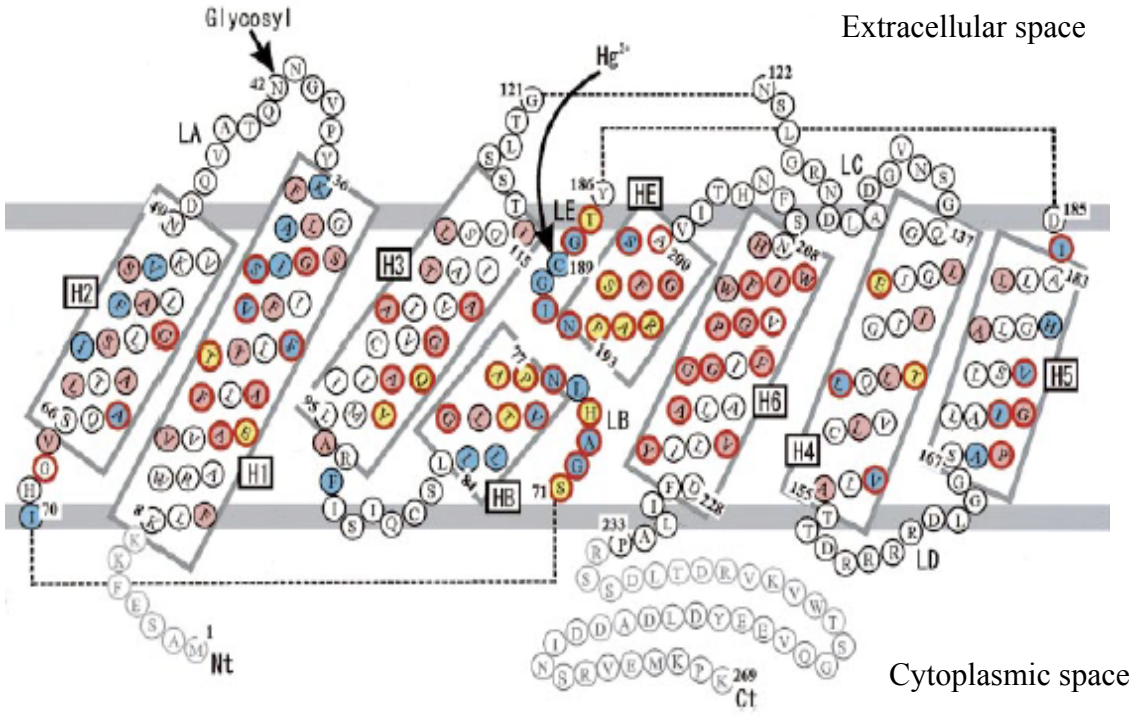

Figure 3. Schematic representation of the water pore. The gray bands represent the plasma membrane. The arrow indicates that the mercury ion binds to Cys 189 (Murata 2000).

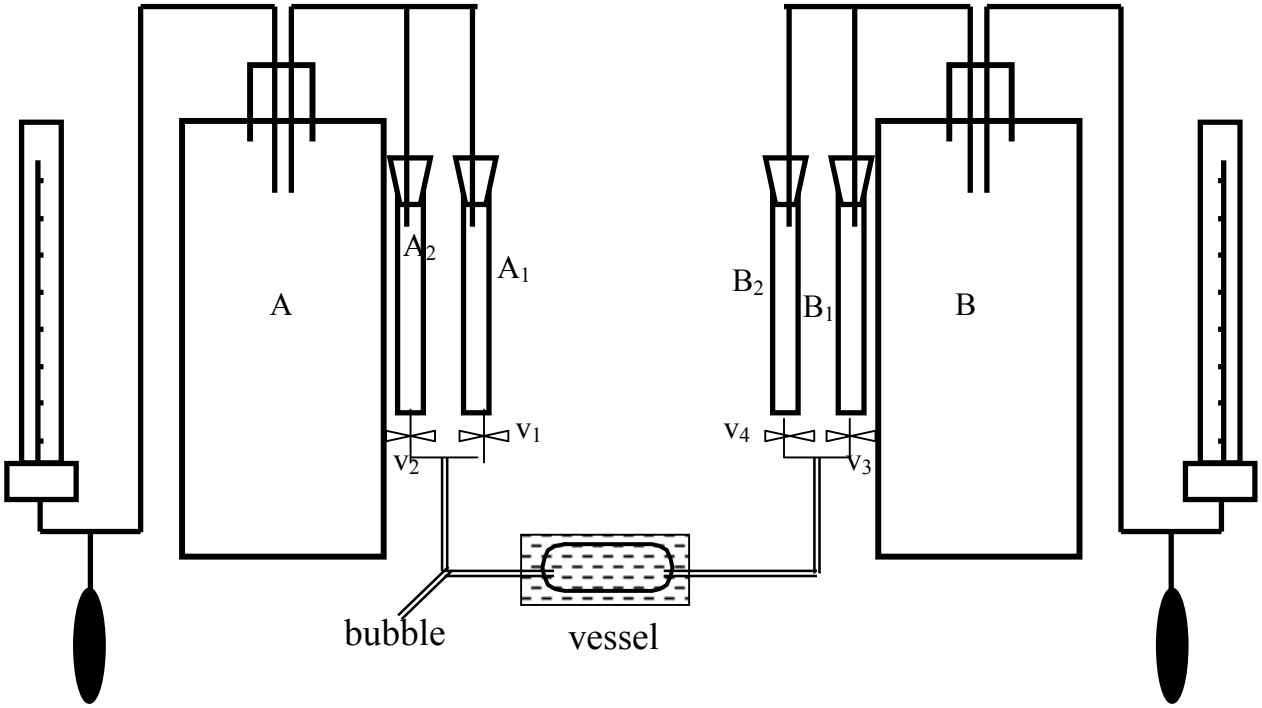

Figure 4. Schematic drawing of the pressurized setup. Two pressure reservoirs (A & B) are connected to the solution reservoirs (Res A_1, A_2, B_1, B_2). Res A_1 and B_1 contains trypan blue in PBS solution. Res B_2 contains $HgCl_2$ in PBS solution. The flows of each reservoir are controlled by the valves (v_1, v_2, v_3 and v_4)

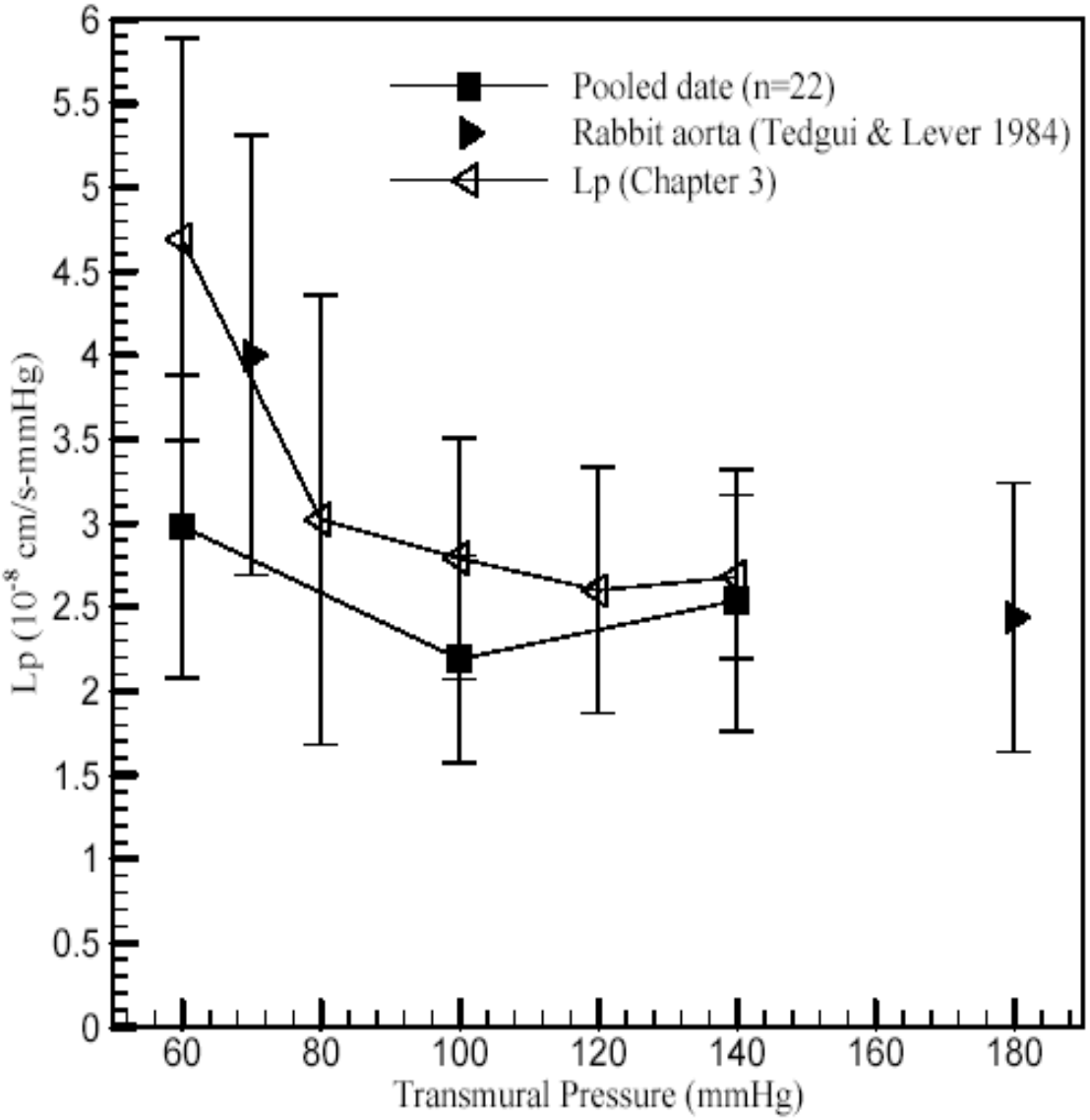

Figure 5. The hydraulic conductivity of the rat aorta averaging of all vessels (n=22, n=number of rats used), comparing with Chapter 3. The differences between the new data presented here, that function as the controls for this paper, and the historic data are statistically insignificant (P>0.05). The Lp drops 27% from 60 to 100 mmHg in the present data. The results were quantitatively agreed with that of the rabbit aorta (Tedgui 1984).

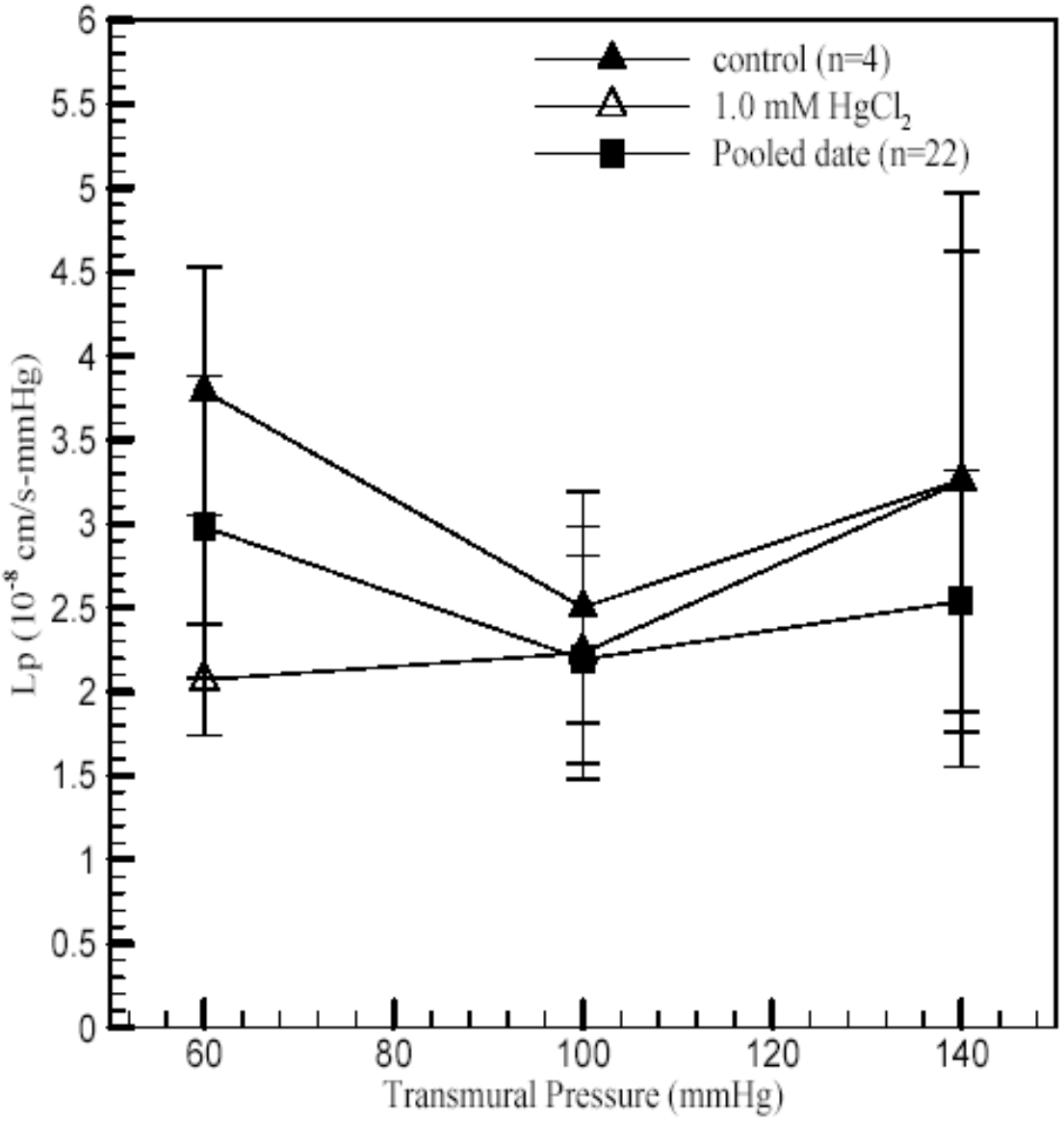

Figure 6a. The hydraulic conductivity of the rat aorta with and without AQP with $HgCl_2$ concentration of 1.0 mM (n=4). The Lp of the rat with AQP has a high value at 60 mmHg and drops 34% at 100 mmHg ($P<0.05$). It is statistically insignificant comparing the control data and pooled data. Lp drops about 45.4% at 60 mmHg after the inhibitor ($P<0.05$) of each vessel. The curve of Lp after inhibitor is relatively flat ($P>0.05$) and does not appear significantly different from the control at the higher pressures. The Lp drops 30% at 60 mmHg by the pooled data ($P<0.05$).

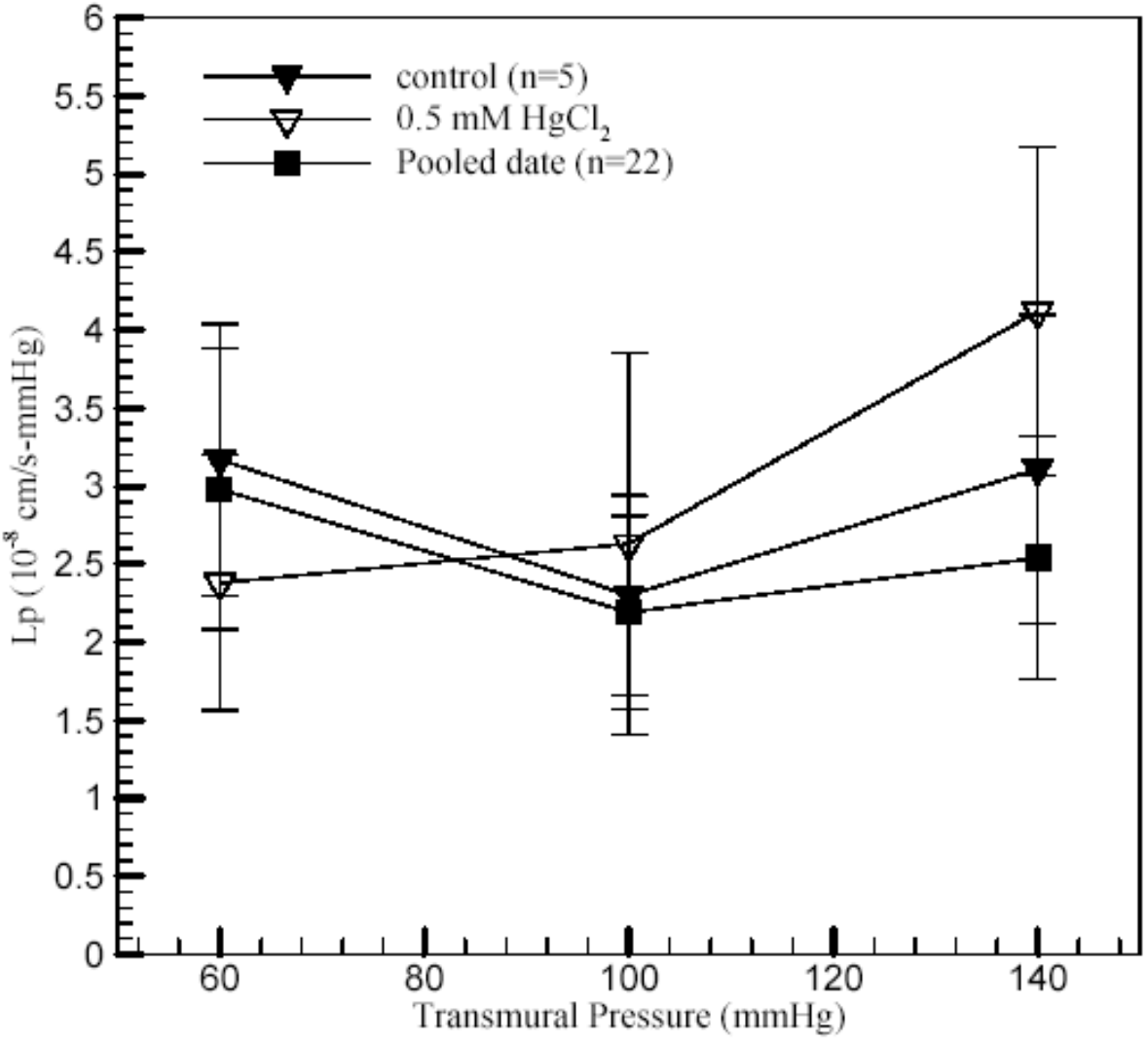

Figure 6b. The hydraulic conductivity of the rat aorta with and without AQP with $HgCl_2$ concentration of 0.5 mM (n=5). The Lp of the rat with AQP has a high value at 60 mmHg and drops 23.0% at 100 mmHg. The control data is statistically insignificant compared to the pooled data. The Lp drops about 24.9% at 60 mmHg after the inhibitor ($P<0.05$) with each vessel. The curve of Lp after inhibitor is relatively flat ($P>0.05$) and appears to show artifacts at the two higher pressures. The Lp drops 20% at 60 mmHg with the pooled data ($P<0.05$).

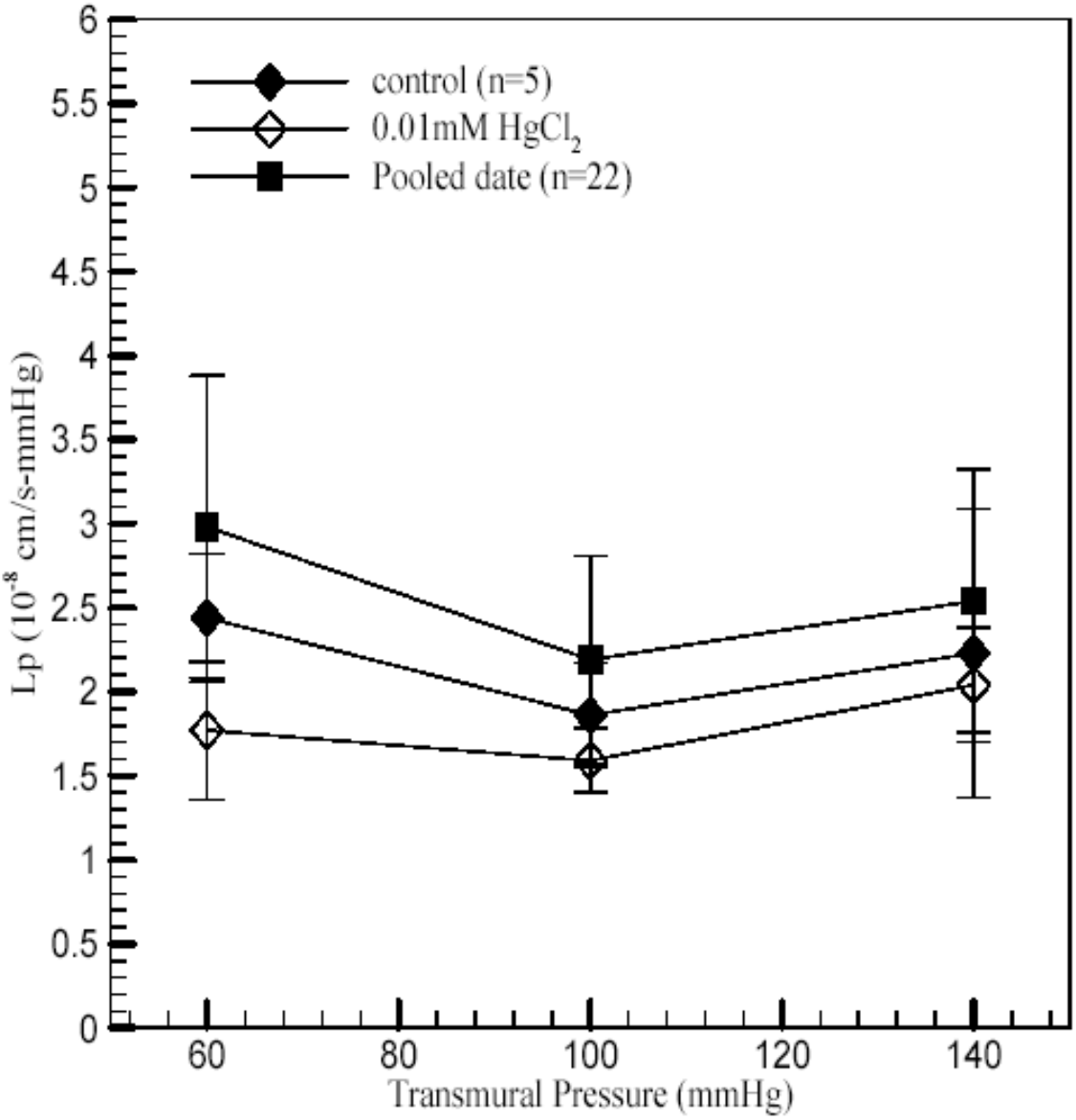

Figure 6c. The hydraulic conductivity of the rat aorta with and without AQP with $HgCl_2$ at a concentration of 10 μM (n=5). The Lp of the rat with AQP has a high value at 60 mmHg and drops 23.8% at 100 mmHg. The pool data drops 28% from 60 to 100 mmHg ($P<0.05$). The pooled is statistically insignificant compared to control data. The Lp drops ~27.4% from its value on the same vessels and ~41% from the pooled control at 60 mmHg after the exposure to the inhibitor. The visible drops at 100 and 140 mmHg are of questionable statistical significance. The Lp curve after inhibitor is relatively flat ($P>0.05$).

Chapter 6

Models for the Filtration Flows in Arteries and Veins and their Effect on the Growth of Macromolecular Leakage Spots in their Intimas

This chapter will now codify the experimental information gathered from the previous chapters and from the literature in models for the filtration water flow problems in the three different vessels. These models are prerequisite for the corresponding mass transfer problem needed to understand the macromolecular transport in these vessels. The working hypothesis is that differences in the macromolecular transport in these vessels may determine their different susceptibilities to at least early stage atherosclerosis. We first provide a brief background, including motivation, and then formulate appropriate models for the different vessels in detail.

1. Background

Atherosclerosis is a disease mainly of large arteries, becoming evident when the arterial wall thickens near the lumen (Vander 2001) Atherosclerosis appears to begin with the delivery of low-density lipoprotein (LDL) from the blood into the vessel wall, where it accumulates. Blood-borne monocytes enter the arterial intima in regions with high subendothelial lipid concentration, becoming macrophages that attempt to scavenge the extracellular cholesterol lodged in the intima. When overwhelmed, they, along with other smooth muscle-derived scavenger cells, progress to form foam cells. This accumulation of lipid and necrotic cells appears to comprise the earliest lesions

((Simionescu 1986, Steinberg 1983)) that can develop into stenoses leading to blockage, rupture or clot formation.

Atherosclerosis normally occurs in the large arteries and/or in the aortic valve but not in the pulmonary artery (PA) or in veins. In humans, the pulmonary artery is vulnerable only in the presence of pulmonary hypertension (Duff 1951). (Curiously, some data suggest that rabbit pulmonary artery appears to be similar to rabbit aorta in its proclivity toward developing atherosclerosis (Schwenke 1997) and a comparison of the PA of the rabbit with that of an animal without this unusual susceptibility is worthy of study.) Veins normally do not develop atherosclerosis. However, when veins, such as the saphenous vein, which is frequently used in coronary bypass procedures, are placed in arterial conditions, i.e., high transmural pressure, atherosclerosis often develops (Lever 1996) along with vessel remodeling. After 6 to 12 years, 71% of such vein grafts develop atherosclerosis and their structures resemble arterial fatty streaks (Berceli 1991).

Since aorta is one of the major vessels where the disease takes place, and the largest vessel, it has drawn extensive attention and there are numerous studies in this area. The aorta typically consists of a monolayer of endothelial cells (EC) at the luminal side, a sub-endothelial intima and an internal elastic laminar (IEL), below which is the tunica media that comprises circa 99% of the total vessel wall thickness. The media have a repeated structure of elastin and smooth muscle cells (SMC). Stemerman *et al*. (Stemerman 1986) found that large macromolecules do not cross the endothelium uniformly at short circulation times, but rather focally. Weinbaum *et al* (Weinbaum 1985) proposed a mathematical model for macromolecular leakage assuming that it proceeds through transiently open or poorly formed endothelial cell junctions associated

with cells in mitosis or with dying cells. The normal endothelial cell junction is less than 7 nm wide ((Bell 1974b), (Bell 1974a), (Majno 1961), (Packham 1967), (Sprague 1980)), which is far smaller than the size of an LDL molecule (22 nm). Lin *et al*. (Lin 1988) observed the association of both Evans Blue albumin and Lucifer-Yellow LDL crossing of the endothelium with mitotic cells. Various measurements ((Lin 1988), (Lin 1989), (Truskey 1992)) have associated a fraction of these leaky cells with mitotic and dying cells. Lin *et al*. found that 99% of cell in mitosis leaked, while Truskey *et al*. found 25% of the leakage sites were associated with cells in mitosis. Chuang *et al*. (Chuang 1990) studied the growth of horseradish peroxidase (HRP) tracer spots around such an isolated leak as a function of tracer circulation time and found spot growth that was too fast to be consistent with a purely diffusive transport for any reasonable diffusivity. Various mathematic models have since attempted to interpret the tracer spot growth. The early models ((Truskey 1981), (Fry 1985), (Fry 1987)) were one-dimensional – with variation only in the direction normal to the endothelium – and were thus unable to address the issue of isolated spot growth. Early two dimensional models ((Weinbaum 1985), (Tzeghai 1986), (Weinbaum 1988b), (Wen 1988)) incorporated only limited structural information about the wall (generally they considered the endothelium and lumped the rest of the wall into a uniform medium) and considered diffusion alone, or convection/diffusion mainly in the direction normal to the endothelial surface, and could not describe the observed spot growth. Yuan *et al*. (Yuan 1991) proposed a two-dimension convection/diffusion model that included the intima region and the IEL explicitly, with the IEL assumed to be an appreciable transport barrier to encourage transport parallel to the endothelium, but they assumed that the porosities and

characteristic transport parameters of intima and media were the same. They were also unable to account for the observed spot growth. Huang *et al*. (Huang 1994) noticed that Frank and Fogelman's ultra-rapid freezing/rotary shadow etching study (Frank 1989) actually revealed that the structure of the subendothelial intima was ultra-porous. Their *ab initio* theory for the intimal transport parameters showed that the intima provided almost two orders of magnitude less flow resistance than did the media. Huang *et al* 's model incorporated these radically different, structure-based parameters into a two-dimensional convection/diffusion model. The model predicted that a convective flow in the intima, mainly in the direction parallel to the endothelium, carried tracer that had been advected into the aortic intima through a leaky junction, thereby quickly forming large spots that agreed with experiment. Eventually, the tracer seeped into the media. Thus the early time filtration and macromolecular transport into the aortic wall appears to be reasonably well understood, i.e., theory and experiment agree.

If the triggering events for the disease in the large arteries are water-driven lipid transport across focal sites in the vessel endothelium and its sub-endothelial water-driven spread and its accumulation there, it is natural to wonder if and how these processes are radically different in resistant and disease-prone vessels. Much of this thesis has been concerned with experiments aimed at beginning to answer this question. These will provide the guidance for constructing mathematical models which should be able to quantitatively explain observed data and to make predictions that should address this question. We briefly review some of the relevant results and then, based on these results, formulate a mathematical model for the filtration flow in the PA and IVC.

The PA and IVC are accustomed to much lower physiological pressure, 16 and 5 mmHg, respectively, than the aorta. The PA has a structure that is similar to the aorta, but with a thinner wall (78.9±3.3 μm in rat, (Chapter 2)) than the aorta (145±9.7 μm, (Chapter 2)), and a much higher elastin content. Since the vein is normally exposed under lower lumen pressure, the vein has different structure and a thinner wall (66.1±4.1 μm, (Chapter 2)) than the arteries. The venous wall has a large lumen, fewer SMC, less elastin content, but much more collagen fibers. We found that the IVC has an incomplete IEL and its media is comprised of sparse elastin, SMCs and abundance of collagen fibers. Importantly, our ultrastructural studies with ruthenium red revealed that all three vessels had intima or intimal-like structures. These facts are consistent with our findings (Chapter 3) that Lp for these vessels increases in the order aorta, PA, IVC. Surprisingly, the overall transmural water flux ($L_p\Delta P$) through the walls of all three of these vessels turned out to be very similar, although the details of the flow fields may turn out to be quite different. It thus appears likely that convective transport cannot be neglected in the PA or the IVC, and that the filtration problems for these vessels may play a central role in understanding their differences.

We have observed (Chapter 4) that HRP tracer penetrates the vessel endothelium in the PA and the IVC focally, as in the aorta, for short circulation times. Thus a two-dimensional model is necessary, as in the aorta. Moreover, by following Chuang *et al.*'s (Chuang 1990) procedure, we found that spots in the PA and in the aorta were surprisingly similar in size and rate of growth. Thus we would expect a similarly strong intimal water flow parallel to the endothelium in the PA as in the aorta, but a much weaker one in the IVC, despite a similar overall flow. We shall therefore explicitly

account for the intima in all of the models below. We are now ready to propose a mathematical model for the filtration flow field as the appropriate route to address the above questions. Lp and other data from our own measurements (Chapter 3) will provide critical parameter inputs. Future work will link this flow field to a convective-diffusive mass transport model.

2. Water Filtration Model for the PA

2.1. Mathematical Formulation

The model for the PA will be almost identical in form to that for the aorta (Huang 1994) but will differ in one of its boundary conditions and in its parameters. The IVC model will differ in other ways. We begin with the model for the PA.

Since the vessel wall is typically much thinner than the vessel diameter, we shall consider the vessel wall to be flat. Consider a round, axisymmetric slab of a vessel wall whose z-axis passes through the center of an assumed circular leaky cell and is perpendicular to the vessel endothelium. Despite the abuse of geometry, we assume that the vessel wall is periodic in this slab. Cylindrical coordinates describe the system. The z coordinate is defined in the direction normal to the endothelial surface with z=0 at the IEL and pointing toward the adventitia. The local r coordinate is, in the context of the whole artery wall, a radial position in the "plane" parallel to the endothelium. We assume axisymmetry in this model about $r^*=0$. A high, reference pressure in the lumen above the vessel endothelium forces water to cross the endothelium and to enter the artery wall by passing through all of the inter-endothelial junctions, but fluid that bears large solute molecules can only enter through the rare junctions that leak, here the central cell only. Since both the intima and the media are porous media, we shall define velocities in a

local volume-averaged sense, so that the velocity is defined as a continuous, differentiable function everywhere in the tissue and in the tissue interstices. As such, the transport through them is a Darcy flow:

$$u_k^* = -\frac{Kp_k^*}{\mu^*}\frac{\partial p_k^*}{\partial r^*}, \text{ and } w_k^* = -\frac{Kp_k^*}{\mu^*}\frac{\partial p_k^*}{\partial z^*}, \; k\text{= i (intima), m (media),} \qquad \text{(1a-b)}$$

where $\underline{u}^*=(u^*, w^*)$, u^* and w^* are the horizontal (r^* direction) and normal (z^* direction) velocities, respectively. K_p^* (different for the intima and for the media) is the Darcy permeability, μ^* is the fluid viscosity and p^* is the pressure. The continuity equation, or conservation of fluid mass, for an incompressible flow is

$$\nabla \cdot \underline{u}_k^* = \frac{1}{r^*}\frac{\partial}{\partial r^*}\left(r^* u_k^*\right) + \frac{\partial w_k^*}{\partial z^*} = 0, \; k\text{= i (intima), m (media),} \qquad \text{(2a)}$$

Combining Eqs (1) and (2a), we get

$$0 = \nabla^2 p_k^* \; k\text{=i(intima),m(media).} \qquad \text{(2b)}$$

Here asterisks denote the dimensional variables. We introduce the following non-dimensional variables:

$$r = \frac{r^*}{L_m^*}, \; z = \frac{z^*}{L_m^*}, \; P = \frac{p^*}{P_L^*}, \; Kp = \frac{Kp^*}{Kp_m^*}, \; U = \frac{u^*}{Lp_m^* P_L^*}, \; W = \frac{w^*}{Lp_m^* P_L^*},$$

where $Kp_m^* = Lp_m^* \mu^* L_m^*$. L_m^* is the thickness of the media, P_L^* is the lumen pressure, and Lp_m^* is the hydraulic conductivity of the media. Then Eqs. (1) and (2) in the dimensionless form become:

$$U_k = -\frac{\partial P_k}{\partial r}, \; W_k = -\frac{\partial P_k}{\partial z}, \qquad \text{(3a, b)}$$

$$\frac{1}{r}\frac{\partial}{\partial r}(rU) + \frac{\partial W}{\partial z} = 0. \qquad \text{(4a)}$$

$$0 = \nabla^2 p_k \; k\text{=i(intima), m(media).} \qquad \text{(4b)}$$

Fluid enters the intima and can spread in the (local) radial direction, which means that it would flow towards r=0 for $0<r<R_1$, and away from r=0 for $R_2<r<\xi$. As noted, the intimal thickness is much less than the media thickness L_m and than the distance 2ξ between adjacent leaky cells. Thus, as a result of the separation of scales in the intima, one has a boundary-layer type analysis that, to leading order, has no variation in U in the z-direction across the intima. Integrating Eq. (4a) in the z-direction across the intima yields:

$$\frac{dU_k}{dr}+\frac{U_k}{r}=\frac{1}{\eta}\left(W_i(r)-W_m(r,z=0)\right), \tag{5}$$

where $\eta = Kp_iL_i$, W_i and $W_m(z=0)$ are the velocities in the z-direction across the endothelium far from the leaky junctions and across the IEL, respectively. Equation (5) has implicitly used the boundary condition that W at the IEL is continuous, i.e., its intima and media value are the same at z=0. Note that these velocities are presumed to be continuous functions of r away from the leaky junction and, as such, do not explicitly consider the normal junctions or the IEL fenestrae.

It is now necessary to prescribe the boundary conditions on the r- surfaces r=0, R_1, ξ, the edge $r=\xi$ of the periodic unit, and at the three z-surfaces, the endothelium, the IEL (both assumed here to be infinitely thin) and the media-adventitial boundary.

At r=0 and ξ, symmetry and periodicity conditions lead to no flow in the r-direction:

$$U=0 \text{ at } r=0,\ \xi. \tag{6}$$

The pressure is also continuous in the intima beneath the leak junction (inner and outer junction radii R_1 and R_2, respectively).

$$P_i(r=R_1) = P_i(r=R_2). \tag{7}$$

At the media-adventitial boundary,

$$P_m = P_i \text{ at } (z=0) \tag{8a}$$

$$P_m = 0 \text{ at } z=1. \tag{8b}$$

At the IEL, the normal velocity W is characterized by a hydraulic conductivity through the IEL and linearly related to the pressure difference: across the IEL, vis.,

$$W_m = Lp_I(P_i - P_m) \text{ at } z=0. \tag{9a}$$

Here Lp_I is the hydraulic conductivity of the IEL, and Lp_I is defined by equation (9b), but where the pressures are replaced by the area-average (subscript "mean") over a circular slab of radius equal to half the mean distance between IEL fenestrae of their values as calculated from a very simplified local model (Yuan 1991). This model considers a circular slab of intima, IEL and media with a single, circular fenstral pore through which all water traversing the IEL passes at its center and periodic boundary conditions at its outer edge. It takes the intimal pressure as uniform and known and one-dimensional flow through the fenestra. The result is $\left(W_m^i\right)_{mean}/Lp_m P_i = \left(P_m^i\right)_{mean}/P_i = W_f \phi_I$ and

$$Lp_I = \frac{W_f \phi_I}{1 - W_f \phi_I}, \tag{9b}$$

where $\phi_I = a_f^2/\xi_I^2$ and a_f is the radius of an IEL fenestra. W_f, the water velocity through the fenestra divided by $Lp_m p_i$, is given by:

$$W_f = \frac{(L_m/L_I)(Kp_i/Kp_m)}{1 + G_0(L_m/L_I)(Kp_i/Kp_m)},$$

with

$$G_0 = \phi_I + \sum_{n=2}^{\infty} \frac{2a_f J_1(\nu_n a_f)}{\nu_n \coth(\nu_n)\xi_I^2 J_0^2(\nu_n \xi_I)}.$$

On the endothelial surface, at the normal junctions,

$$W_i\,(z = -L_i) = L\mathrm{p}_e(1-P_i), \quad R_2 \le r \le \xi \quad . \tag{10a}$$

$$0 \qquad , \qquad 0 \le r \le R_1 \; . \tag{10b}$$

Note that Huang *et al*. (Huang 1994) assumed that (10a) also applies for $0 \le r \le R_1$. This distinction should not change the results significantly since $R_1 << \xi$. Here the subscripts I, e denote the IEL and the normal endothelial junctions, respectively.

The velocity W_j across the leaky cleft, in relation to the local pressure, is

$$W_j\,(z = -L_i) = L\mathrm{p}_j(1-P_i(R_1)), \tag{11}$$

where $L\mathrm{p}_j$ is the hydraulic conductivity of the leaky junction. Neglecting the resistance of the junction fibers, one can assume that the flow across the junction is Poiseuille flow through a parallel channel. Inserting the result into Starling's law (Yuan 1991) gives

$$Lp_j = \frac{(\Delta R)^2}{12\mu L_j Lp_m^*},$$

where $\Delta R = R_2 - R_1$ and L_j^* are the width and depth of the leaky junction. Note that ΔR is of the order of tens of nanometers, whereas R_1 is of the order of ten microns (Chapter 4). As such, $\Delta R << R1, R2$. At the leaky junction $R_1 < r < R_2$ across which the water flow in the intima is conserved, it demands the following matched condition:

$$W_j \Delta R = L_i(U_{i2}(R_2) - U_{i1}(R_1)). \tag{12}$$

Since $W_j >> W_m$, we have deleted W_m from the left side of (12).

Clearly the model depends on the sizes of extracellular structures and on fluid and filtration properties. We shall discuss these parameters after presenting the analytic solutions to the model.

2.2. Solution for Water Velocity and Pressure Distribution

The water velocity and pressure distribution that satisfy boundary conditions (6), (8), and (10) can be expressed as follows. For the intima,

$$P_{i1} = a_1 I_0(\lambda_1 r) + A_0 + \sum_{n=1}^{\infty} A_n \frac{\lambda_1^2 \sinh(\mu_n)}{\lambda_1^2 + \mu_n^2} J_0(\mu_n r), \tag{13a}$$

$$U_{i1} = -a_1 Kp_i \lambda_1 I_1(\lambda_1 r) + \sum_{n=1}^{\infty} A_n \frac{\lambda_1^2 \mu_n Kp_i \sinh(\mu_n)}{\lambda_1^2 + \mu_n^2} J_1(\mu_n r), \tag{13b}$$

$$P_{i2} = b_2(\alpha I_0(\lambda_2 r) + K_0(\lambda_2 r)) + \frac{Lp_e}{Lp_e + Lp_I} + \frac{Lp_I}{Lp_e + Lp_I} A_0 + \sum_{n=1}^{\infty} A_n \frac{\lambda_1^2 \sinh(\mu_n)}{\lambda_2^2 + \mu_n^2} J_0(\mu_n r), \tag{13c}$$

$$U_{i2} = -b_2 Kp_i \lambda_2 (\alpha I_1(\lambda_2 r) - K_1(\lambda_2 r)) + \sum_{n=1}^{\infty} A_n \frac{\lambda_1^2 \mu_n Kp_i \sinh(\mu_n)}{\lambda_2^2 + \mu_n^2} J_1(\mu_n r), \tag{13d}$$

with $\lambda_1^2 = \frac{Lp_I}{L_i Kp_i}$, $\lambda_2^2 = \frac{Lp_I + Lp_e}{L_i Kp_i}$, $\alpha = \frac{K_1(\lambda_2 \xi)}{I_1(\lambda_2 \xi)}$.

As for the media, we have

$$P_m = A_0(1-z) + \sum_{n=1}^{\infty} A_n \sinh(\mu_n(1-z)) J_0(\mu_n r), \tag{14a}$$

$$W_m = A_0 + \sum_{n=1}^{\infty} A_n \mu_n \cosh(\mu_n(1-z)) J_0(\mu_n r), \tag{14b}$$

$$U_m = \sum_{n=1}^{\infty} A_n \mu_n \sinh(\mu_n(1-z)) J_1(\mu_n r). \tag{14c}$$

Here J_q is the Bessel function of the order q. I's and K's are modified Bessel functions of the first and the second kinds, respectively. The μ_n are the positive roots of $J_1(\mu_n \xi)=0$. The unknown coefficients a_1, b_2, A_0 and A_n can be now determined by applying the rest of the boundary conditions. Eq. (7) leads to

$$a_1 I_0(\lambda_1 R_1) - b_2(\alpha I_0(\lambda_2 R_2) + K_0(\lambda_2 R_2)) + \left(1 - \frac{Lp_I}{Lp_e + Lp_I}\right) A_0 + \sum_{n=1}^{\infty} A_n \lambda_1^2 \sinh(\mu_n) \left(\frac{J_0(\mu_n R_1)}{\lambda_1^2 + \mu_n^2} - \frac{J_0(\mu_n R_2)}{\lambda_2^2 + \mu_n^2} \right) = \frac{Lp_e}{Lp_e + Lp_I} \quad , \tag{15}$$

Applying Eq. (9), with the aid of orthogonality of Bessel functions, yields

$$-a_1 Lp_I \int_0^{R_1} I_0(\lambda_1 r) r J_0(\mu_l r) dr - b_2 Lp_I \int_{R_1}^{\xi} (\alpha I_0(\lambda_2 r) + K_0(\lambda_2 r)) r J_0(\mu_l r) dr + A_0 \Delta_{0l} + \sum_{n=1}^{\infty} A_n \Delta_{nl}$$

$$= \int_{R_1}^{\xi} \frac{Lp_e Lp_I}{Lp_e + Lp_I} r J_0(\mu_l r) dr \quad (l = 0,1,2,\ldots), \tag{16}$$

where $\Delta_{0l} = \delta_{0l}(1 + Lp_I) \int_0^{\xi} r J_0(\mu_l r) dr - Lp_I \left(\int_0^{R_1} r J_0(\mu_l r) dr + \frac{Lp_I}{Lp_e + Lp_I} \int_{R_1}^{\xi} r J_0(\mu_l r) dr \right)$,

$$\Delta_{nl} = \delta_{nl}(\mu_n \cosh(\mu_n) + Lp_I \sinh(\mu_n)) \int_0^{\xi} r J_0(\mu_l r) J_0(\mu_n r) dr$$

$$- Lp_I \sinh(\mu_n) \lambda_1^2 \left[\int_0^{R_1} \frac{r J_0(\mu_l r) J_0(\mu_n r)}{\mu_n^2 + \lambda_1^2} dr + \int_{R_1}^{\xi} \frac{r J_0(\mu_l r) J_0(\mu_n r)}{\mu_n^2 + \lambda_2^2} dr \right].$$

From Eq. (12), we have

$$a_1 (\lambda_1 L_i Kp_i I_1(\lambda_1 R_1) + \Delta RLp_j I_0(\lambda_1 R_1)) - b_2 \lambda_2 L_i Kp_i (\alpha I_1(\lambda_2 R_2) - K_1(\lambda_2 R_2)) + A_0 \Delta RLp_j$$

$$+ \sum_{n=1}^{\infty} A_n \lambda_1^2 \sinh(\mu_n) \left[\frac{Kp_i \mu_n L_i}{\lambda_2^2 + \mu_n^2} J_1(\mu_n R_2) - \frac{Kp_i \mu_n L_i}{\lambda_1^2 + \mu_n^2} J_1(\mu_n R_1) + \frac{\Delta RLp_j}{\lambda_1^2 + \mu_n^2} J_0(\mu_n R_1) \right] = \Delta RLp_j \tag{17}$$

Eqs. (15)–(17) constitute a set of linear equations for a_1, b_2, A_0 and A_n. Retaining a finite number of terms, say N, for A_n, the system can be written in a form of (N+3)× (N+3) matrix. It can in principle be solved numerically using standard matrix inversion techniques. We have carried out some numerical solutions of these equations (not presented here) and found that N=20 was sufficient, i.e., doubling to N=40 did not change the results noticeably.

3. Filtration Model for the IVC

3.1. Mathematical Formulation

The IVC has the same governing equations (Eqs. (1)-(2)) as the PA and the aorta. The boundary conditions of the IVC are very similar to those of the PA and the aorta, except for the boundary conditions, Eqs. (10) and (12), at the IEL surface z=0. See Figure 3.

Since the IVC has incomplete IEL, we assume that, rather than being governed by a Starling condition, the flow simply satisfies continuity of both pressure and normal velocity at z=0, i.e.,

$$P_{\mathrm{i}} = P_{\mathrm{m}}, \tag{18a}$$

$$W_{\mathrm{i}} = W_{\mathrm{m}}, \tag{18b}$$

The matching condition then becomes

$$(W_{\mathrm{j}} - W_{\mathrm{m}}(\mathrm{z}=0))\Delta R = L_{\mathrm{i}}(U_{\mathrm{i2}}(\mathrm{R}_2) - U_{\mathrm{i1}}(\mathrm{R}_1)). \tag{19}$$

Compared to Eq. (12) in the aorta/PA model, we account in (19) for the leaky flow into the underlying media $W_{\mathrm{m}}(\mathrm{z}=0)$ in view of incomplete IEL for the IVC.

3.2. Solution for Water Velocity and Pressure Distribution

The water velocity and pressure distribution that satisfy boundary conditions (6), (8), and (18b) can be expressed as follows. For the intima,

$$P_{i1} = \frac{A_0 r^2}{4 L_i K p_i} + a_1 - \sum A_n \frac{\cosh(\mu_n)}{L_i K p_i \mu_n} J_0(\mu_n r) \tag{20a}$$

$$U_{i1} = -\frac{A_0 r}{2 L_i} - \sum A_n \frac{\cosh(\mu_n)}{L_i} J_1(\mu_n r) \tag{20b}$$

$$P_{i2} = b_2\left(\alpha I_0(\lambda r) + K_0(\lambda r)\right) + 1 - \frac{A_0}{L p_e} - \sum_{n=1} A_n \frac{\mu_n \cosh(\mu_n)}{L_i K p_i\left(\lambda^2 + \mu_n^2\right)} J_0(\mu_n r) \tag{20c}$$

$$U_{i2} = b_2 \lambda K p_i\left(-\alpha I_1(\lambda r) + K_1(\lambda r)\right) - \sum_{n=1} A_n \frac{\mu_n^2 \cosh(\mu_n)}{L_i\left(\lambda^2 + \mu_n^2\right)} J_1(\mu_n r), \tag{20d}$$

where $\lambda^2 = \dfrac{Lpe}{L_i K p_i}$

As for the media, the solution is:

$$P_m = A_0(1 - z) + \sum_{n=1} A_n \sinh(\mu_n(1 - z)) J_0(\mu_n r) \tag{21a}$$

$$W_m = A_0 + \sum_{n=1} A_n \mu_n \cosh(\mu_n(1-z)) J_0(\mu_n r) \tag{21b}$$

$$U_m = \sum_{n=1}^{\infty} A_n \mu_n \sinh(\mu_n(1-z)) J_1(\mu_n r) \tag{21c}$$

Similar to the procedures outlined in section 2.2, the values of the unknown coefficients a_1, b_2, A_0 and A_n are the result of solving the following equations:

$$\begin{aligned} &a_1 - b_2\left(\alpha I_0(\lambda R_1) + K_0(\lambda R_1)\right) + A_0\left(\frac{R_1^2}{4L_i Kp_i} + \frac{1}{Lp_e}\right) \\ &+ \sum_{n=1}^{\infty} A_n J_0(\mu_n R_1) \frac{\cosh(\mu_n)}{L_i Kp_i}\left(\frac{\mu_n}{\mu_n^2 + \lambda^2} - \frac{1}{\mu_n}\right) = 1 \end{aligned} \tag{22}$$

From the matching condition Eq. (19), we obtain

$$\begin{aligned} &a_1 \Delta R Lp_j - b_2 L_i \lambda Kp_i\left(\alpha I_1(\lambda R_2) - K_1(\lambda R_2)\right) + A_0\left(\frac{R_1}{2} + \frac{\Delta R Lp_j R_1^2}{4L_i Kp_i} + \Delta R\right) \\ &+ \sum_{n=1}^{\infty} A_n \cosh(\mu_n)\left[J_1(\mu_n R_1) - \frac{\mu_n^2}{\mu_n^2 + \lambda^2} J_1(\mu_n R_2) - J_0(\mu_n R_1)\Delta R\left(\frac{Lp_j}{L_i Kp_i \mu_n} - \mu_n\right)\right] = \Delta R Lp_j \end{aligned} \tag{23}$$

From boundary condition Eq. (18a),

$$\begin{aligned} &a_1 \int_0^{R_1} r J_0(\mu_l r) dr + b_2 \int_{R_1}^{\xi} \left(\alpha I_0(\lambda r) + K_0(\lambda r)\right) r J_0(\mu_l r) dr + A_0 \Delta_{0l} \\ &- \sum_{n=1}^{\infty} A_n \Delta_{nl} = -\int_0^{\xi} r J_0(\mu_l r) dr \end{aligned} \tag{24}$$

where $\Delta_{0l} = \frac{1}{4L_i Kp_i}\int_0^{R_1} r^3 J_0(\mu_l r) dr - \delta_{nl}\int_0^{\xi} r J_0(\mu_l r) dr$,

$$\Delta_{nl} = \frac{\cosh(\mu_n)}{L_i Kp_i}\left(\frac{1}{\mu_n}\int_0^{R_1} r J_0(\mu_n r) J_0(\mu_l r) dr + \frac{\mu_n}{\mu_n^2 + \lambda}\int_{R_1}^{\xi} r J_0(\mu_n r) J_0(\mu_l r) dr\right) - \delta_{nl} \sinh(\mu_n)\int_0^{\xi} r J_0(\mu_n r) J_0(\mu_l r) dr$$

The unknown coefficients can be solved numerically by standard matrix inversion via a finite number of truncation, as mentioned earlier in section 2.2.

4. Parameters in the model

The models proposed above contains a number of parameters, such as Lp for endothelium and IEL and Kp for the intima and media that require some discussion before numerical solution.

Let us first discuss the parameters that are easy to obtain. The parameters, such as the radius R_1 of the endothelial cells and the wall unit radius ξ can be estimated either from literatures or from our experiments. From the results of Heath and Smith (Heath 1979), the diameters of the ECs of the pulmonary artery vary from the smallest of 10 μm to the largest of 30 μm. From the silver lining experiment, we measured the cell radius is 12μm for the PA (Chapter 4). By the same methods, we have determined that the IVC has an average endothelial cell radius of 11μm (Chapter 4). Huang *et al*. (Huang 1994) and Yin *et al*. (Yin 1997) determined the values of ξ for their tissues (aorta and aortic valve, respectively) from the average number density of leaks found in HRP spot size experiments. We can also estimate a corresponding ξ value from our HRP experiment on pulmonary artery, although due to the sample size, the error bars are large. The value is about 600 μm for both the PA and the IVC. Since the models turn out to be rather insensitive to the exact value taken for the width ΔR of the leaky cleft, we initially take it to be similar to the aorta, which was 20 nm. (Wen 1988). Tarbell (Tarbell 2003) stated that the leaky junctions of endothelium had the dimensions on the order of 30 to 1000 nm. This seems reasonable since the amount of tracer entering through the leak seems similar to that in the aorta.

The thickness of the pulmonary artery wall L_w depends on the sizes and types of the animals we investigate. From Tompkins' work (Tompkins 1989), L_w for squirrel

monkeys (weight 700-1000g) is about 78 μm. However, Lever and Jay (Lever 1990) had the thickness of the media L_m is about 97 μm for rabbits weighing from 2 to 2.5 kg. We use values for the thicknesses L_m and L_w for rats from our ultrastructure experiments (Chapter 2). The aorta has a wall thickness of 145±9.7 μm, the PA 78.9±3.3 μm, and the IVC 66.1±4.1 μm in our male Sprague-Dawley rat model.

The Lps for the model derive directly from our measurements. We measured the *L*ps of the vessel with both intact and denuded vessel wall and calculated *L*p of the endothelium by assuming that the 1/Lp for the layers add like resistances in series (See Chapter 3). We found that *L*p of aortic endothelium is $4x10^{-11}$ cm^2s/g and that about 50% of the overall wall resistance derives from the media, $4x10^{-11}$ cm^2s/g. The PA has a larger $Lp_{endothelium}$ ($4x10^{-10}$ cm^2s/g) and Lp_{media} ($2x10^{-10}$ cm^2s/g). Most flow resistance in the IVC is from the endothelium. The $Lp_{endothelium}$ is $6x10^{-10}$ cm^2s/g and Lp_{media} is $20x10^{-10}$ cm^2s/g. The Darcy's permeability of the media is related to the hydraulic conductivity of the media by $Kp_m=Lp_m\mu L_m$, where μ is the water viscosity, and thus derives from the measured Lp values. Note that Lp_I contains detailed structural parameters ϕ_I and a_f for the IEL, which have been measured/estimated for the rat aorta by Huang *et al*'s (Huang 1998) experimental paper as 5% for ϕ_I, and 1μm for a_f. We shall begin by presuming that the PA values are the same or slightly larger (due to the thinner PA IEL).

It is worth noting that in order to fit the experimental spot size data, Huang *et al.* (Huang 1994) did not use the measured Lp values available in the literature at the time from Tedgui and Lever (Tedgui 1984), but rather estimated them using other criteria. Moreover, the values for ϕ_I and a_f determined in Huang *et al* (Huang 1998) turned out to be different from those assumed earlier by Huang *et al.* (Huang 1994). Thus, the first job

in solving this problem is to go back to the aorta model with Huang *et al.*'*s* (Huang 1994) parameters and to reproduce their results, among which is the curve showing that the convection front that caries the tracer in the intima is able to estimate the observed HRP spot growth. Then one must reexamine the aortic parameters in light of the currently known values. Using these experimentally measured parameters one needs to see if the model still produces an intimal convection front that roughly tracks the HRP spot growth. If not, one needs to see if there is enough wiggle room left in the remaining estimated parameters (e.g., $L\mathrm{p}_\mathrm{I}$, $L\mathrm{p}_\mathrm{j}$, $K\mathrm{p}_\mathrm{i}$) so that they remain of reasonable sizes, yet allow the model to account for these data. Only at that point will it make sense to proceed to the numerical solutions of the present models for the filtration flow in the PA and the IVC. This work is under way presently.

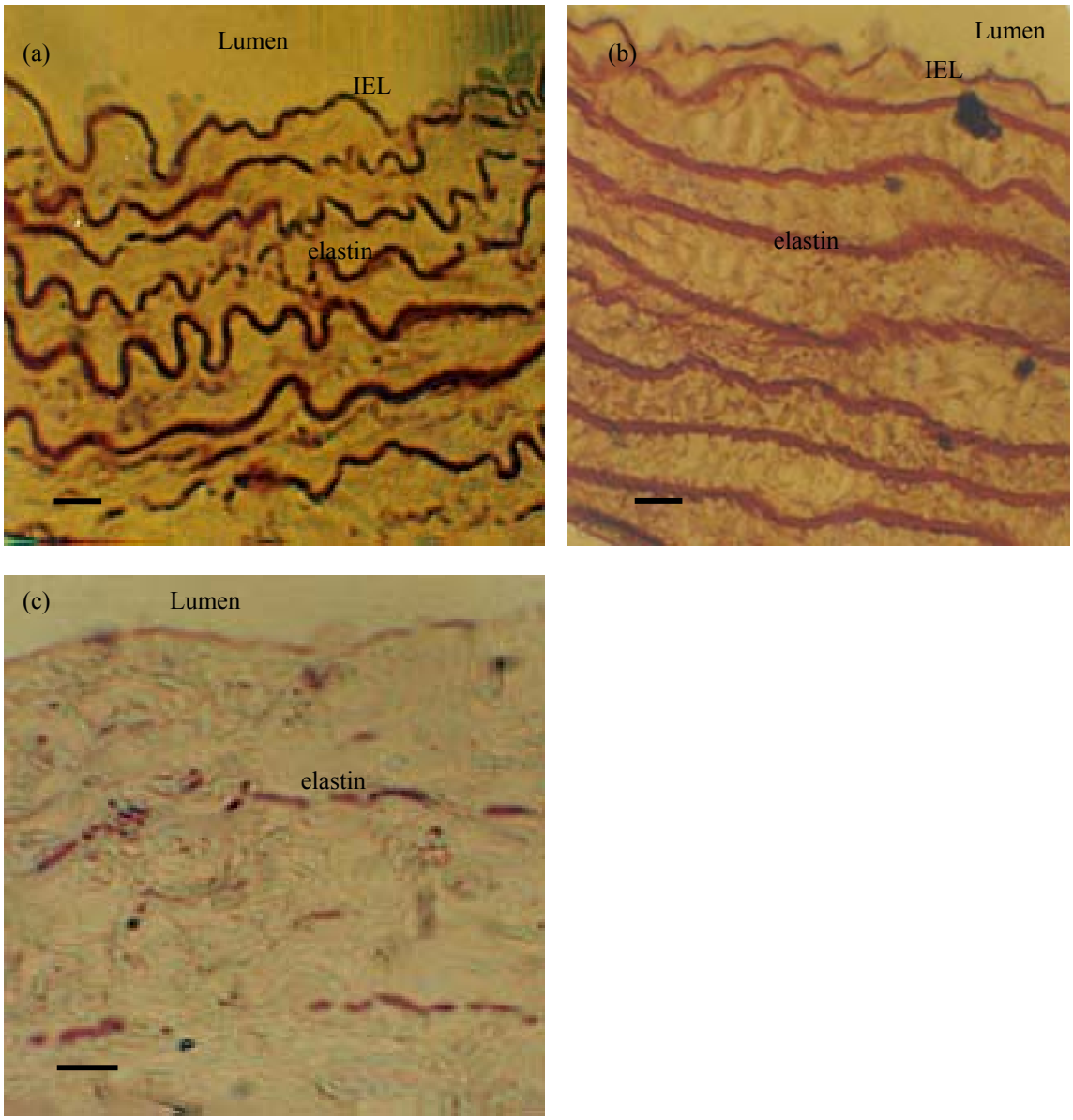

Figure 1. Vessel wall structure: Light microscopic views of100 nm thick sections stained with orcein, which specifically highlights elastin in red. (a) The pulmonary artery has a wall thickness of 78.9±3.3 μm (mean± SD) at zero pressure. It has a complete internal elastic lamina (IEL) (3.2±0.7 μm thick) and continuous wavy layers of elastin (0.4% orcein stain). (b) The aorta has a wall thickness of 145±9.7μm at zero pressure (Chapter 2). It has a complete IEL (4.6±1.6 μm) and continuous layers of elastin (0.4% orcein stain). (c) The inferior vena cava has a wall thickness of 66.1±4.1 μm at zero pressure. It has an incomplete IEL (the broken red line just below the lumen) and only sparse bits of elastin throughout (1.0% orcein stain). Bar=10 μm.

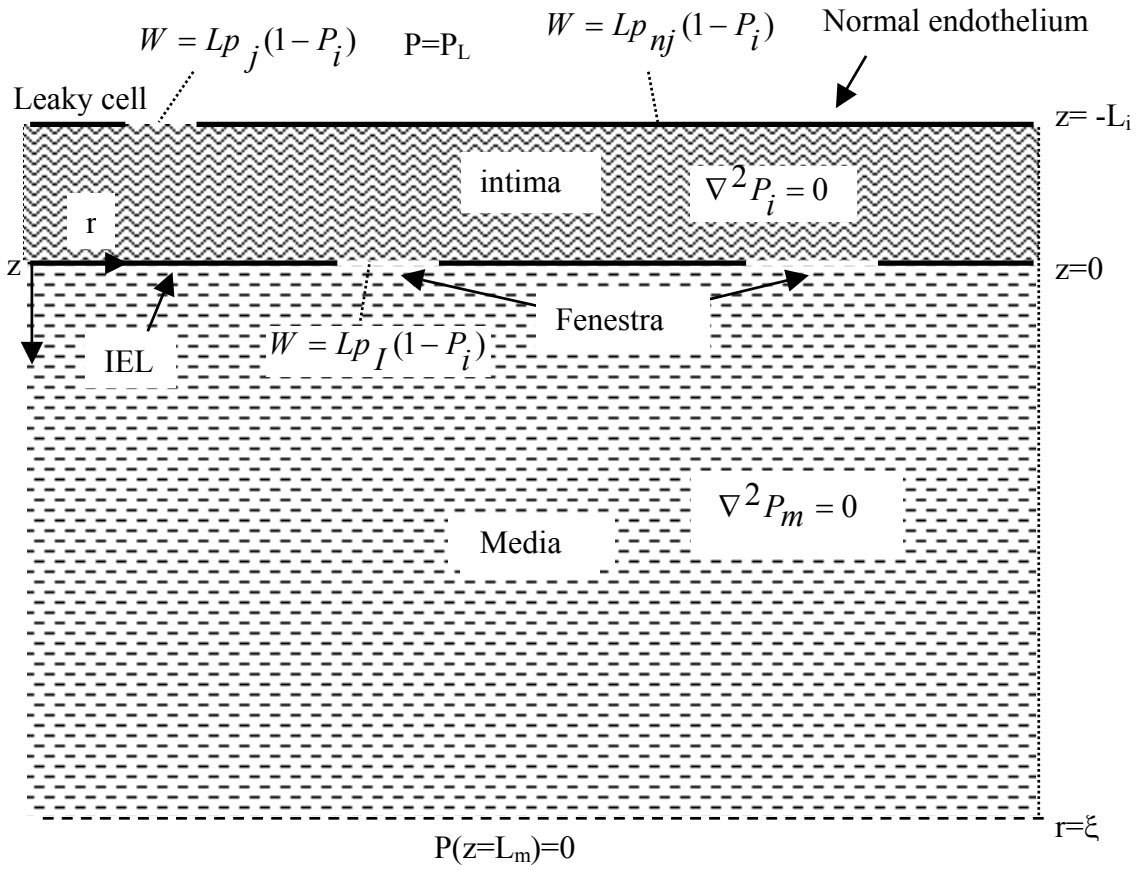

Figure 2. Schematic illustration of the periodic wall unit of the PA and aorta. The figure shows endothelial layer with a leaky cell at the origin, intima and internal elastic laminar (IEL) and media. The PA and aorta have a complete IEL. There is a pressure jump across the IEL.

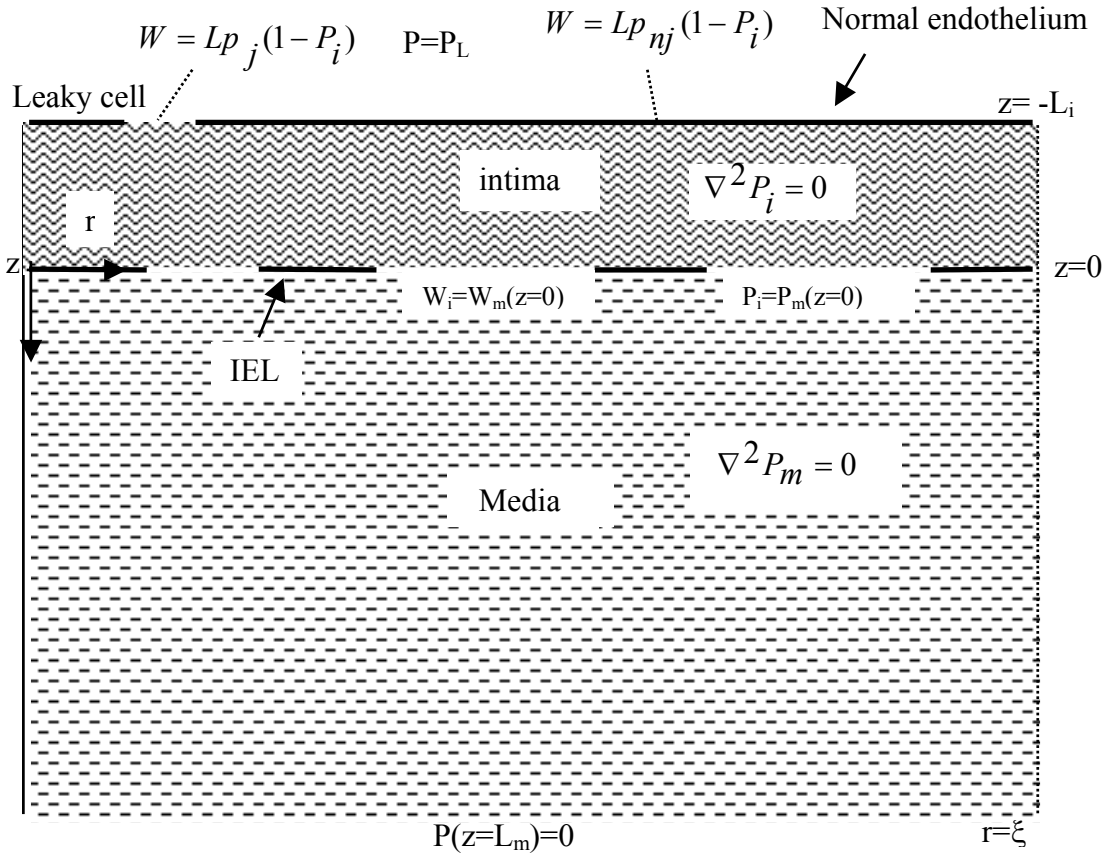

Figure 3. Schematic illustration of the periodic wall unit of the IVC. The figure shows endothelial layer with a leaky cell at the origin, intima and incomplete internal elastic laminar (IEL) and media. The pressure and the normal velocity across the IEL are continuous.

Chapter 7

Conclusions

As mentioned several times throughout this thesis, the aorta, pulmonary artery and inferior vena cava have very different susceptibilities to atherosclerosis. What have we learned about the features of transmural water and macromolecular transport in these vessels that may help us understand this difference in susceptibilities? The structures of the PA and aortic walls are similar, but differ substantially from that of the IVC. This is consistent with the very similar HRP tracer spot growth in the PA and aorta, which is very different from that in the IVC; IVC spots start out very large and hardly grow, as opposed to arterial spots that start small, but grow very quickly. The hydraulic conductivities of all three endothelia are likely very similar, but those of their medias increase sharply from aorta to PA to IVC. The combination is such that the overall transmural water flows in all three vessels are surprisingly similar, despite their very different normal transmural pressures. As a consequence, it is likely that macromolecular transport into the PA and the aorta are superficially similar; they both likely involve strong convection-driven transport parallel to the endothelium in their intimas. On the other hand, convection in the IVC, although of the same magnitude as in the arteries, is likely to involve a much smaller change in overall flow direction in the intima, and likely remains predominantly in the direction normal to the endothelium. Z. Zeng in our group is currently developing detailed solutions to the theory in Chapter 6 (coupled to a detailed associated mass transfer theory), which should clarify this issue.

How do these facts relate to the differences in vessel susceptibility to atherosclerosis? At this point we can only speculate. Our best guess is that, although convection seems to force similar amounts of macromolecular tracers into the walls of all three of these vessels, the critical

question for triggering early lesion formation is, how much of the LDL convected into the intima binds to intimal extracellular matrix? Since the aortic media is much denser than its intima, much higher lipid concentrations exist in its intima near a localized leak than in its media. The kinetics of lipid binding to intimal extracellular matrix depend on the local lipid concentration, and not on the concentration integrated across the vessel wall that one observes in the spot size studies. As such, it is possible that in the PA and the IVC, lipid that enters the wall distributes much better between the intima and media, rather than building up to high levels in the intima. Therefore the lower intima lipid concentration means that the kinetics of lipid binding to intimal extracellular matrix would be much slower than in the aortic intima. As such, it may be easily cleaned up by natural mechanisms. Current studies by other PhD students in our group should shed some light on this hypothesis. These include confocal microscopy studies to experimentally access and differentiate the tracer concentration in the intima from that in the media. It also includes the solution of Zeng's convection-diffusion transport model for the pulmonary artery. These theoretical solutions will also predict the portion of the tracer accumulation in the tracer spot that is in the intima and the portion that is in the media. This theoretical development also includes the coupling of Zeng's transport model to Yin *et al*'s (Yin 1997) model for the formation and growth of extracellular lipid liposomes in the intima. The goal is to see how these likely differences in intimal lipid concentration translate into differences in the rate of extracellular lipid accumulation in the vessel intima. At that point we shall see if these differences correlate with and lend some understanding to the known differences in vessel susceptibility to atherogenesis.

Bibliography

Aleo MF, F. Morandini, F. Bettoni, S. Tanganelli, A. Vezzola, R. Giuliani, N. Steimberg, Pl Apostoli, and G. Mazzoleni. 2002. Antioxidant poteintial and gap junction-mediated intercellular communication as early biological markers of mercuric chloride toxicity in the MDCK cell line. *Toxicology in Vitro* 16: 457-65

Baldwin AL, and L. M. Wilson. 1993. Endothelium increases medial hydraulic conductance of aorta, Possibly by release of EDRF. *American Journal of Physiology* 264: H26-H32

Baldwin AL, L. M. Wilson and B. R. Simon. 1992. Effect of pressure on hydraulic conductance. *Arteriosclerosis and Thombosis* 12: 163-71

Baldwin AL, M. J. Lever, and C. G. Caro. 1983. Effect of noradrenaline, sodium nitrite, and isosorbide dinitrate on albumin transport in the wall of the excised rabbit common carotid artery. *Atherosclerosis* 46: 1-11

Bell FP, I. L. Adamson, and C. Schwartz. 1974b. Aortic endothelial permeability to albumin: focal and regional patterns of uptake and transmural distribution of ^{131}I-albumin in the young pig. *Exp. Mol. Pathol.* 20: 57-68

Bell FP, A. S. Gallus, and C. Schwartz. 1974a. Focal and regional patterns of uptake and the transmural distribution of ^{131}I-fibrinogen in the pig aorta in vivo. *Exp. Mol. Pathol.* 20: 281-92

Berceli SA, H.S. Borovetz, R.A. Sheppeck, H.H. Moosa, V.S. Warty, M.A. Armany, and I.M. Herman. 1991. Mechanisms of vein graft atherosclerosis LDL metabolism and endothelial actin reorganizaton. *J. Vascular Surgery* 13: 336-47

Bozzola JJ, and L.D. Russell. 1992. *Electron Microscopy Principles and Techniques for Biologists*. Sudbury, Massachusetts: Jones and Bartlett Publishers

Brossman W. 1992. Pulmonary hypertension. In *Heart disease: a textbook of cardiovascular medicine*, ed. E Braunwald, pp. 790-816. Philadelphia: Saunder

Brown BP, and D. D. Heistad. 1986. Capacitance of the rabbit portal vein and inferior vena cava. *J. Physiol.* 381: 417-25

Chang YS, Munn, L., Hillsley, M.V., Dull, R.O., Yuan, J., Lakshminarayanan, S., Gardner, T.W., Jain, R.K., and J.M. Tarbell. 2000. Effect of vscular endothelial growth factor on cultured endothlial cell monolayer transport properties. *Microvascular research* 59: 265-77

Chen YL, K.M. Jan, H.S. Lin, and S. Chien. 1995. ultrasructural studies on macromolecular permeability in relation to endothelial cell turnover. *Atherosclerosis* 118: 89-104

Cho MR, D. W. Knowles, B. L. Smith, J. J. Mooulds, P. Agre, N. Mohandas, and D. E. Golan. 1999. Membrane dynaimcs of the water transport protein Aquaporin-1 in intact human red cells. *Biophysical Journal* 76: 1136-44

Chuang P, J. Cheng, S. Lin, K.M. Jan, D. Wang, and S. Chien. 1990. Macromolecular transport across arterial and venous endothelium in rats: Studies with Evans Blue-Albumin and Horseradish Peroxidase. *Arteriosclerosis* 10: 188-97

DeMaio L, J. M. Tarbell, R. C. Scaduto, Jr., T. W. Gardner, and D. A. Antonetti. 2003. A transmural pressure gradient induces mechanical and biological adaptive responses in endothelial cells. *Am. J. Physiol Heart Circ. Physiol* 286: H731-H41

Dhar P, G. Jayaraman, N. Karmakar, and S. C. Manchanda. 1996. Effect of pressure on transmural fluid flow in different de-endothelialised arteries. *Med. & Biol. Eng. & Comput.* 34: 155-9

Duff GL, and G.C. McMillan. 1951. Pathology of atherosclerosis. *Am. J. Med* 11: 92-108

Fortin MG, N. A. Morrison, and D. P. Verma. 1987. Nodulin-26, a peribacteroid membrane nodulin is expressed independently of the development of the peribacteroid compartment. *Nucleic Acids Res* 15: 813-24

Frank JS, and A.M. Fogelman. 1989. Ultrastructure of the intima in WHHL and Cholesterol-Fed rabbit aortas prepared by Ultra-Rapid Freezing and Freeze-Etching. *Journal of Lipid Research* 30: 967-78

Fry DL. 1985. Mathematical models of arterial transmural transport. *American Journal of Physiology* 245: H977-H91

Fry DL. 1987. Mass transport, atherogenesis, and risk. *Arteriosclerosis* 7: 88

Gerrity RG, M. Richardson, J.B. Somer, F.P. Bell, and C.J. Schwartz. 1977. Endothelial cell morphology in areas of *in vivo* Evans Blue uptake in the aorta of young pigs. II. Ultrastructure of the intima in areas of differing permeability to proteins. *American Journal of Pathology* 89: 313-34

Haldenby KA, D. C. Chappell, C. P. Winlove, K. H. Parker and J. A. Firth. 1994. Focal and regional variations in the composition of the glycocalyx of large vessel endothelium. *J. Vasc. Res.* 31: 2-9

Heath D, and P. Smith. 1979. The pulmonary endothelial cell. *Thorax* 34: 200-8

Hu X, R. H. Adamson, B. Liu, F. E. Curry, and S. Weinbaum. 2000. Starling forces that oppose filtration after tissue oncotic pressure is increased. *Am J Physiol Heart Circ Physiol* 279: H1724-H36

Huang AL, K.M. Jan, and S. Chien. 1992. Role of intercellular junctions in the passage of horseradish Peroxidadse across aortic endothelium. *Laboratory Investigation* 67: 201

Huang Y, D. Rumschitzki, S. Chien, and S. Weinbaum. 1994. A fiber matrix model for the growth of macromolecular leakage spots in the arterial intima. *Journal of Biomechanical Engineering* 116: 430-45

Huang Y, D. Rumschitzki, S. Chien, and S. Weinbaum. 1997. A fiber matrix model for the filtration through fenestral pores in a compressible arterial intima. *American Journal of Physiology* 272: H2023

Huang Y, K.M. Jan, D. Rumschitzki, and S. Weinbaum. 1998. Structural changes in rat aortic intima due to transmural pressure. *Journal of Biomechanical Engineering* 120: 476

Inglesby MK, Elder T. J., and S. H. Zeronian. 2002. Aggregation of direct dyes investigated by molecular modeling. *Texile Res J.* 72: 231-9

Iverius PH. 1972. The interaction between human plasma lipoproteins and connective tissue glycosaminoglycans. *J. Biol. Chem.* 247: 26.7-2613

Johanson U, M. Karlsson, I. Johansson, S. Gustavsson, S. Sjovall, L. Fraysse, A. R. Weig, and P. Kjellbom. 2001. The complete set of genes encoding major intrinsic proteins in Arabidopsis provides a framework for a new nomenclature for major intrinsic proteins in plants. *Plant Physiol* 126: 1358-69

Johnson M, and J. M. Tarbell. 2001. A biphasic, anisotropic model of the aortic wall. *J. of Biomech. Eng* 123: 52-7

Karmakar N, and J. Lever. 1994. Effect of high molecular weight solutes on fluid flux across the arterial wall. *Heart and Vessels* 9: 275-82

Kim WS, Tarbell JM. 1994. Macromolecular transport through the deformable porous media of artery wall. *Journal of Biomechanical Engineering* 116: 156-63

Klanchar M, and J. Tarbell. 1987. Moeling water flow through arterial tissue. *Bull. Math. Biol* 49: 651-69

Knox P, J. R. Levick and J. N. McDonald. 1988. Synovial fluid -- its mass, macromolecular content and pressure in major limb joints of the rabbit. *Q. J. Exp. Physiol.* 73: 33-45

Lark MW, T. Yeo, H. Mar, S. Lara, I. Hellstrom, K. Hellstrom, and T.N. Wight. 1988. Arterial chondroitin sulfate proteoglycan: Localization with a monoclonal antibody. *Journal of Histochemistry and Cytochemistry* 36: 1211-21

Lever MJ, and M.T. Jay. 1990. Albumin and Cr-EDTA uptake by systemic arteries, veins and pulmonary artery of rabbit. *Arterioscler Thromb* 10: 551-8

Lever MJ, and N. Sharifi. 1987. The effects of transmural pressure and perfusate albumin concentration on the hydraulic conductivity of the iolated rabbit common caarotid artery. *J. Physiol.* 387: P68

Lever MJ, T.J. Mark and P.J.Coleman. 1996. Plasma protein entry and retention in the vascular wall:possible factors in atherogenesis. *Canadian Journal of Physiology and Pharmacology* 74: 818-23

Levick JR. 1994. An analysis of the interaction between interstitial plasma protein, interstitial flow, and fenestral filtration and its application to synovium. *Microvascular research* 47: 90-125

Lin S, K.M. Jan, G. Schuessler, S. Weinbaum and S. Chien. 1988. Enhanced macromolecular permeability of aortic endothelial cells in association with mitosis. *Arteriosclerosis* 73: 223-32

Lin S, K.M. Jan, S. Weinbaum and S. Chien. 1989. Transendothelial transport of Low Density Lipoprotein in association with cell mitosis in rat aorta. *Arteriosclerosis* 9: 230-5

Luft JH. 1971a. Ruthenium red and violet. I. Chemistry, purification, methods of use for electron microscopy and mechanism. *Anat. Rec.* 171: 347-68

Luft JH. 1971b. Ruthenium red and violet. II. Tine structural localization in animal tissues. *Anat. Rec.* 171: 369-416

Majno G, G. E. Palade, and G. L. Schoetl. 1961. Studies in inflammation. II. The site of action of histamine and serotonin along the vascular tree: a topographic study. *J. Biophys. Biochem. Cytol.* 11: 567-629

McCandless BK, M.R. Powers, J.A. Cooper and A.B. Malik. 1991. Effect of albumin on hydraulic conductivity of pulmonary artery endothelial monolayers. *American Journal of Physiology* 260: L571-L6

Mountcastle VB, ed. 1968. *Medical Physiology*, Vols. 1 & 2. Saint Louis: C.V. Mosby Co.

Murata K, K. Mitsuoka, T. Hirai, T. Walz, P. Agre, J. B. Heymann, A. Engel, and Y. Fujiyoshi. 2000. Structural determinants of water permeation through aquaporin-1. *Nature* 407: 599

Nielsen S, B. L. Smith, E. I. Christensen, and P. Agre. 1993. Distribution of the aquaporin CHIP in secretory and resorptive epithelia and capillary endothelia. *Proc. Natl. Acad. Sci. USA* 90: 17275-7279

Niemietz CM, and S. D. Tyerman. 2002. New potent inhibitors of aquaporins: silver and gold compounds inhibit aquaporins of plants and human origin. *FEBS Letters* 531: 443-7

Packham MA, H. C. Rowsell, L. Jorgensen, and J. F. Mustard. 1967. Localized protein accumulation in the wall of the aorta. *Exp. Mol. Pathol.* 7: 214-32

Preston GM, J. S. Jung, W. B. Guggino and P. Agre. 1993. The mercury-sensitive residue at cysteine 189 in the CHIP28 water channel. *The Journal of Biological Chemistry* 268: 17-20

Ross R. 1986. The pathogenesis of atherosclerosis - an update. *N. Eng. J. Med* 314: 488-500

Schnitzer JE, and P. Oh. 1996. Aquaporin-1 in plasma membrane and caveolae provides mercury-sensitive water channels across lung endothelium. *American Journal of Physiology (Heart Circ. Physiol)* 270: H416-H22

Schwenke DC. 1997. Comparison of aorta and pulmonary artery II. LDL transport and metabolism correlate with susceptibility to atherosclerosis. *Circulation Research* 81: 346-54

Selzer A. 1987. Changing aspects of the natural histor of valvular aortic stenosis. *N. Eng. J. Med* 317: 91-8

Shanahan CM, Connolly D. L., Thson K. L., Cary Nr., Osbourn J. K., Agre P., and P. L. Weissberg. 1999. Aquaporin-1 is expressed by vascular smooth muscle cells and mediates rapid water transport across vascular cell membranes. *J. Vasc. Res.* 36

Sidel VW, and A. K. Solomon. 1957. Entrance of water into human red cells under an osmotic pressure gradient. *J. Gen. Physiol.* 41: 243-57

Silberberg A. 1990. The physiological role of a thick gel-like layer over the endothelial surface (Abstract). *Int. J. Microcirc. Clin Exp* 9: 204

Simionescu N, E. Vasile, F. Lupu, G. Popescu, and M. Simionescu. 1986. Prelesional events in atherogenesis. Accumulation of extracellular cholesterol-rich liposomes in the arterial intima and cardiac valves of the hyperlipidemic rabbit. *American Journal of Pathology* 123: 109-25

Sprague EA, M. A. Frankel, M. R. Hagens, G. B. Wilhelm, and C. J. Schwartz. 1980. Observations on vascular surface membrane charge distribution. In

Hemodynamics and the arterial wall, ed. RM Nerem, and J. R. Guyton, pp. 11-8. Houston: Univ. of Houston Press

Steinberg D. 1983. Liporoteins and atherosclerosis: A look back and a look ahead. *Arteriosclerosis* 3: 283-301

Stemerman MB, E.M. Morrel, K.R. Burke, C.K. Colton, K.A. Smith, and R.S. Lees. 1986. Local variation in arterial wall permeability to Low Density Lipoprotein in normal rabbit aorta. *Arteriosclerosis* 6: 64-9

Sui HX, B. Han, J. K. Lee., P. Walian and B. K. Jap. 2001. Structural basis of water-specific transport through the AQP1 water channel. *Nature* 414: 872

Tarbell JM. 2003. Mass transport in arteries and the localization of atherosclerosis. *Annu. Rev. Biomed. Eng.* 5: 79-118

Tarbell JM, L. Demaio, and M.M. Zaw. 1999. Effect of pressure on hydraulic conductivity of endothelial monolayers: Role of endothelial cleft shear stress. *J. Appl.Physiol.* 87: 261-8

Tedgui A, and M.J. Lever. 1987. Effect of pressure and intimal damage on ^{131}I-Albumin and [^{14}C]Sucrose spaces in aorta. *American Journal of Physiology* 253: H1530-H9

Tedgui A, and M.J. Lever. 1984. Filtration through damaged and undamaged rabbit thoracic aorta. *Am. J. Physiol* 247: H784-H91

Tompkins RG, M.L. J.J. Schnitzer, and M.L. Yarmush. 1989a. Macromolecular transport within heart valves. *Circulation Research* 64: 1213-23

Tompkins RG, M.L. Yarmush, J.J. Schnitzer, C.K. Colton, K.A. Smith and M.B. Stemerman. 1989b. Low-Density Lipoprotein transport in blood vessel walls of squirrel monkeys. *American Journal of Physiology* 257: H452-H64

Truskey GA, C.K. Colton and K.A. Smith. 1981. Quantitative analysis of protein transport in the arterial wall. In *Structure and Function of the Circulation*, ed. CJ Schwartz, J.T. Werthessen and S. Wolf, pp. 287-355. New York: Plenum Publishing Corporation

Truskey GA, W.L. Rogerts, R.A. Herrmann, and R.A. Malinauskas. 1992. Measurement of endothelial permeability to ^{125}I-Low Density Lipoproteins in rabbit arteries by use of *en face* preparations. *Circulation Research* 71: 883-97

Tzeghai G, P. Ganatos, R. Pfeffer, S. Weinbaum, and A. Nir. 1986. A theoretical model to study the effect of convection and leaky junctions on macromolecular transport in artery walls. *Journal of Theoretical Biology* 121: 141-62

VanBavel E, P. Siersma, and J. A. E. Spaan. 2003. Elasticity of passive blood vessels: a new concept. *Am. J. Physiol Heart Circ. Physiol* 285: H1986-H2000

Vander A, J. Sherman, and D. Luciano. 2001. *Human Physiology: the Mechanisms of Body Function*. New York: McGraw Hill Companies, Inc. 450 pp.

Vargas CB, F.F. Vargas, J.G. Pribyl, and P.L. Blackshear. 1979. Hydraulic conductivity of the endothelial and outer layers of the rabbit aorta. *American Journal of Physiology* 236: H53-H60

Vargas FF, P. Sanabria, H. Osorio, and C. Schulz. 1986. Hydraulic conductivity of venous endothelium as measured with a volume clamp method. *American Journal of Physiology* 251: H676-H80

Verkman AS. 1992. Water channels in cell membranes. *Annu. Rev. Physiol.* 54: 97-108

Vink H, and B. R. Duling. 1996. Identification of distinct luminal domains for macromolecules, erythrocytes and leukocytes within mammalian capillaries. *Circ. Res.* 79: 581-9

Vlad M, G. Uza, M. Zirbo and D. Olteanu. 1995. Free radicals, ceruloplasmin, and copper concentration in serum and aortic tissue in experimental atherosclerosis. *Nutrition* 11: 588-91

Waltz T, B. L. Smith, M. L. Zeidel, A. Engel, and P. Agre. 1994. Biologically active two-dimensional crystals of Aquaporin CHIP. *J. Biol. Chem.* 269: 1583-6

Weinbaum S, G. Tzeghai, P. Ganatos, R. Pfeffer, and S. Chien. 1985. Effect of cell turnover and leaky junctions on arterial macromolecular transport. *American Journal of Physiology* 248: H945-H60

Weinbaum S, G. Wen, P. Ganatos, R. Pfeffer, M.M.L. Lee,and S. Chien. 1988b. On the time-dependent diffusion of macromolecules through transient open junctions and theri subendothelial spread, I. Short-time model for cleft exit region. *Journal of Theoretical Biology* 135: 1-30

Wen G, S. Weinbaum, P. Ganatos, R. Pfeffer, and S. Chien. 1988. On the time-dependent diffusion of macromolecules through transient open junctions and their subendothelial spread, II. Long-time model for interaction between leakage sites. *Journal of Theoretical Physiology* 135: 219-53

Wen Q, F. Diecke, P. Iserovich, K. Kuang, J. Sparrow, and J. Fischbarg. 2001. Immunocytochemical localization of Aquaporin-1 in bovine corneal endothelial cells and keratocytes. *Exp. Biol. Med.* 226: 463-7

Wight TN, and R. Ross. 1975. Proteoglycans in primate arteries. I. Ultrastrucural localization and distribution in the intima. *Journal of Cell Biology* 67: 660-74

Wight TN, M. W. Lark, and M. G. Kinsella. 1987. Blood vessel proteoglycans. *Biology of Proteoglycans*: 267-300

Wilson JD, E. Braunwald, K. J. Isselbacher, R. G. Petersdorf, J. B. Martin, A. S. Fauci, and R.K. Root. 1991. *Harrison's Principles of Internal Medicine*. New York: McGraw-Hill

Yamartino E, Jr.,R. Bratzler, C. Colton, K. Smith and R. Lees. 1974. Hydraulic permeability of arterial tissue. *Circulation 49-50, Suppl* 3: 273

Yin Y, K. Lim, S. Weinbaum, S. chien, and D. Rumschitzki. 1997. A model for the initiation and growth of extracellular Lipid Liposomes in arterial intima. *American Journal of Physiology* 272: H1033

Yuan F, S. Chien and S. Weinbaum. 1991. A new view of convective-diffusive transport processes in the arterial intima. *Journal of Biomechanical Engineering* 113: 314-29

Zeng Z, Y. Y. Yin, A. Huang, K. M. Jan, and D. S. Rumschitzki. 2005. Macromolecualr transport in heart valves. I. Studies with Horseradish Peroxidase. *Am J Physiol Heart Circ Physiol* to be submitted

Zhang R, A. N. van Hoek, J. Biwersi, and A. S. Verkman. 1993. A point mutation at Cysteine 189 blocks the water permeability of rat kidney water channel CHIP28k. *Biochemistry* 32: 2938-41

Zhu F, E. Tajkhoshid, and K. Schulten. 2002. Pressure-induced water transport in membrane channels studied by molecular dynamics. *Biophysical Journal* 83: 154-60